Confined Atomic Systems

A thesis presented in partial fulfilment of the

requirements for the degree of

Doctor of Philosophy

in

Mathematical Physics

at Massey University, Albany,

New Zealand

Mustafa Hasanbulli

2015

Abstract

In this thesis, we investigate physical properties of various atomic systems such as hydrogen, helium and argon confined in a soft–wall potential of the form $V_s(r) = (r/r_0)^N$, where r_0 is the radius of the spherical confinement and N is the stiffness controlling variable. Our main purpose is to introduce a confinement for atomic systems that is flexible in terms of stiffness of the confining walls. However, this brings its complications such as non–existence of analytic solutions to the non–relativistic Schrödinger equation for this particular problem, and non–availability of good basis sets for studying electronic properties of such systems. Therefore, at first, we treat the problem in pure numerical fashion. Based on our experience on the numerical data, we then attempt to design basis sets that can be used in quantum chemical software packages. We compare our results to known theoretical and experimental results and, in return, make a decision on the quality of the basis sets. To our knowledge, systems confined in this type of potential has not yet been studied, and, we believe that this study will open up new research areas in this field. Possible applications are in high–pressure simulations of atomic, or molecular systems.

Acknowledgements

This research project would not have been successful without the support of many people. I would like to express my deep gratitude towards my supervisor Distinguished Prof. Peter Schwerdtfeger for all his support, help, guidance and vision. He was always within reach when I needed his help. I would also like to thank my co–supervisor Prof. Boris Pavlov for all the exciting discussions on Mathematics. In addition, my thanks to the old and new members of the CTCP for all the lunch breaks and our awesome challenging discussions, specially Dr. Michael Wormit, Dr. Andreas Hauser and Dr. Florian Senn. One special thanks goes to Dr. Jonas Kortner. If it wasn't for him, I wouldn't be able to make it this far. He repeatedly explained very trivial concept without losing his patience. And, thanks to him I was able to grasp the basics. I would also like to thank Nik Harris for his support, courage, patience and care. Without him, this journey would be a very difficult one. Last but not least, I am grateful to have the love, respect and appreciation of my mother and sisters.

Contents

List of Figures

List of Tables

Chapter 1

Introduction and Motivation

Confined atomic systems such as the hard–wall confined hydrogen have been the focus of many researchers for decades. Many authors tried to understand the behaviour of these atomic systems when exposed to high pressures. When Michels et al. [47] introduced the model of the confined hydrogen atom at the center of an impenetrable spherical box in 1937, he aimed to study how the pressure (as the derivative of the total energy with respect to the confinement volume) and dipole polarisability evolve as a function of compression. Since then, a number of research articles have been produced discussing the model of confinement for different sizes as well as different geometrical shapes.

As a first approximation, the behaviour of a system (an atom, or a molecule, etc.) subject to extreme pressures can be simulated by placing it in a box of impenetrable walls, where the infinite potential should simulate the pressure induced by confining the system. Under these conditions, the particle wave function must vanish at the wall, i.e., it should satisfy Dirichlet boundary conditions. spatial confinement causes certain changes in the observable properties of the system such as the energy spectrum, transition frequencies and transition probabilities as well as the polarisability.

The confinement model is also useful to systematically study effects on an atom,

or molecule trapped in a microscopic cavity, such as in fullerenes. We expect that the observables for such systems will change due to the spatial confinement as mentioned earlier. Moreover, the same situation occurs at a nanoscopic scale in artificial systems constructed within semiconductors such as two–dimensional quantum wells, quantum wires and quantum dots. Metal properties, astrophysical spectroscopic data, phase transitions, matter embedded in electric fields, nuclear models are some of the many possible applications of confined systems.

1.1 A Look Back

In 1937, Michels et al. [47] proposed a model to study ground state energy shifts and polarisability changes for the hydrogen atom when subjected to uniform compression. In their model, it is assumed that the nuclear charge is located at the center of an impenetrable spherically symmetric box of radius r_0. Thus, the angular functions of the free atom are unaffected by the confinement which implies that they remain spherical harmonic functions. The radial Schrödinger equation, in atomic units (a.u.), for the confined hydrogen atom is given by

$$\left(-\frac{1}{r^2}\frac{\mathrm{d}}{\mathrm{d}r}\left(r^2\frac{\mathrm{d}}{\mathrm{d}r}\right)+\frac{l(l+1)}{r^2}-\frac{2}{r}+2V_h(r)\right)R(r)=2ER(r),$$

where the confining potential $V_h(r)$ has the form,

$$V_h(r)=\begin{cases} 0, & \text{if} \quad r<r_0 \\ +\infty, & \text{if} \quad r\geq r_0. \end{cases}$$

Since the wave function must vanish for $r \geq r_0$, we restrict our attention to the region where $r < r_0$. Thus, the radial Schrödinger equation takes the form

$$\left(-\frac{1}{r^2}\frac{\mathrm{d}}{\mathrm{d}r}\left(r^2\frac{\mathrm{d}}{\mathrm{d}r}\right)+\frac{l(l+1)}{r^2}-\frac{2}{r}\right)R(r)=2ER(r), \tag{1.1}$$

with the Dirichlet boundary condition

$$R(r_0) = 0 \tag{1.2}$$

Michels et al. [47] proposed the following ansatz

$$R(r) = \frac{1}{r}\mathrm{e}^{-r/a} f(r),$$

which transforms Eq. (1.1) to

$$\left(\frac{\mathrm{d}^2}{\mathrm{d}r^2} - \frac{2}{a}\frac{\mathrm{d}}{\mathrm{d}r} - \frac{l(l+1)}{r^2} + \frac{2}{r}\right) f(r) = 0,$$

where

$$a = \sqrt{-\frac{1}{2E}} \quad \text{or,} \quad E = -\frac{1}{2a^2}. \tag{1.3}$$

For the unconfined hydrogen atom, i.e., when $\lim_{r\to+\infty} R(r) = 0$ and $a = n$ with $n \in \mathbb{N}^+$, we get the usual energy eigenvalues given by

$$E = -\frac{1}{2n^2}. \tag{1.4}$$

However, for the confined hydrogen atom the wave function must vanish at a finite value of the radial variable r_0. Therefore a cannot always be an integer. Hence, Michels et al. [47] proposed a power series solution of the form

$$f(r) = \sum_{l+1}^{+\infty} b_s r^s,$$

where the boundary condition becomes

$$f(r_0) = \sum_{l+1}^{+\infty} b_s r_0^s = 0.$$

This equation determines the perturbed values of a and E where they restricted their attention to ground state ($n = 1, l = 0$) and computed the ground state energy

shift for $r_0 = 5, 6, 7$ and 8 atomic units (a.u.).

Following Michels et al.'s [47] results, in 1938, Sommerfeld and Walker [64] published a research article proposing an exact formal expression for the wave functions of the confined hydrogen atom. Their claim on astrophysical importance of the model heated the research on this particular system. One can easily rewrite Eq. (1.1) in the following form, for $l = 0$,

$$\left(\frac{\mathrm{d}^2}{\mathrm{d}r^2} + \frac{2}{r}\frac{\mathrm{d}}{\mathrm{d}r} + 2E + \frac{2}{r}\right)R(r) = 0, \tag{1.5}$$

since

$$\frac{1}{r^2}\frac{\mathrm{d}}{\mathrm{d}r}\left(r^2\frac{\mathrm{d}}{\mathrm{d}r}\right) = \frac{\mathrm{d}^2}{\mathrm{d}r^2} + \frac{2}{r}\frac{\mathrm{d}}{\mathrm{d}r}.$$

Similarly, energy eigenvalues are given by Eq. (1.3). The ansatz of the form

$$R(\rho) = \mathrm{e}^{-\rho/2}F(\rho), \quad \rho = \frac{2r}{a},$$

where a in Eq. (1.3) transforms Eq. (1.5) into

$$\rho F''(\rho) + (2 - \rho)F'(\rho) + (a - 1)F(\rho) = 0. \tag{1.6}$$

Eq. (1.6) is a typical example of Kummer's differential equation[1]. Its solution at the origin is the confluent hypergeometric function ${}_1F_1(1 - a, 2, \rho)$. When a boundary condition similar to (1.2) is imposed, in order to find the energy eigenvalues, it is necessary to solve the equation

$${}_1F_1(1 - a, 2, \rho_0) = 0.$$

As soon as the values of a are determined, one can find the energy eigenvalues using the relationship stated in (1.3). However, the lack of algorithms as well as computational codes, and, of course, even computers capable of executing them,

[1] See Appendix B.

made it impossible to obtain accurate results at the time that Sommerfeld and Walker published their work [64]. Instead, they solved the problem by using analytical expansions of the hypergeometric functions to estimate the energy levels. They computed the ground state energy for $r_0 = 2, 3$ and 4 a.u. It is also important to note that Sommerfeld and Walker [64] also tried to estimate the critical cage radius r_c, i.e., the radius at which the binding energy becomes zero as r_0 becomes smaller. The total energy of the system becomes positive for $r_0 < r_c$. The r_c value could be important when constructing the partition function of the atom and the pressure ionization of ground and excited states.

Later in 1946, de Groot and ten Seldam [17] computed energy level shifts for excited states. They treated the radial Schrödinger equation with a non–zero angular momentum number subject to the boundary condition (1.2). Their ansatz is

$$R(\rho) = \mathrm{e}^{-\rho/2}\rho^l F(\rho)$$

where they showed that $F(\rho)$ satisfies Kummer's differential equation whose regular solution at the origin is given by the confluent hypergeometric function ${}_1F_1$, similar to Sommerfeld and Walker [64].

As stated earlier, when $r_0 \to +\infty$, the expansion of F becomes a polynomial with a being a positive integer where the energies are given by the well known formula in Eq. (1.4). On the other hand, when r_0 is finite, the values of a are in general non–integers, furthermore, they can be imaginary when the energy value is positive. de Groot and ten Seldam [17] computed how, under pressure, the hydrogen atom energies change for the $1s, 2s$ and $3s$ states. See Table 1.1.

de Groot and ten Seldam [17] also solved the problem for the region corresponding to the total energy $E > 0$. Although their results were considered to be exact for some time, later calculations showed inaccuracies for some of them. de Groot and ten Seldam were the first to realize that for small values of r_0 the expectation value of the kinetic energy is higher than that the Coulomb potential.

Table 1.1: Ground state energy eigenvalues (E_h) obtained by Michels et al. [47], Sommerfeld and Walkers [64] and de Groot and ten Seldam [17] as a function of the box radius r_0 (a.u.)

r_0	E(1s)	E(2s)	E(2p)
2.0	-0.1250^a		
3.0	-0.44^a		
4.0	-0.48^a		
5.0	-0.49659^b		
6.0	-0.49928^b		
7.0	-0.49986^b	-0.0974^c	-0.1058^c
8.0	-0.49997^b	-0.1055^c	-0.1124^c
10.0		-0.1162^c	-0.1194^c
15.0		-0.12451^c	-0.12477^c
20.0		-0.12499^c	-0.12500^c
$+\infty$	-0.50000^c	-0.12500^c	-0.12500^c

[a]Reference [64]
[b]Reference [47]
[c]Reference [17]

Goodfriend [27] used linear variation functions method[2] to study the confined hydrogen atom. He developed a formalism in which the basis set does not satisfy the boundary conditions. His calculations were carried out only for s states. A trial wave function was constructed out of $1s, 2s$, and $3s$ functions corresponding to the free hydrogen atom;

$$\psi(r) = c_1\phi_1(r) + c_2\phi_2(r) + c_3\phi_3(r),$$

where

$$\begin{aligned}
\phi_1(r) &= \frac{\mathrm{e}^{-r}}{\sqrt{\pi}}, \\
\phi_2(r) &= \frac{1}{4\sqrt{2\pi}}(2-r)\,\mathrm{e}^{-r/2}, \\
\phi_3(r) &= \frac{1}{81\sqrt{3\pi}}\left(27 - 18r + 2r^2\right)\mathrm{e}^{-r/3}.
\end{aligned}$$

Clearly, these functions do not satisfy the boundary conditions given in Eq. (1.2). However, the requirement is that the wave function ψ expanded in eigenfunctions

[2]See Appendix F.

of the unconfined system must satisfy the boundary condition, i.e.,

$$\psi(r_0) = c_1\phi_1(r_0) + c_2\phi_2(r_0) + c_3\phi_3(r_0) = 0.$$

This can be seen as a configuration interaction calculation for the confinement. It is worthy to note that, in order to represent the wave function in tight regimes, i.e. when r_0 gets relatively small, it is necessary to increase the number of functions in the expansion. Hence, with smaller r_0 the expansion becomes larger.

Goodfriend successfully showed that energy determination equation is given by

$$\begin{vmatrix} H_{11} - ES_{11} & H_{12} - ES_{12} & H_{13} - ES_{13} & \phi_1(r_0) \\ H_{21} - ES_{21} & H_{22} - ES_{22} & H_{23} - ES_{13} & \phi_2(r_0) \\ H_{31} - ES_{31} & H_{32} - ES_{32} & H_{33} - ES_{13} & \phi_3(r_0) \\ \phi_1(r_0) & \phi_2(r_0) & \phi_3(r_0) & 0 \end{vmatrix} = 0,$$

where Hamiltonian and overlap integrals are given by

$$H_{ij} = \left\langle \phi_i \middle| \mathcal{H} \middle| \phi_j \right\rangle$$

and

$$S_{ij} = \left\langle \phi_i \middle| \phi_j \right\rangle,$$

respectively. The integrals involved must be evaluated between 0 and r_0.

Table 1.2 depicts the results obtained by Goodfriend [27]. Despite the fact that he used only three terms in the wave function expansion, the agreement with the results by de Groot and ten Seldam [17] is good in most cases. However, for $r_0 = 7$ a.u., the energy reported by Goodfriend [27] for the first excited state is about 50% lower than that obtained by de Groot and ten Seldam [17].

In recent years, there has been an increased interest in the study of confined systems.

Table 1.2: Energies (E_h) obtained by Goodfriend [27] for levels 1s and 2s as a function of r_0 (a.u.) as compared with de Groot and ten Seldam [17]

r_0	E(1s)	Ref. [17]
1.902	−0.0556	−0.0566
2	−0.1250	−0.1250
3	−0.4240	−0.4475
4	−0.4832	−0.4852
5	−0.4964	−0.49659
7	−0.4999	−0.49986
$+\infty$	−0.5000	−0.50000
r_0	E(2s)	Ref. [17]
7	−0.0513	−0.0974
10	−0.1120	−0.1162
20	−0.1249	−0.12499
$+\infty$	−0.1250	−0.12500

One can nominate two reasons for such immense interest in these systems. First is the variety of real problems related with atoms and molecules under high pressures, near–surface donor states, and impurity binding energies in quantum wells are a few to count. Second, many free quantum systems can be solved easily if one confines them within a box with impenetrable walls. The energy eigenvalues of the free system can be obtained when the size of the confinement approaches infinity, as, for instance, in quantum anharmonic oscillator.

Besides accurate energy levels for the hard–wall confined hydrogen atom, many authors have considered physical properties such as hyperfine splitting, nuclear magnetic shielding, polarisability and pressure. Aquino [4] was one of the leading authors in this field of research to present accurate calculations for physical properties. In his paper, he used the Campoy–Palma (CP) method to accurately calculate ground level energy shifts of the hard–wall confined hydrogen atom. The CP method is designed for polynomial potentials. However, the hard–wall confined hydrogen atom has the potential

$$-\frac{1}{r}+V_h(r)=-\frac{1}{r}+\begin{cases} 0 & \text{if} \quad r\le r_0, \\ +\infty & \text{if} \quad r>r_0. \end{cases} \tag{1.7}$$

Table 1.3: The energy eigenvalues of ground state and first two excited states ($l = 0$) for hard–wall confined hydrogen atom by Aquino [4].

r_0[a]	Energies[a]		
	$1s$	$2s$	$3s$
1.0249	1.99998832673	14.73265476650	36.54667692735
2.0000	−0.12500000000	3.32750915649	9.31415043551
4.0867	−0.48533085511	0.38576150184	1.77514809767
7.0000	−0.49986257755	−0.05126039361	0.39224114311
8.0000	−0.49997510044	−0.08473872135	0.24649197699
10.0000	−0.49999926328	−0.11280621029	0.09142232240
17.0000	−0.49999999999	−0.12487792105	−0.04045674563
25.0000	−0.50000000000	−0.12499976370	−0.05459245098
48.0000	−0.50000000000	−0.12500000000	−0.05555555553
$r_0 = +\infty$[b]	−0.50000000000	−0.12500000000	−0.05555555556

[a]The energies are in hartrees and the distances in bohrs.
[b]Free hydrogen atom.

Aquino [4] solved this problem by writing the Schrödinger equation in the following form

$$r^2\psi'' = -2r\psi' + l\,(l+1)\,\psi - 2r\psi - 2Er^2\psi,$$

and expanding the wave function ψ at the point where the initial value is known, i.e., $\psi\,(0) = 0$. Table 1.3 summarizes his results for ground state and first two excited state energy shifts. It is notable that with increasing radius r_0 of the confinement, the energies approach the free hydrogen atom energies as one expects.

In the same paper, Aquino calculated position expectation values using the Hellmann-Feynman theorem which states that

$$\frac{\mathrm{d}E}{\mathrm{d}\alpha} = \left\langle \frac{\partial H}{\partial \alpha} \right\rangle,$$

where α is any parameter in the Hamiltonian. Adding αr^n, $n \in \mathbb{Z}$, to the original Hamiltonian $\mathcal{H}$ and solving the eigenvalue problem for

$$h = \mathcal{H} + \alpha r^n,$$

Table 1.4: The expectation values of ground state and first excited state ($l = 0$) for hard–wall confined hydrogen atom by Aquino [4].

	$1s$		$2s$	
r_0[a]	$\langle 1/r \rangle$	$\langle r \rangle^2$	$\langle 1/r \rangle$	$\langle r \rangle^2$
0.53622	4.7862828706	0.0768911073		
1.05486	2.5750499876	0.2796999371		
2.00000	1.5351617064	0.8748255394	1.64627014	1.3320904
3.04187	1.1878909423	1.6552712120		
4.08667	1.0683597490	2.3160511520		
4.93358			0.63685783	8.6689450
7.00000	1.0013470611	2.9655475140	0.41884859	16.7757750
9.00000	1.0000601992	2.9976710450		
10.00000	1.0000116928	2.9994595080	0.29883743	28.5243200
12.00000	1.0000003947	2.9999750180		
15.00000			0.25415513	39.7375090
16.00000	1.0000000002	2.9999999640		
20.00000			0.25017311	41.8491300
30.00000			0.25000008	41.3338400
$r_0 = +\infty$[b]	1.0000000000	3.0000000000	0.25000000	42.0000000

[a]The distances are in bohrs.
[b]Free hydrogen atom.

reduces the computation of $\langle r^n \rangle$ to the computation of

$$\langle r^n \rangle = \left\langle \frac{\partial h}{\partial \alpha} \right\rangle .$$

Table 1.4 shows some of their results. It is not surprising that their results approach the expectation values of free hydrogen atom with increasing radius r_0.

In addition to energy shifts and expectation values, Aquino also calculated hyperfine splittings and nuclear magnetic shielding constants, polarisabilities and pressure. We will focus on these physical properties later in the section, as Aquino et al. [5] presented much improved results later in 2007.

When energy shifts of the hard–wall confined hydrogen atom have been understood well, many researchers started focusing on other physical properties of the system. One important reason being that our understanding of the interiors of planets like Jupiter and Saturn depends on our knowledge of the properties of the hydrogen

atom at high pressures. Guillot's [28] model is based on the assumption that both planets consist of three globally homogeneous regions: a dense core, an atomic or metallic hydrogen envelope, and a molecular hydrogen envelope. Astrophysicists pointed out that the study of hydrogen at high pressures is one of the key problems in modern physics and astrophysics. As a result, a great amount of experimental and theoretical work has been done on properties of the hydrogen atom at high pressures. See, for example, Ashcroft [8]. However, one should note that such a model system may be far fetched to describe extremely dense hydrogen, which becomes metallic at very high pressures.

The biggest difficulty in such studies is the lack of the exact analytical form of the wave function due to non–standard boundary conditions. Analytic approximation methods developed so far to handle confined systems are mainly based on perturbation methods, semi–classical WKB techniques and variational methods. However, as far as the accuracy of the predicted energy eigenvalues are concerned, the variational approach seems to be the most effective one.

Dutt et al. [19] used a two–parameter variational trial wave function method [67], which results in the energy eigenvalues of $1s, 2p$ and $3d$ states of confined hydrogen atom with accuracy within 0.5% as compared to the exact value obtained by solving the Schrödinger equation numerically. However, a good wave function producing correct energy eigenvalues is not guaranteed to give accurate properties of the system such as the dipole polarisability. Method used in [67] predicts the dipole polarisability of a hard–wall confined hydrogen atom with reasonably good accuracy up to a certain range of the radius. Although extensive theoretical work has been done on the dipole polarisabily of many atoms, these cases are for free atoms. Therefore, Dutt et al. [19] saw the necessity of a study that mainly gives both upper and lower bounds for the dipole polarisability of an hard–wall confined hydrogen atom. As a result, they conclude that the variational wave function method presented in [67] is a reliable enough method to study spectroscopic parameters such as the magnetic shielding factor for all ranges of radius r_0.

In 2002, Montgomery [48] studied the hard–wall confined hydrogen atom problem using a method introduced by Ley-Koo and Rubinstein [41], where he presented exact numerical ground state energy eigenvalues. In addition, the static and dynamic dipole polarisability of the system has been calculated using variational perturbation theory. The variational perturbation method is shown to be quite stable even far into the anomalous dispersion region.

In the following years, research on finding accurate ground state dipole polarisabilities concentrated on studying trends in polarisabilities with changing confinement radius. Laughlin [38] derived first–order $1s$ and $2p$ wave functions of a hard–wall confined hydrogen–like atom to predict the large–box asymptotic forms of the $1s$–$2p$ oscillator strength and ground state static dipole polarisability. It was found that the deviations from the free atom values behave as e^{-Zr_0} in the case of the oscillator strength, and as e^{-2Zr_0} in the case of the dipole polarisability. For the positive energy region, they implemented Rayleigh–Schrödinger perturbation theory to calculate dipole polarisabilities.

Borrows and Cohen [14] presented analytical closed form solutions for the first–order perturbation corrections appropriate to the dipole polarisation of all s states. They provided *exact* solutions in terms of confluent hypergeometric functions by exploiting several well–known recurrence and differential relations for these functions. Their technique is the first one that provides exact values for dipole polarisability and shielding factors. Additionally, the procedure is easily extended to states of non–zero angular momentum as well as higher multipole perturbations.

Aquino et al. [5] were able to obtain eigenvalues for the confined hydrogen atom with accuracy up to 100 decimal digits. They employed two different methods with agreeing results. The first method is based on a formal solution of the confluent hypergeometric function, while the second method involves a series expansion method. As we refer and compare our results to their result, we see it fit to present

their approach to the problem. The stationary Schrödinger equation is given by

$$-\frac{1}{2}\nabla^2\psi + V(r)\psi = E\psi. \tag{1.8}$$

For the confined hydrogen atom, they considered the potential in (1.7). As usual, they separated the wave function as

$$\psi(r,\theta,\phi) = R(r)Y_{lm}(\theta,\phi) \tag{1.9}$$

Substitution of (1.9) into Eq. (1.8) yields the radial Schrödinger equation

$$\frac{1}{2}\frac{1}{r^2}\frac{\mathrm{d}}{\mathrm{d}r}\left(r^2\frac{\mathrm{d}R(r)}{\mathrm{d}r}\right) + \left(V(r) + \frac{l(l+1)}{2r^2}\right)R(r) = ER(r). \tag{1.10}$$

For the region of interest, i.e., for $r \leq r_0$, the previous equation becomes

$$-\frac{1}{2}\frac{1}{r^2}\frac{\mathrm{d}}{\mathrm{d}r}\left(r^2\frac{\mathrm{d}R(r)}{\mathrm{d}r}\right) + \left(\frac{l(l+1)}{2r^2} - \frac{1}{r}\right)R(r) = ER(r),$$

where the Dirichlet boundary condition is given by

$$R(r_0) = 0.$$

Substitutions

$$a = \frac{1}{\sqrt{-2E}} \quad \text{and} \quad \rho = \frac{2r}{a} \tag{1.11}$$

transform the radial Schrödinger equation into

$$\frac{\mathrm{d}^2R(r)}{\mathrm{d}\rho^2} + \frac{2}{\rho}\frac{\mathrm{d}R(r)}{\mathrm{d}\rho} - \left(\frac{1}{4} - \frac{a}{\rho} + \frac{l(l+1)}{\rho^2}\right)R(r) = 0. \tag{1.12}$$

Aquino et al. [5] used the ansatz

$$R(\rho) = \mathrm{e}^{-\rho/2}\rho^l F(\rho)$$

which in return they arrived at the Kummer's differential equation

$$\rho \frac{\mathrm{d}^2 F(\rho)}{\mathrm{d}\rho^2} + (2l + 2 - \rho)\frac{\mathrm{d}F(\rho)}{\mathrm{d}\rho} - (l + 1 - a)F(\rho) = 0.$$

It is essential that the wave function has a finite value at the origin. That is why F must be a confluent hypergeometric function defined by

$$F(\rho) = {}_1F_1(l + 1 - a, 2l + 2, \rho).$$

It is well-known that ${}_1F_1$ is defined and yields a polynomial with a finite number of terms if $l + 1 - a$ is an integer and is negative. Therefore, letting n_r be a non-negative integer, define

$$-n_r = l + 1 - a.$$

Substitution of a yields the discrete energy eigenvalues given by

$$E_m = -\frac{1}{2m^2}, \quad m = n_r + l + 1.$$

When the hydrogen atom is enclosed in a spherical box with radius r_0, the Dirichlet boundary condition requires that $F = 0$ at $r = r_0$. Then, the allowed energies are found when

$${}_1F_1(l + 1 - a, 2l + 2, \rho_0) = 0.$$

For a given value of l, the first root of the polynomial corresponds to the energy of the lowest state ($n = 1$) and the successive roots are the excited states. Aquino et al. [5] used *Maple*'s root-finding function `fsolve` with the command `fulldigits` to ensure accuracies up to 100 significant figures. Their results for the ground state are presented in Table 1.5. Physical properties such as hyperfine splitting, nuclear magnetic shielding and the dipole polarisability are among the results Aquino et al. [5] presented. We omit these results as we present them in comparison to our results in the following section.

Table 1.5: Ground state 1s ($n = 1, l = 0$) energy of the confined hydrogen atom as a function of the box radius r_0.

r_0[a]	Energies[a]
0.5	14.747970030350279644598703765880615668472656184029 33
0.6	9.527707806146348161148737309004361666743550361003 49
0.7	6.469926127251261996193642455671406362657384786309 81
0.8	4.543380181009424336282743526815948945496313684707 60
0.9	3.262189536240118583882596061256307004974818769466 12
1.0	2.373990866103663727195906546113493079636937450659 97
1.2	1.269315015103739248025860860102452867969840586965 87
1.5	0.437018065247255850763110083187139463347563094812 63
1.7	0.139100928095954333035977576717866658760127007378 79
2.0	−0.125000000000000000000000000000000000000000000000 00
2.5	−0.334910185427921056513891973797366068567332788073 08
3.0	−0.423967287733453673913769533645925912797102939494 47
4.0	−0.483265302078022026214682311928753117255903478780 57
5.0	−0.496417006591452221323524379721599282322004492626 57
6.0	−0.499277286372115035056660315118618957995418019251 11
7.0	−0.499862577551405716245466710332615799078546936913 83
8.0	−0.499975100445740595490766927591499679270698746193 90
9.0	−0.499995654219019010768943175327305378948733380023 80
10.0	−0.499999263281525452542754690318164954701889999075 69
14.0	−0.499999999498264132081461431785892355814155697127 32
20.0	−0.499999999999993551989358444271366577401429115880 84

[a]The energies are in hartrees and the distances in bohrs.

And, very recently, Ferreyra and Proetto [20] presented a very extensive study on the hard–wall confined hydrogen atom summarising and, possibly, finalising all the mystery behind hard–wall confined hydrogen atom. They successfully clarified the issue of the quantum numbers and the ordering of the energy levels of the hard–wall confined hydrogen atom, the size dependence of the lowest electronic states of the problem has been found, rigorous analytical approximations have been derived in the physically relevant limits of weak and strong confinement, and the application of a modified version of the virial theorem, valid for confined systems, has been exemplified, together with a discussion of Kato's cusp condition and the essential role played by the electronic density alone as an alternative basic variable. Their result provide a basis for the important problem of doping with impurities of semiconductor heterostructure such a quantum dots.

1.2 Motivation

First study of a confined atomic system by Michels et al. [47] came out of curiosity. They wanted to know what would happen to physical properties of a single hydrogen atom when you "squeeze" it enough. Easy nature of the problem gained the interest of other researchers quickly. Although the first steps were to improve the accuracy of the numerical calculations for the ground state total energy of the hard–wall confined hydrogen atom, authors started to approach the problem using different techniques. Advances in computer science allowed us to develop better algorithms and write more efficient codes and, ultimately, that meant better and more accurate results. With an increased interest into the hard–wall confined hydrogen atom, it was only natural to wonder what would happen if multi–electron atoms were squeezed in a similar fashion. Based on the techniques, researchers were able to simulate the hard–wall confined helium atom. Although the problem seemed easy, the hard-wall confined helium atom proved to be a more difficult case. As expected, the electron–electron interaction in helium was one of the main reasons for many difficulties encountered. However, this did not stop the research and, now, we have a reasonably good understanding of both of these special confined systems.

In this thesis, we present a detailed study of confined hydrogen and helium atoms, but with a slight twist. Our main focus, initially, will be the soft–wall confined hydrogen atom. The fundamental difference between the hard–wall and the soft–wall confined hydrogen atoms is the fact that, with a soft-wall confinement, we are able to control the stiffness of the confining cavity. Although introduction of such confinements bring several difficulties to the study, it is interesting to see the converging similarities of both confinement types. Our approach, in its nature, is similar to the hard–wall confined hydrogen atom. However, the treatment to this new problem is very different.

Although our reason to study such systems is purely theoretical curiosity, we

believe this will clear the way to new discussions and theories.

Organisation of this thesis is as follows. Chapter 2 gives a brief introduction to atomic theory for systematic introduction of terminology and notations used in the thesis. Although it may seem that this chapter is elementary in its nature, we believe a condensed overview is needed to reduce the original physical problem to the corresponding technical one. Our new approach to the confined hydrogen atom and our findings are presented in Chapter 3. Even–tempered basis sets for the soft–wall confined hydrogen atom is presented in Chapter 4. This chapter also includes a study of physical properties such as the electron correlation and the dipole polarisability of the soft–wall confined hydrogen atom. Based on our experience and results with even–tempered basis sets, in Chapter 5, we repeat calculations with even–tempered basis sets to illustrate the ground state energy shifts, the electron correlation and the dipole polarisability of the soft–wall confined helium and argon atoms. And, finally, we summarize our finding in Chapter 6 and look into possible extensions of this interesting topic.

Remark 1 *Throughout the thesis, we will assume a general knowledge of linear algebra, general vector spaces, linear, adjoint and self-adjoint operators, and Hilbert spaces.*

Remark 2 *Unless specified otherwise, every wave function ψ, being a solution of a stationary Schrödinger equation with discrete spectrum will be a vector in the Hilbert space L^2 of square integrable functions:*

1. $\psi \in L^2$,
2. *the integral of $|\psi|^2$ over all space is time–independent,*
3. ψ *is well–defined, continuous and smooth everywhere, except locations where the potential of the system becomes infinite.*

Remark 3 *Throughout the thesis, we assume to work in atomic units. For a brief explanation reader can refer to Appendix A.*

Chapter 2

Atomic Theory

According to quantum mechanics, a stationary state of an N–electron atom is described by a wave function $\psi(\mathbf{r}_1, \ldots, \mathbf{r}_N)$, where $\mathbf{r}_i$ represents the space coordinates of the electron i (we neglect spin in this and the following formalism). The wave function is assumed to be continuous with respect to the space variables and is a solution to the stationary wave equation

$$\mathcal{H}\psi(\mathbf{r}_1, \ldots, \mathbf{r}_N) = E\psi(\mathbf{r}_1, \ldots, \mathbf{r}_N),$$

where $\mathcal{H}$ is the Hamiltonian operator for the atomic system. The wave equation is an eigenvalue problem and solutions exist for only certain values of E. These values are known as the eigenvalues of the operator and they represent the possible values of the total energy of the system. Following the mathematical terminology, the set of all eigenvalues is referred to as the eigenvalue spectrum of the operator.

The Hamiltonian operator $\mathcal{H}$ depends on the atomic system as well as on the underlying quantum mechanical formalism. For non–relativistic calculations, the normal starting point is Schrödinger's equation where $\mathcal{H}$, in atomic units, is given as

$$\mathcal{H} = \sum_{i=1}^{N}\left(-\frac{1}{2}\nabla_i^2 - \frac{Z}{r_i}\right) + \sum_{i>j}^{N}\frac{1}{r_{ij}}. \tag{2.1}$$

Here Z is the nuclear charge of the atom, $r_i = |\mathbf{r}_i|$ is the distance of electron i from nucleus and $r_{ij} = \left|\mathbf{r}_i - \mathbf{r}_j\right|$ is the distance between electron i and electron j. The above Hamiltonian is valid under the assumption that relativistic effects can be neglected and that the atomic nucleus can be treated as a point charge of infinite mass.

2.1 Normalisation

The Hamiltonian operator (2.1) has both a discrete and a continuous spectrum. Eigenfunctions belonging to the discrete spectrum are square integrable and represent bound states. Often these eigenfunctions are assumed to be normalised, i.e,

$$\int_{\mathbf{r}} \left|\psi\left(\mathbf{r}_1, \ldots, \mathbf{r}_N\right)\right|^2 \mathrm{d}\mathbf{r}_1 \ldots \mathrm{d}\mathbf{r}_N \equiv \langle \psi \,|\, \psi \rangle = 1,$$

where the integral sign means integration over all space coordinates. For normalised eigenfunctions, Born [11] interpreted

$$\left|\psi\left(\mathbf{r}_1, \ldots, \mathbf{r}_N\right)\right|^2 \mathrm{d}\mathbf{r}_1 \ldots \mathrm{d}\mathbf{r}_N$$

as the probability of finding the electrons in the generalised volume element $\mathrm{d}\mathbf{r}_1 \ldots \mathrm{d}\mathbf{r}_N$ centred at $\mathbf{r}_1, \ldots, \mathbf{r}_N$.

2.2 Antisymmetry

Identical particles are particles that cannot be distinguished from one another, even in principle. There are two main categories of identical particles: bosons which can share quantum states, and fermions which do not share quantum states due to the Pauli exclusion principle. Electrons are in the latter category of indistinguishable particles. Therefore, the Hamiltonian operator must be invariant under any

permutation of the electron coordinates. As a consequence, if $\psi(\mathbf{r}_1, \ldots, \mathbf{r}_N)$ is an eigenfunction of $\mathcal{H}$ with eigenvalue E, so is

$$\mathcal{P}_{ij}\psi\left(\mathbf{r}_1, \ldots, \mathbf{r}_i, \ldots, \mathbf{r}_j, \ldots, \mathbf{r}_N\right) = -\psi\left(\mathbf{r}_1, \ldots, \mathbf{r}_j, \ldots, \mathbf{r}_i, \ldots, \mathbf{r}_N\right),$$

where $\mathcal{P}_{ij}$ is the permutation operator and the minus sign accounts for the fact that electrons are fermions (plus sign for bosons) and obey Fermi-Dirac statistics. Hence, the general eigenfunction of $\mathcal{H}$ with eigenvalue E can be obtained as a linear combination of functions for which the coordinates have been permuted. It is, however, an experimental fact that only linear combinations that result in completely antisymmetric eigenfunctions give a correct description of fermionic system. One possible representation for such an antisymmetric eigenfunction is given by the linear combination

$$\frac{1}{\sqrt{N!}} \sum_{\mathcal{P}} (-1)^p \mathcal{P}\psi(\mathbf{r}_1, \ldots, \mathbf{r}_N),$$

where p is the parity of the permutation and the sum $\mathcal{P}$ is over all $N!$ permutations. For future use, we introduce the antisymmetrisation operator $\mathcal{A}$ defined by

$$\mathcal{A} = \frac{1}{\sqrt{N!}} \sum_{\mathcal{P}} (-1)^p \mathcal{P}.$$

To see the effect of such operator, consider the a three–electron eigenfunction. Then, we have

$$\begin{aligned}\mathcal{A}\psi(\mathbf{r}_1, \mathbf{r}_2, \mathbf{r}_3) = \frac{1}{\sqrt{3!}} \big[&\psi(\mathbf{r}_1, \mathbf{r}_2, \mathbf{r}_3) - \psi(\mathbf{r}_1, \mathbf{r}_3, \mathbf{r}_2) \\ &+ \psi(\mathbf{r}_2, \mathbf{r}_3, \mathbf{r}_1) - \psi(\mathbf{r}_2, \mathbf{r}_1, \mathbf{r}_3) + \psi(\mathbf{r}_3, \mathbf{r}_1, \mathbf{r}_2) - \psi(\mathbf{r}_3, \mathbf{r}_2, \mathbf{r}_1)\big]\end{aligned}$$

An antisymmetric eigenfunction is identically zero when two electrons with the same spin occupy the same position in space. Due to the continuity of the eigenfunction with respect to the spatial variables, it follows that the absolute

value of the eigenfunction is small whenever two electrons with the same spin are close together.

2.3 Angular Properties

The non–relativistic Hamiltonian commutes with the total orbital angular momentum operator

$$\mathbf{L} = \sum_{i=1}^{N} \mathbf{l}_i$$

as well as with the total spin angular momentum operator

$$\mathbf{S} = \sum_{i=1}^{N} \mathbf{s}_i,$$

i.e,

$$[\mathcal{H}, \mathbf{L}] = [\mathcal{H}, \mathbf{S}] = 0$$

and thus $\mathcal{H}, \mathbf{L}^2, L_z, \mathbf{S}^2$ and S_z define a set of mutually commuting operators. This implies that simultaneous eigenfunctions of all these operators exist, and we have

$$\begin{aligned}
\mathcal{H}\psi(\mathbf{q}_1, \ldots, \mathbf{q}_N) &= E\psi(\mathbf{q}_1, \ldots, \mathbf{q}_N), \\
\mathbf{L}^2\psi(\mathbf{q}_1, \ldots, \mathbf{q}_N) &= L(L+1)\psi(\mathbf{q}_1, \ldots, \mathbf{q}_N), \\
L_z\psi(\mathbf{q}_1, \ldots, \mathbf{q}_N) &= M_L\psi(\mathbf{q}_1, \ldots, \mathbf{q}_N), \\
\mathbf{S}^2\psi(\mathbf{q}_1, \ldots, \mathbf{q}_N) &= S(S+1)\psi(\mathbf{q}_1, \ldots, \mathbf{q}_N), \\
S_z\psi(\mathbf{q}_1, \ldots, \mathbf{q}_N) &= M_S\psi(\mathbf{q}_1, \ldots, \mathbf{q}_N).
\end{aligned}$$

These eigenfunctions will be denoted as

$$\psi(\gamma L M_L S M_S; \mathbf{r}_1, \ldots, \mathbf{r}_N),$$

where γ represents additional quantum numbers needed to completely specify the state.

2.4 Parity

In addition to the angular momentum quantum numbers LM_LSM_S, the eigenfunctions of the Hamiltonian can be denoted by their parity. The parity operator Π is defined by the relation

$$\Pi(\mathbf{r}_1, \ldots, \mathbf{r}_N) = \psi(-\mathbf{r}_1, \ldots, -\mathbf{r}_N).$$

From the definition, it is clear that $\Pi^2 = 1$ which implies the eigenvalues of Π are $\pi = \pm 1$. The parity operator commutes with the Hamiltonian and the angular momentum operator, hence the atomic eigenfunction may be taken also as eigenfunctions of Π. Eigenfunctions belonging to the eigenvalues +1 and −1 of the parity operator are said to be *even* and *odd*, respectively.

2.5 One–electron Systems

For most realistic potentials, the Schrödinger equation in Cartesian coordinates cannot be solved by simply trying to separate the wave function in these coordinates. However, one–electron systems belongs to the class of systems where Schrödinger's equation can be solved analytically for a Coulomb potential. Moreover, the results concerning these systems form the basis of most of the approximate methods for more complex many–electron systems. A very useful case is when the potential has spherical symmetry. Then, we can express the Schrödinger equation in spherical coordinates which, in return, results in an equation which becomes separable.

Introducing the spherical coordinates, i.e.,

$$x = r\sin\theta\cos\phi,$$
$$y = r\sin\theta\sin\phi,$$
$$z = r\cos\theta,$$

after some elaborate calculations, one can show that

$$\frac{\partial^2}{\partial x^2}+\frac{\partial^2}{\partial y^2}+\frac{\partial^2}{\partial z^2}=\frac{1}{r^2}\left[\frac{\partial}{\partial r}\left(r^2\frac{\partial}{\partial r}\right)+\frac{1}{\sin\theta}\frac{\partial}{\partial\theta}\left(\sin\theta\frac{\partial}{\partial\theta}\right)+\frac{1}{\sin^2\theta}\frac{\partial^2}{\partial\phi^2}\right].$$

It is important that we define an arbitrary axis, in this case z–axis, in relation to which all the angles are measured. This axis has special importance in the case that the symmetry of the potential is axially distorted. Introducing the spherical coordinates, the Schödinger equation is separable and takes the following form

$$-\frac{1}{2r^2}\left[\frac{\partial}{\partial r}\left(r^2\frac{\partial\Psi}{\partial r}\right)+\left(\frac{1}{\sin\theta}\frac{\partial}{\partial\theta}\left(\sin\theta\frac{\partial\Psi}{\partial\theta}\right)+\frac{1}{\sin^2\theta}\frac{\partial^2\Psi}{\partial\phi^2}\right)+2r^2V(r)\Psi\right]=E\Psi \quad (2.2)$$

Assuming that the potential depends on solely on r and is independent of the angular variables, we can use separation of variables method to separate Eq. (2.2). Let

$$\Psi\left(r,\theta,\phi\right)=R\left(r\right)Y\left(\theta,\phi\right).$$

Substitution of Ψ into Eq. (2.2) gives

$$\begin{aligned}\frac{1}{Y\left(\theta,\phi\right)}\left(\frac{1}{\sin\theta}\frac{\partial}{\partial\theta}\left(\sin\theta\frac{\partial Y\left(\theta,\phi\right)}{\partial\theta}\right)+\frac{1}{\sin^2\theta}\frac{\partial^2Y\left(\theta,\phi\right)}{\partial\phi^2}\right)\\ +\frac{1}{R\left(r\right)}\frac{\partial}{\partial r}\left(r^2\frac{\partial R\left(r\right)}{\partial r}\right)+2r^2\left(V\left(r\right)-E\right)=0.\end{aligned} \quad (2.3)$$

Since this equation must be valid for all variables, the only possibility is that each term equals a constant. In this way, we can separate the Schrödinger equation into

the following two differential equations

$$\frac{1}{Y\left(\theta,\phi\right)}\left(\frac{1}{\sin\theta}\frac{\partial}{\partial\theta}\left(\sin\theta\frac{\partial Y\left(\theta,\phi\right)}{\partial\theta}\right)+\frac{1}{\sin^2\theta}\frac{\partial^2 Y\left(\theta,\phi\right)}{\partial\phi^2}\right)=-L^2, \tag{2.4}$$

and

$$\frac{1}{R\left(r\right)}\frac{\partial}{\partial r}\left(r^2\frac{\partial R\left(r\right)}{\partial r}\right)-2r^2\left(V\left(r\right)-E\right)=L^2. \tag{2.5}$$

We first attempt to solve the angular part in Eq. (2.4). Rearranging the equation and using the ansatz $Y\left(\theta,\phi\right)=P\left(\theta\right)F\left(\phi\right)$, we can separate the angular part into the following equations

$$L^2\sin^2\theta+\frac{\sin\theta}{P\left(\theta\right)}\frac{\mathrm{d}}{\mathrm{d}\theta}\left(\sin\theta\frac{\mathrm{d}P\left(\theta\right)}{\mathrm{d}\theta}\right)=m_l^2, \tag{2.6}$$

and

$$\frac{1}{F\left(\phi\right)}\frac{\mathrm{d}^2F\left(\phi\right)}{\mathrm{d}\phi^2}=-m_l^2. \tag{2.7}$$

Azimuthal part in (2.7), together with the boundary condition $F\left(\phi\right)=F\left(\phi+2\pi\right)$, is easily solved by considering the corresponding auxiliary equation which in return gives[1]

$$F\left(\phi\right)=\frac{1}{\sqrt{2\pi}}\mathrm{e}^{\mathrm{i}m_l\phi}.$$

Solving the polar part depends on making the substitution $x=\cos\theta$. Then, Eq. (2.6) becomes the associated Legendre differential equation

$$\left(1-x^2\right)\frac{\mathrm{d}^2P}{\mathrm{d}x^2}-2x\frac{\mathrm{d}P}{\mathrm{d}x}+\left(L^2-\frac{m_l^2}{1-x^2}\right)P=0.$$

The solutions of Legendre differential equation are well known associated Legendre functions given by

$$P_{m_l}^{l}\left(x\right)=\frac{\left(-1\right)^{m_l}}{2^l l!}\left(1-x^2\right)^{m_l/2}\frac{\mathrm{d}^{l+m_l}}{\mathrm{d}x^{l+m_l}}\left(x^2-1\right)^l,$$

[1]Note that we already include the normalisation constant.

such that

$$L^2 = l(l+1), \quad L^2 - m_l^2 \geq 0, \quad l > |m_l|, \quad l > m_l > -l,$$

for $l \in \mathbb{Z}_+$.

At this point, we can form the solutions of angular part of the Schödinger equation which Table 2.1 shows some of the spherical harmonics for various values of l and m_l.

Next step is to solve the radial part of the Schödinger equation, that is to solve

$$\frac{\mathrm{d}}{\mathrm{d}r}\left(r^2 \frac{\mathrm{d}R(r)}{\mathrm{d}r}\right) + \Big(2r^2 \left(E - V(r)\right) - l(l+1)\Big) R(r) = 0. \tag{2.8}$$

To find the radial part, we must know the specific r–dependence of the potential energy term. It is possible to write Eq. (2.8) in a simpler way by means of the following transformation

$$R(r) = \frac{1}{r} P(r).$$

Then, we have

$$\left(\frac{\mathrm{d}^2}{\mathrm{d}r^2} - \frac{l(l+1)}{r^2} - 2V(r) + 2\mathrm{E}\right) P(r) = 0. \tag{2.9}$$

Since $\Psi\left(r, \theta, \phi\right)$ must be everywhere finite, $P(r)$ should satisfy the boundary condition (also known as the cusp condition)

$$P(0) = 0. \tag{2.10}$$

2.5.1 Bound State Solutions

Square integrable solutions to Eq. (2.9) satisfying boundary condition (2.10) exist for certain values of energy E, where $E < 0$. The different solutions $P(r)$ belonging to these energy values may be distinguished by the quantum number l. This number also specifies the number of nodes of the solution besides the origin. It

Table 2.1: Examples of normalised spherical harmonics.

l	m_l	$Y_l^{m_l}(\theta,\phi)$
0	0	$\sqrt{\frac{1}{4\pi}}$
1	0	$\sqrt{\frac{3}{4\pi}}\cos\theta$
1	1	$\sqrt{\frac{3}{8\pi}}\sin\theta e^{i\phi}$
2	0	$\sqrt{\frac{5}{16\pi}}\left(3\cos^2\theta-1\right)$
2	1	$\sqrt{\frac{15}{8\pi}}\sin\theta\cos\theta e^{i\phi}$
2	2	$\sqrt{\frac{15}{32\pi}}\sin^2\theta e^{2i\phi}$

Table 2.2: Example plots of spherical harmonics.

$Y_2^0(\theta,\phi)$	
$Y_2^1(\theta,\phi)$	
$Y_4^1(\theta,\phi)$	

is customary to denote the orbital angular momentum with the spectroscopic notation

$$\begin{array}{cccccccccc} l = 0 & 1 & 2 & 3 & 4 & 5 & 6 & 7 & 8 \ldots \\ s & p & d & f & g & h & i & k & l \ldots \end{array}$$

and to use a principal quantum number n defined by

$$n = l + v + 1,$$

where v is the number of nodes of the radial function not counting the zero at the origin. As an example, the radial function $P(2s; r)$ corresponds to an orbital angular momentum $l = 0$ and has one node away from the origin. Thus, we can specify the one–electron wave function

$$\Psi(\mathbf{q}) = \frac{1}{r} P(nl; r) Y_{lm_l}\left(\theta, \phi\right),$$

where $\mathbf{q} = \left(r, \theta, \phi\right)$, completely by using three quantum numbers nlm_l.[2] We can denote them as either $\Psi(nlm_l; \mathbf{q})$, or, $\langle \mathbf{q} \,|\, nlm_l \rangle$. If the coordinate is not important, one can use the notation $|nlm_l\rangle$. In order to normalise the wave functions, $P(nl; r)$ should satisfy

$$\int_0^{+\infty} P^2(nl; r)\, \mathrm{d}r = 1.$$

Even for normalised wave functions, there is a trivial arbitrariness between $P(nl; r)$ and $-P(nl; r)$. To resolve this, we use the convention that the radial functions should be positive near the origin.

For small r, we expand the radial function in a power series of the form

$$P(nl; r) = a_0 r^s + a_1 r^{s+1} + \cdots .$$

Since $\Psi(\mathbf{q})$ must be finite everywhere, we see that $s \geq 1$. Substituting this into

[2] One would normally consider four quantum numbers to specify the wave function. Because we are omitting the spin component, we ignore the forth quantum number, m_s.

Eq. (2.9) and collecting terms of the same order in r, we see that, for small r,

$$\frac{1}{r}P\left(nl;r\right) \propto r^{l}.$$

Therefore, the probability of finding electron close to the nucleus rapidly decreases for increasing l and it is finite only for $l = 0$. For $r \to +\infty$, it is readily seen that the radial function decreases exponentially since

$$P\left(nl;r\right) \propto \mathrm{e}^{-r\sqrt{2|E|}}.$$

Table 2.3 shows some of the normalised eigenfunctions of hydrogen atom with $V(r) = -1/r$.

Table 2.3: Normalised radial functions for $V(r) = -1/r$.

$$P\left(1s;r\right) = 2r\mathrm{e}^{-r}$$

$$P\left(2s;r\right) = \frac{1}{\sqrt{2}}r\mathrm{e}^{-1/2}\left(1-\frac{r}{2}\right)$$

$$P\left(2p;r\right) = \frac{1}{2\sqrt{6}}r^{2}\mathrm{e}^{-r/2}$$

$$P\left(3s;r\right) = \frac{2}{3\sqrt{3}}r\mathrm{e}^{-r/3}\left(1-\frac{2r}{3}+\frac{2r^{2}}{27}\right)$$

$$P\left(3p;r\right) = \frac{8}{27\sqrt{6}}r^{2}\mathrm{e}^{-r/3}\left(1-\frac{r}{6}\right)$$

$$P\left(3d;r\right) = \frac{4}{81\sqrt{30}}r^{3}\mathrm{e}^{-r/3}$$

2.5.2 Continuum State Solutions

For positive energy regime, $E > 0$, the electron is no longer bound to the nucleus and it behaves, for large r, essentially like a free particle. It can be shown that there is a solution to the radial equation (2.9) for every positive E, and a continuous spectrum of positive eigenvalues adjoins the discrete levels of negative energy. See Figure 2.1.

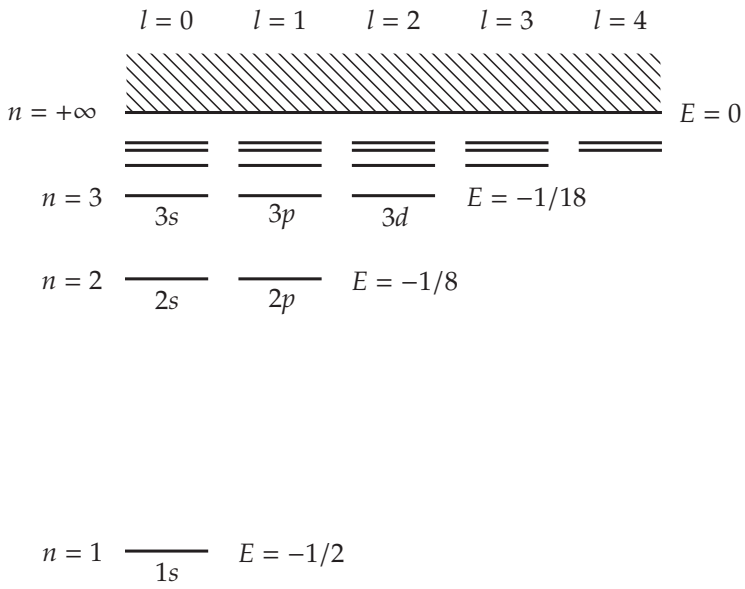

Figure 2.1: The discrete and continuous parts of the spectrum of hydrogen atom.

Let

$$E = \frac{k^2}{2}.$$

Then, the radial equation can be written as

$$\left(\frac{\mathrm{d}^2}{\mathrm{d}r^2} - 2V(r) - \frac{l(l+1)}{r^2} + k^2\right) P(kl;r) = 0,$$

where k together with the angular momentum number l are now used to label the different radial functions. For an electron moving in Coulomb field of the nucleus with charge Z the asymptotic form of the radial function is

$$P(kl;r) \propto \sin\left(kr - \frac{l\pi}{2} + \frac{Z\log(2kr)}{k} + \sigma_l\right),$$

where σ_l, the Coulomb phase shift, is given by

$$\sigma_l = \arg\Gamma\left(l + 1 - \mathrm{i}\frac{Z}{k}\right),$$

where Γ is the gamma function defined for complex numbers with a positive real

part, and it is defined via a convergent improper integral of the form

$$\Gamma(t) = \int_0^{+\infty} x^{t-1} \mathrm{e}^{-x} \mathrm{d}x.$$

If the continuum solutions are normalised in the Dirac sense such that

$$\int_0^{+\infty} P(kl; r) P(k'l; r) \, \mathrm{d}r = \delta(E - \mathrm{E}'),$$

then,

$$\left|\phi(klm_l; \mathbf{r})\right|^2 \mathrm{dE}\mathrm{d}q$$

can be interpreted as the probability that the electron is in the generalised volume element $\mathrm{d}q$ centered at q and has energy in the interval dE centred at $E = k^2/2$.

2.6 Many–electron Systems

The exact forms of the wave functions for many–electron systems are not known. Therefore, one must instead find approximate wave functions. One possibility that provides more insight into the nature of approximate wave functions is to replace the non–relativistic Hamiltonian $\mathcal{H}$ by one for which the Schrödinger equation is solvable.

2.6.1 Central–field Approximation

In the central–field approximation, the full Hamiltonian is replaced with the separable Hamiltonian $\mathcal{H}_0$[3]

$$\mathcal{H} \approx \mathcal{H}_0 = \sum_{i=1}^{N} \left(-\frac{1}{2}\nabla_i^2 - \frac{Z}{r_i} + V(r_i) \right),$$

[3]We assume to work in spherical coordinates, i.e., $\mathbf{q} = (r, \theta, \phi)$.

where the effective potential $V(r)$ approximates the effects of the Coulomb repulsion among the electrons.

The approximate Hamiltonian $\mathcal{H}_0$ as well as the full Hamiltonian commutes with the total angular momentum operators $\mathrm{L}^2, L_z, \mathrm{S}^2$ and S_z and we may choose the eigenfunctions of $\mathcal{H}_0$ to be the eigenfunctions of these operators. If

$$\mathcal{H}_0 \psi_0 (\mathbf{q}_1, \ldots, \mathbf{q}_N) = E_0 \psi_0 (\mathbf{q}_1, \ldots, \mathbf{q}_N),$$

then, since $\mathcal{H}_0$ is separable, the eigenvalues and eigenfunctions can be written as

$$E_0 = \sum_{i=1}^{N} E_i$$

and

$$\psi_0 (\mathbf{q}_1, \ldots, \mathbf{q}_N) = \prod_{i=1}^{N} \psi (\alpha_i; \mathbf{q}_i), \tag{2.11}$$

respectively, where the individual eigenfunctions are solutions to the one–electron equation

$$\left(-\frac{1}{2} \nabla^2 + U(r) \right) \psi (\alpha_i; \mathbf{q}) = E \psi (\alpha_i; \mathbf{q}),$$

with

$$U(r) = -\frac{Z}{r} + V(r).$$

As we have discussed earlier, the one–electron eigenfunction can be written as

$$\psi (\alpha; \mathbf{q}) = \frac{1}{r} P (nl; r) Y_{lm_l} (\theta, \varphi),$$

where the solutions are characterised by the quantum numbers $\alpha = nlm_l$. Note that for a general potential $U(r)$, the one–electron energy E, contrary to the Coulomb case, depends on n and l.

The Hamiltonian $\mathcal{H}_0$ is invariant with respect to permutations of the electron coordinates. Therefore, any permutation of these coordinates in the product function (2.11) also leads to an eigenfunction. By combining permuted product

functions, we can form the following antisymmetric function

$$\Psi(\mathbf{q}_1, \ldots, \mathbf{q}_N) = \mathcal{A} \prod_{i=1}^{N} \psi(\alpha_i; \mathbf{q}_i).$$

This function can also be represented as a Slater determinant

$$\Psi(\mathbf{q}_1, \ldots, \mathbf{q}_N) = \frac{1}{\sqrt{N!}} \begin{vmatrix} \psi(\alpha_1; \mathbf{q}_1) & \psi(\alpha_1; \mathbf{q}_2) & \cdots & \psi(\alpha_1; \mathbf{q}_N) \\ \psi(\alpha_2; \mathbf{q}_1) & \psi(\alpha_2; \mathbf{q}_2) & \cdots & \psi(\alpha_2; \mathbf{q}_N) \\ \vdots & \vdots & & \vdots \\ \psi(\alpha_N; \mathbf{q}_1) & \psi(\alpha_N; \mathbf{q}_2) & \cdots & \psi(\alpha_N; \mathbf{q}_N) \end{vmatrix}.$$

In this expression, it is seen that the total wave function $\Psi(\mathbf{q_1}, \ldots, \mathbf{q}_N)$ vanishes if two electrons have the same value of the four quantum numbers. Thus, for allowed states of the atom, no two electrons can share the same value of the four quantum numbers. This is the Pauli exclusion principle in the form originally discovered by Pauli in 1925. Note also that the determinant vanishes whenever $\mathbf{q}_i = \mathbf{q}_j$.

The parity operator, which changes the sign of all coordinates, commutes with the Hamiltonian of the system. To determine the parity of the Slater determinant, we need the parity of the each orbital building the Slater determinant which is given by $(-1)^l$. The Slater determinant itself must therefore have the parity

$$\pi = (-1)^{l_1} (-1)^{l_2} \cdots (-1)^{l_N} = (-1)^{\sum_i l_i},$$

which is even or odd depending on whether the sum of the orbital angular momentum quantum numbers is even or odd.

2.6.2 Electron Configuration

As seen above, an eigenfunction of the central–field effective Hamiltonian $\mathcal{H}_0$ can be written as a Slater determinant. The corresponding energy E_0 is then given by the sum of the energies of the orbitals appearing in the determinant, i.e.,

$$E_0 = \sum_{i=1}^{N} E_i.$$

Orbitals with n and l quantum numbers are said to belong to the same subshell and are called equivalent orbitals. Correspondingly, we may loosely speak of electrons belonging to the same subshell and refer to them as equivalent electrons. Since the energy of a orbital depends only on the n and l quantum numbers, the energy E_0 is entirely determined by the electron configuration (besides Russel–Sanders coupling which can split the energy levels for the same configuration), i.e., the distribution of orbitals with respect to the subshells.

A general electron distribution (or, configuration) is given by

$$(n_1 l_1)^{w_1} (n_2 l_2)^{w_2} \cdots (n_m l_m)^{w_m}, \quad N = \sum_{j=1}^{m} w_j,$$

where $w_1, w_2, \ldots$ are the occupation numbers of the orbitals in the different subshells. The corresponding energy can be given as

$$E_0 = \sum_{j=1}^{m} w_j E_{n_j l_j},$$

where E_{nl} denotes the energy of the orbital in an nl subshell. Often the electron configurations are denoted by means of the spectroscopic symbols given in Section 2.5.1. For instance, $1s^2 2s^2 2p^2$ means that there are two electrons in each of the $1s$, $2s$ and $2p$ subshells. According to the Pauli exclusion principle there can be at most two electrons in each orbital, and thus there can be at most $2\,(2l + 1)$ electrons in a subshell nl. A subshell which is fully occupied is said to be closed,

in contrast to a partially occupied shell which is said to be open. The energy of a configuration is given by the occupation number of each subshell. Therefore, the ground (lowest energy) configuration for a particular atom should be obtained by successfully filling the electron subshells with the lowest energies E_{nl} leading to a number of closed subshells and at most one open shell. This is the so–called "Aufbau" principle formulated by Bohr in 1922 to explain the periodic table of elements.

The concept of configuration has a simple interpretation. For light atoms, the experimental energy levels often appear in closely spaced groups. When a central–field calculation is performed using a suitable potential $V(r)$, it is found that the average energy of each of these groups correspond reasonably well with the energy of a certain configuration, and this it is possible to assign configuration labels to the groups. Furthermore, if the assignment of the configuration has been done correctly, it is seen that the number of states in a group is equal to the number of determinants of the corresponding configuration.

Chapter 3

The Soft–Wall Confined Hydrogen Atom

Over the years, with increased interest in confined systems, new types of confinements have been introduced. Some of these systems consisted of hard [17, 47, 64] and soft [24, 41, 46] confinements. Some authors also studied systems confined within various geometrical shapes [40, 42, 43]. In addition, spherical off–center confined atoms were particular interest as well. For example, in the theory of endohedral compounds, for atoms rapped in fullerene cages, there exist experimental and theoretical studies that shows that the confined atom is not at the center of $M@C_{60}$ $(M = Li, Na, K)$[18, 68].

In this section, we would like to introduce a rather general confinement model compared to the hard–wall problem. This model will allow us to control the stiffness of the confinement in addition to the spatial confinement parameter. We call this type "soft–wall" confinement. Such a confinement does not possess a discontinuity like the hard–wall potential (or some other impenetrable boxes in use). This simplifies its use enormously in conjunction with existing numerical algorithms/software packages to study (unconfined) many–electron systems, and clears the way for quantum theoretical studies of atoms or molecules in potentials with various stiffness levels.

3.1 A New Confinement Potential

Consider the following confinement potential

$$V_s(r) = \left(\frac{r}{r_0}\right)^N, \tag{3.1}$$

where r_0 defines the radius and $N \in \mathbb{N}$ the stiffness of the confinement. By increasing the stiffness, the slope of the potential curve around r_0 is made steeper, and thus, the potential wall becomes less penetrable, i.e., stiffer, see Fig. 3.1. It is readily seen that $V_s(r) \to V_h(r)$ as $N \to +\infty$. Together with potential $V_s(r)$, Eq. (1.10) becomes

$$\left[-\frac{1}{2}\frac{\mathrm{d}^2}{\mathrm{d}r^2} + \frac{l(l+1)}{2r^2} - \frac{1}{r} + \left(\frac{r}{r_0}\right)^N\right] P(r) = EP(r). \tag{3.2}$$

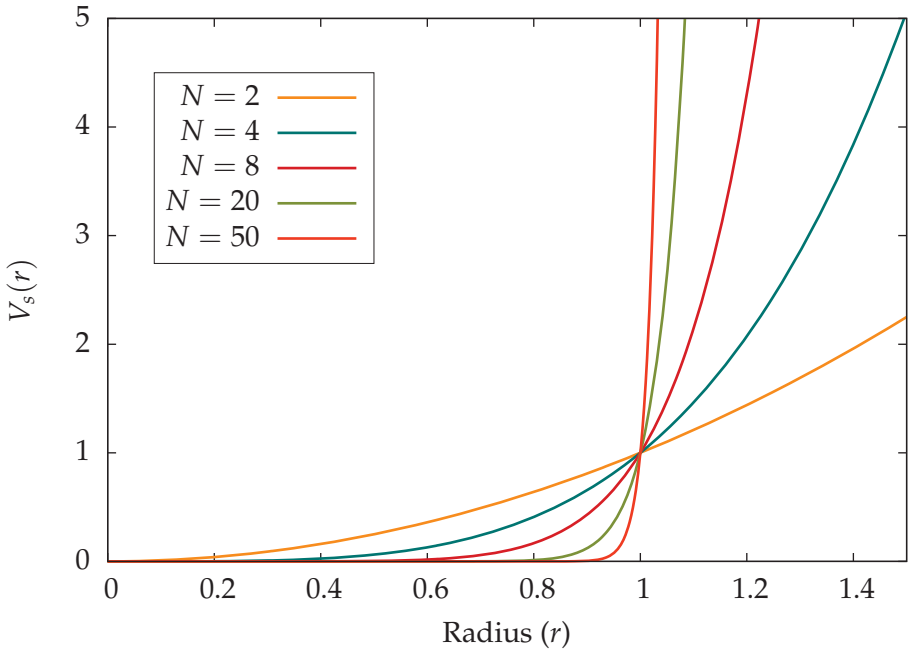

Figure 3.1: Plots of $V_s(r)$ at $r_0 = 1$ a.u. with different stiffness levels. The distances are in bohrs.

It is obvious that Eq. (3.2) does not have any discontinuities at r_0 and that the Hamiltonian of Eq. (3.2) is bounded from below and the spectrum is discrete for $N \geq 1$. Thus, the Dirichlet boundary condition $P(r_0) = 0$ which has been employed in the case of $V_h(r)$ is no longer required. Solutions to Eq. (3.2) can be expected to

decay quite rapidly for $r > r_0$, even more though if the stiffness increases.

Before we continue with the detailed numerical study of the soft–wall confined hydrogen atom, we would like to present the analytical asymptotic form of the solutions to Eq. (3.2).

Remark 4 *In what follows, unless stated otherwise, the energies are in hartrees and the distances in bohrs.*

3.2 Asymptotic Form of Solutions

Before we attempt the numerical solution of the soft–wall confined hydrogen atom, we consider the asymptotic behaviour of the radial wave functions $P(r)$. Let us consider Eq. (3.2) in the following form,

$$\left[-\frac{1}{2}\frac{\mathrm{d}^2}{\mathrm{d}r^2} + \frac{l(l+1)}{2r^2} + \left(\frac{r}{r_0}\right)^N - \frac{1}{r} - E\right]P(r) = 0. \tag{3.3}$$

We are interested in the asymptotic behaviour of the wave functions $P(r)$ as $r \to +\infty$. In the asymptotic limit, for $N \geq 1$, the term in brackets of Eq. (3.3) is dominated by the kinetic energy and $(r/r_0)^N$ terms, and, therefore, we may disregard the Coulomb, angular momentum and energy terms. In return, we arrive at the differential equation

$$-\frac{1}{2}\frac{\mathrm{d}^2P(r)}{\mathrm{d}r^2} + \left(\frac{r}{r_0}\right)^N P(r) = 0. \tag{3.4}$$

Hence, it is sufficient to study the asymptotic behaviour of solutions of Eq. (3.4), which for $N = 2$ is identical to the one-dimensional harmonic oscillator differential equation.

First, we introduce necessary concepts that will help us with the rest of this section. Consider the following differential equation

$$\frac{\mathrm{d}^2y(z)}{\mathrm{d}z^2} + b^2z^{c-2}y(z) = 0, \tag{3.5}$$

where $z, b \in \mathbb{C}$, $y \in C^2(\mathbb{C})$[1] and $c \in \mathbb{R} \setminus \{0\}$. Now, let us consider the following transformation

$$y(z) = \sqrt{z}F(z).$$

Simple algebra shows that we can rewrite Eq. (3.5) in the following form

$$\left[z^2\frac{\mathrm{d}^2}{\mathrm{d}z^2} + z\frac{\mathrm{d}}{\mathrm{d}z} + b^2z^c - \frac{1}{4}\right]F(z) = 0. \tag{3.6}$$

Employing the following change of variables

$$\xi = \frac{2b}{c}z^{c/2},$$

one can observe that we have

$$z\frac{\mathrm{d}}{\mathrm{d}z} = z\frac{\mathrm{d}\xi}{\mathrm{d}z}\frac{\mathrm{d}}{\mathrm{d}\xi} = bz^{c/2}\frac{\mathrm{d}}{\mathrm{d}\xi} = \frac{c}{2}\xi\frac{\mathrm{d}}{\mathrm{d}\xi}.$$

Then, the differential equation in Eq. (3.6) takes the form

$$\left[\left(\frac{c}{2}\right)^2\left(\xi^2\frac{\mathrm{d}^2}{\mathrm{d}\xi^2} + \xi\frac{\mathrm{d}}{\mathrm{d}\xi}\right) + \left(\frac{c}{2}\xi\right)^2 - \frac{1}{4}\right]F(\xi) = 0,$$

as a result of operator relation for operations on holomorphic functions

$$\begin{aligned} z^2\frac{\mathrm{d}^2}{\mathrm{d}z^2} + z\frac{\mathrm{d}}{\mathrm{d}z} &= \left(z\frac{\mathrm{d}}{\mathrm{d}z}\right)^2 \\ &= \left(\frac{c}{2}\xi\frac{\mathrm{d}}{\mathrm{d}\xi}\right)^2 = \left(\frac{c}{2}\right)^2\left(\xi^2\frac{\mathrm{d}^2}{\mathrm{d}\xi^2} + \xi\frac{\mathrm{d}}{\mathrm{d}\xi}\right). \end{aligned}$$

Letting $\alpha = 1/c$, we get

$$\xi^2\frac{\mathrm{d}^2F(\xi)}{\mathrm{d}\xi^2} + \xi\frac{\mathrm{d}F(\xi)}{\mathrm{d}\xi} - \left(\xi^2 - \alpha^2\right)F(\xi) = 0, \tag{3.7}$$

which is essentially Bessel's differential equation. Hence, two linearly independent solutions can be taken as Hankel functions, i.e., $F_1(\xi) = H_\alpha^{(1)}(\xi)$ and $F_2(\xi) = H_\alpha^{(2)}(\xi)$.

[1]Set of continuous twice differentiable functions over complex space.

Therefore, after changing back the variables, solutions to Eq. (3.5) become

$$\begin{aligned} y_1(z) &= \sqrt{z}F_1(z) = \sqrt{z}H^{(1)}_{1/c}\left(\frac{2b}{c}z^{c/2}\right), \\ y_2(z) &= \sqrt{z}F_2(z) = \sqrt{z}H^{(2)}_{1/c}\left(\frac{2b}{c}z^{c/2}\right). \end{aligned}$$

It can be shown that solutions $y_1(z)$ and $y_2(z)$ have the asymptotic forms, for fixed c and $|z| \to +\infty$,

$$\begin{aligned} y_1(z) &\sim z^{(c-2)/4}\mathrm{e}^{\gamma}, \quad \text{for} -\pi < \arg(bz^{c/2}) < 2\pi, \\ y_2(z) &\sim z^{(c-2)/4}\mathrm{e}^{-\gamma}, \quad \text{for} -2\pi < \arg(bz^{c/2}) < \pi, \end{aligned}$$

where

$$\gamma = i\frac{2b}{c}z^{c/2}.$$

Observe that Eq. (3.4) is identical to Eq. (3.5) with the substitutions

$$b = i\sqrt{\frac{2}{r_0^N}} \quad \text{and} \quad c = N + 2.$$

Hence, for the two linearly independent solutions we get the following asymptotic forms

$$\begin{aligned} P_1(r) &\sim r^{-N/4}\exp\left(-\frac{2\sqrt{2}}{(N+2)r_0^{N/2}}r^{\left(\frac{N+2}{2}\right)}\right) \\ P_2(r) &\sim r^{-N/4}\exp\left(\frac{2\sqrt{2}}{(N+2)r_0^{N/2}}r^{\left(\frac{N+2}{2}\right)}\right) \end{aligned} \tag{3.8}$$

It is evident that $P_2(r)$ is not normalisable and thus cannot represent a physical state. Thus, we conclude that the asymptotic form of the wave functions is given by $P_1(r)$. An example behaviour is presented in Figure 3.2 for $r_0 = 10$ and $N = 10$.

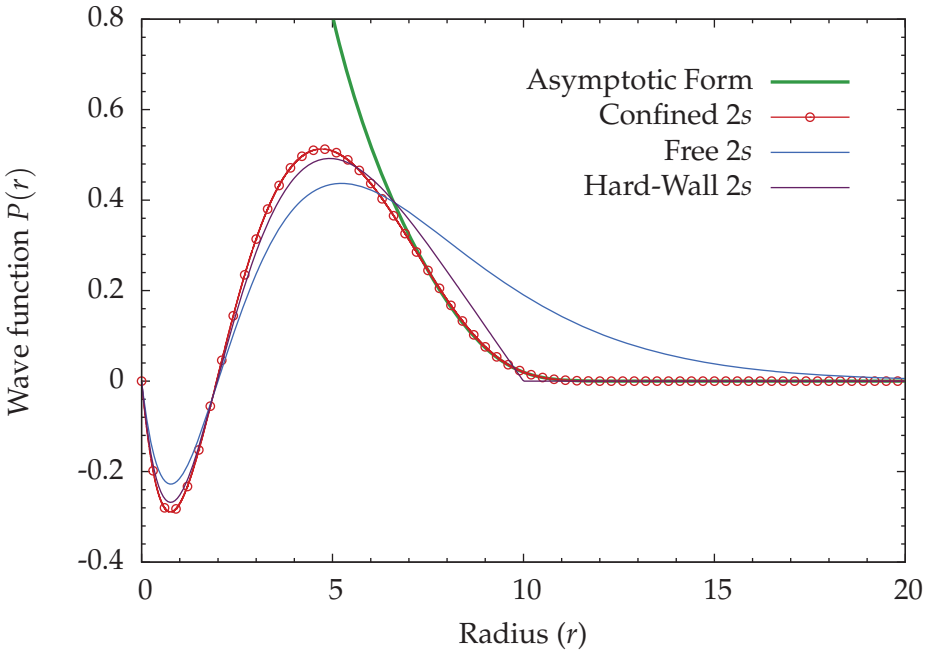

Figure 3.2: 2s normalized wave functions for the system given in Eq. (3.2) with $r_0 = 10, N = 10$, hard–wall problem and free hydrogen atom together with the asymptotic form defined in (3.8).

3.3 Energy Shifts and Long Range Behaviour

In this section, we present results we calculated using Numerov's numerical method[2]. We implemented this method in a C++ software package. The software solution accepts the radius r_0, stiffness N, angular momentum number l and step size to determine the equidistant mesh that the problem will be solved. The core of this software package is the following piece of code

```
1 // Integrate the wave function using Numerov algorithm from left to ↩
    right.
2    m_phi_left[0] = 0;
3    m_phi_left[1] = 1e-15;
4    x = m_grid.xmin;
5    for (size_t i = 1; i <= i_match; i++)
6    {
7       x += m_grid.stepsize;
```

[2]See Appendix C.

```
8         m_phi_left[i+1]  = 2*(1-5*m_c*q(x))*m_phi_left[i];
9         m_phi_left[i+1] -= (1+m_c*q(x-m_grid.stepsize))*m_phi_left[i↩
              -1];
10        m_phi_left[i+1] /= 1+m_c*q(x+m_grid.stepsize);
11    }
12 //Integrate the wave function using Numerov algorithm from right to ↩
      left.
13    m_phi[m_grid.npoints]   = m_phi_right[m_grid.npoints]   = 0;
14    m_phi[m_grid.npoints-1] = m_phi_right[m_grid.npoints-1] = 1e-15;
15    x = m_grid.xmax;
16    for (size_t i = m_grid.npoints-1; i >= i_match; i--)
17    {
18       x -= m_grid.stepsize;
19        m_phi_right[i-1]  = 2*(1-5*m_c*q(x))*m_phi_right[i];
20        m_phi_right[i-1] -= (1+m_c*q(x+m_grid.stepsize))*m_phi_right[i↩
              +1];
21        m_phi[i-1] = m_phi_right[i-1] /= 1+m_c*q(x-m_grid.stepsize);
22    }
```

In short, the code starts the integration from the left boundary (in this case, 10^{-15}) until a pre-defined middle point on the mesh. Then, the same steps happen, but this time from right (the upper integration limit r_{int}) to left. The final step is to find the right matching point to get the complete wave function. In all computations, the step size has been fixed to $\delta r = 0.0001$ whereas the upper integration limit r_{int} has been varied depending on the value of the stiffness parameter. For increasing values of the stiffness parameter N the integration limit has been chosen closer to the confinement radius to avoid numerical instabilities. However, the integration limit has always been kept as large as possible ensuring that the error due to the integration limit is below the numerical accuracy of the method. For instance, for $r_0 = 0.5$ and $N = 5$ the integration limit $r_{\text{int}} = 2$ has been used, while for the same r_0, but N set to 1000, r_{int} has been decreased to 0.51. The results of our calculations are tabulated in Table 3.1 for $n = 1, l = 0$, Table 3.2 for $n = 2, l = 0$, and Table 3.3 for

Table 3.1: Ground state ($n = 1, l = 0$) energy shifts for varying radius values (r_0) and stiffness levels (N).

r_0	$N = 5$	$N = 30$	$N = 50$
0.5	3.862150306076	9.058390885167	10.479866440185
1.0	0.694052667756	1.383461690209	1.614084965380
2.0	−0.244837765152	−0.251289556336	−0.226653788369
3.0	−0.415342574415	−0.450479039698	−0.446462623112
4.0	−0.466149676415	−0.489341519991	−0.488732802799
5.0	−0.484855504835	−0.497740692361	−0.497690793727
8.0	−0.497889269756	−0.499982273061	−0.499984876531
10.0	−0.499255323224	−0.499999348165	−0.499999536920
14.0	−0.499855442874	−0.499999995745	−0.499999996274
r_0	$N = 300$	$N = 1000$	Hard–wall [5]
0.5	13.539524714671	14.293086849057	14.747970030350
1.0	2.146405082002	2.286235411496	2.373990866104
2.0	−0.158521283378	−0.138374191414	−0.125000000000
3.0	−0.432092870340	−0.427302211145	−0.423967287733
4.0	−0.485428322534	−0.484176976365	−0.483265302078
5.0	−0.496968695434	−0.496655598825	−0.496417006591
8.0	−0.499980613771	−0.499977653234	−0.499975100446
10.0	−0.499999448966	−0.499999350945	−0.499999263282
14.0	−0.499999996284	−0.499999996214	−0.499999999498

$n = 2, l = 1$ using nine different confinement radii r_0 and five different values of the stiffness parameter N. It is evident that for any given radius r_0 and increasing stiffness the energy eigenvalues approach the hard–wall energy eigenvalues, as reported, for example, by Aquino et al. [5].

At this point, it is elucidating to analyse the qualitative behaviour of the energy eigenvalues obtained from Numerov's method with respect to the respective hard–wall results for $N \to +\infty$. Therefore, we consider the energy difference

$$\Delta E(r_0, N) = E^s(r_0, N) - E^h(r_0), \tag{3.9}$$

where $E^s(r_0, N)$ is the energy eigenvalue from Numerov's method and $E^h(r_0)$ is the hard–wall energy eigenvalue [5].

Table 3.2: First excited state ($n = 2, l = 0$) energy shifts for varying radius values (r_0) and stiffness levels (N).

r_0	$N = 5$	$N = 30$	$N = 50$
0.5	19.081311562900	47.248837213895	53.765374886926
1.0	6.363958408886	11.581674204770	12.791876509133
2.0	1.910634800501	2.464913655457	2.647016756909
3.0	0.847574257571	0.835884821562	0.883875441697
4.0	0.426951076767	0.309006748521	0.323381261381
5.0	0.219292645822	0.091387693502	0.095069109821
8.0	−0.012580730518	−0.090086502529	−0.091310109820
10.0	−0.063787158449	−0.113849449965	−0.114709479537
14.0	−0.103344941473	−0.123941920638	−0.124140687287
r_0	$N = 300$	$N = 1000$	Hard–wall [5]
0.5	67.365819074030	70.677109607095	72.672039190464
1.0	15.454803449636	16.141184546404	16.570256093470
2.0	3.109005276112	3.240817746926	3.327509156496
3.0	1.032741191614	1.079614183499	1.111684737436
4.0	0.384082266202	0.405245436393	0.420235631714
5.0	0.122680181591	0.133408514493	0.141254203802
8.0	−0.088080812790	−0.086221216598	−0.084738721357
10.0	−0.113963494421	−0.113335010950	−0.112806210296
14.0	−0.124138461355	−0.124074762348	−0.124015029432

We find that the convergence behaviour of the energy difference follows the general functional form

$$\Delta E(r_0, N) \propto \frac{1}{r_0^{\alpha}} \frac{1}{N^{\beta}} \tag{3.10}$$

with $\alpha \approx 2.4$ and $\beta = 0.7$ obtained from a least–squares fit. The convergence behaviour as function of N is displayed in Figure 3.3 for $r_0 = 0.5$ and $r_0 = 1.0$, in Figure 3.4 for $r_0 = r_c^h$ and $r_0 = 2.0$, and in Figure 3.5 for $r_0 = 4.0$ and $r_0 = 5.0$. The figures show that the functional form (3.10) describes the behaviour of the energy differences for large values of N. When N decreases, deviations from the functional form can be observed. The magnitude of the deviations depends on the value of r_0. It becomes smaller for increasing values of r_0. This is easily explained by the fact that for increasing r_0 the confined system converges toward the unconfined system. As a special case, the numerical data for r_0 set to the critical cage radius r_c^h of the spherical box potential has been included (Figure 3.4). The data shows that

Table 3.3: $2p$ state ($n = 2, l = 1$) energy shifts for varying radius values (r_0) and stiffness levels (N).

r_0	$N = 5$	$N = 30$	$N = 50$
0.5	10.881917060199	23.833244509487	27.081706613102
1.0	3.556904137902	5.729302237628	6.324352218426
2.0	1.017532412927	1.152223746319	1.239465370251
3.0	0.418888344006	0.347631573500	0.370076121239
4.0	0.183908145730	0.089949989790	0.096522557215
5.0	0.068320873183	−0.016553332973	−0.014944877584
8.0	−0.061078871637	−0.107149670551	−0.107802732573
10.0	−0.090018946132	−0.119385397810	−0.119835235752
14.0	−0.112629000239	−0.124504265011	−0.124600796241
r_0	$N = 300$	$N = 1000$	Hard–wall [5]
0.5	33.963594670996	35.645418668188	36.658875880189
1.0	7.660654824846	8.006727993178	8.223138316161
2.0	1.467509316719	1.532954379650	1.576018785606
3.0	0.442571280031	0.465532478686	0.481250312527
4.0	0.125926758666	0.136228890316	0.143527083714
5.0	−0.001488519821	0.003758466275	0.007593920467
8.0	−0.106157919012	−0.105207335931	−0.104450066406
10.0	−0.119454360245	−0.119131403612	−0.118859544854
14.0	−0.124599927373	−0.124569344766	−0.124540597990

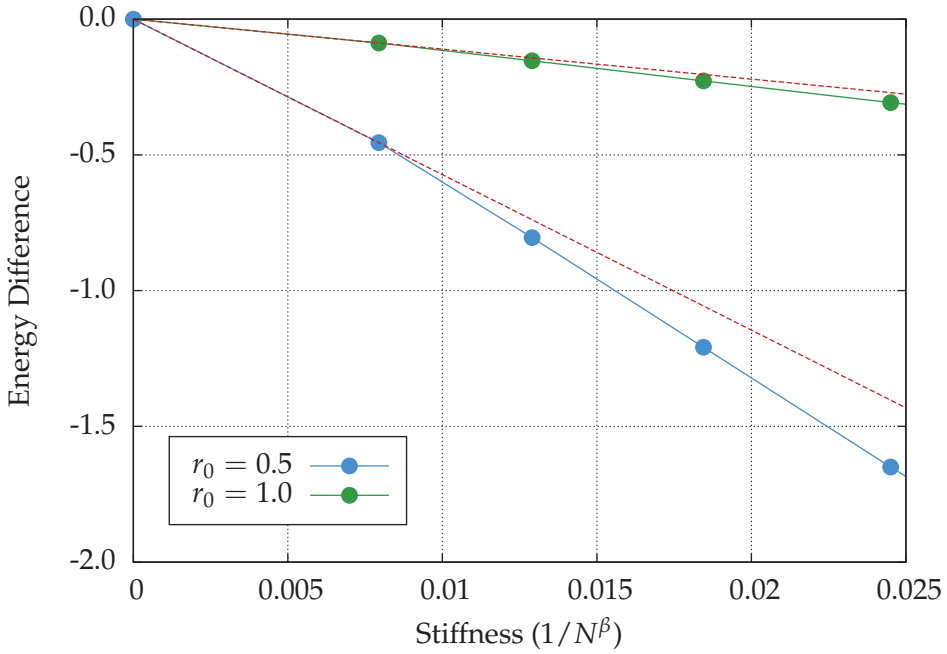

Figure 3.3: Long range behaviour for ground state energy differences ΔE, with respect to hard–wall results [5], for radii $r_0 = 0.5$ and $r_0 = 1.0$ with $\beta = 0.7$. Dashed red lines represent the functional form given in Eq. 3.10

the energy eigenvalues for $r_0 = r_c^h$ are below zero for all N. Thus, the critical cage radius of the confining potential in Eq. (3.1) is found at a smaller radius compared to the spherical box potential.

It is easily observed from Eq. (3.10) that $\Delta E(r_0, N) \to 0$ as either r_0 or N approaches infinity, and this behaviour is already confirmed with the numerical data presented in Tables 3.1, 3.3 and 3.2. Secondly, the convergence to the hard–wall results is greatly reduced as $r_0 \to 0$, see Figure 3.3, 3.4 and 3.5. In contrast, for radii $r_0 \geq 4$, $\Delta E(r_0, N)$ is close to zero for $n = 1, l = 0$.

The presence of a potential defined in Eq. (3.1) can significantly change the energy eigenvalues and the eigenfunctions. To illustrate the changes, the $2s$ wave function of the confined system with $r_0 = 10.0$ a.u. and $N = 10$ is depicted in Figure 3.2 together with the respective functions of the unconfined system and the system confined by the hard–wall potential. It can be observed that the confining potential forces the wave functions to approach zero more rapidly for $r \to +\infty$, as expected also from the asymptotic behaviour, while the radial node of the wave function

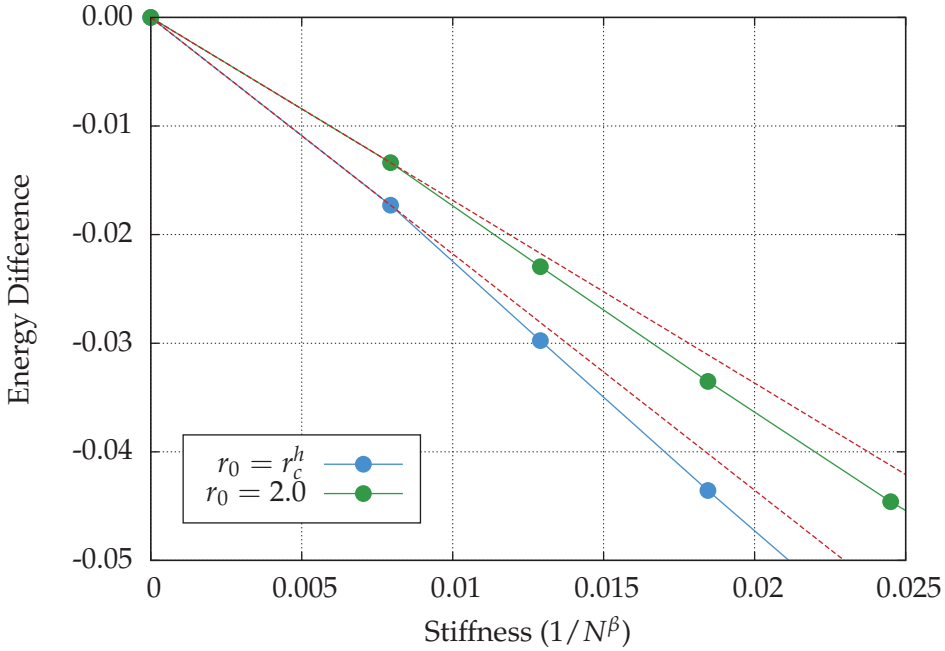

Figure 3.4: Long range behaviour for ground state energy differences ΔE, with respect to hard–wall results [5], for radii $r_c^h = 1.835246330$ and $r_0 = 2.0$ with $\beta = 0.7$, where r_c^h [14] is the critical cage radius for hard–wall. Dashed red lines represent the functional form given in Eq. 3.10

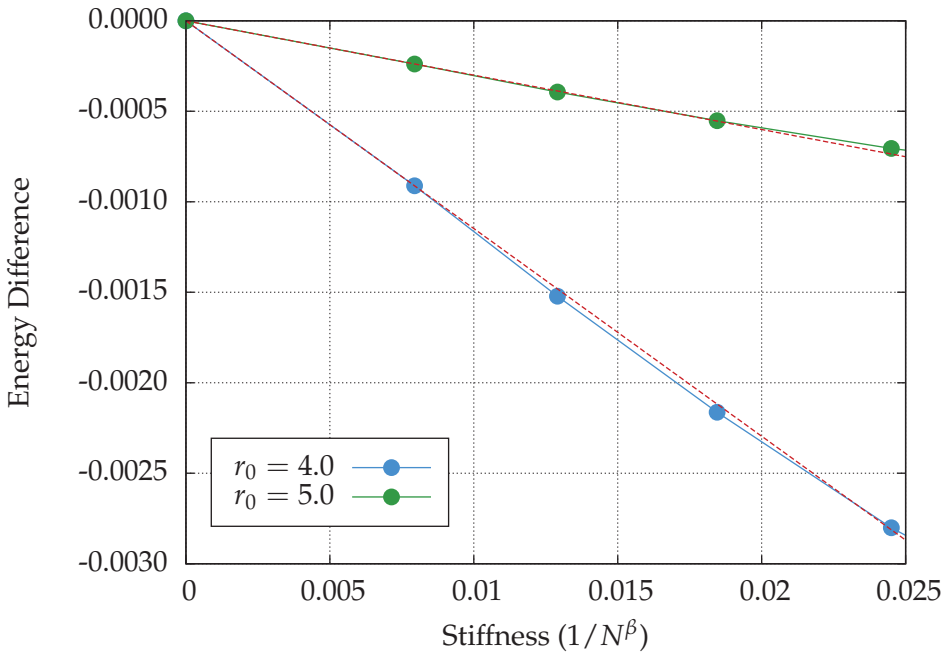

Figure 3.5: Long range behaviour for ground state energy differences ΔE, with respect to hard–wall results [5], for radii $r_0 = 4.0$ and $r_0 = 5.0$ with $\beta = 0.7$. Dashed red lines represent the functional form given in Eq. 3.10

remains mostly unchanged as it is not in too close proximity to the confinement radius. Of course, for smaller confinement radii or for higher angular momentum functions the position of the nodes critically depends on the confinement radius. The shape of the numerical wave functions agrees for $r \to +\infty$ with the asymptotic form of Eq. (3.8). As expected, the wave functions converge for increasing N to the solutions of the hard–wall problem but the convergence is rather slow as can be seen from the small β value of 0.7 in Eq. (3.10). In addition, when r_0 is increased, the eigenfunctions of the system converge toward the wave functions of the free hydrogen atom. This convergence is much faster due to α values of 2.4 shown in Eq. (3.10).

3.4 Radial Expectation Values

In the previous section, we have studied the numerically obtained energy eigenvalues and eigenfunctions of the hydrogen atom confined by the potential $V_s(r)$ with respect to the variation of the parameters r_0 and N. The eigenfunctions can also be used to determine observable properties of the system, like polarisabilities or diamagnetic screening constants, by computing the expectation values of certain operators. Thus, it is interesting to examine the behaviour of the radial expectation values of the confined hydrogen atom for varying N and r_0. We consider only radial expectation values, since the angular part of the eigenfunctions is independent of those parameters. The expectation value of a radial function $f(r)$ with respect to an eigenfunction of the confined hydrogen atom can be calculated using the normalized radial function $P(r)$ introduced in Eq. (1.8) via

$$\begin{aligned} \langle f(r) \rangle &= \int_0^{+\infty} P^*(r) f(r) P(r) \mathrm{d}r \\ &\approx \sum_i^{r_{\mathrm{int}}} P^*(r_i) f(r_i) P(r_i) \, (\Delta r)^2 \end{aligned} \tag{3.11}$$

where Δr is the step size of the grid and r_{int} is the numerical integration limit employed in Numerov's algorithm. For the $1s$, $2s$, and $2p$ eigenstates of the confined hydrogen atom and varying values of N and r_0 the expectation values $\langle r^{-1} \rangle$, $\langle r \rangle$, and $\langle r^2 \rangle$ are given in Tables 3.4, 3.5 and 3.6, respectively. For comparison, the expectation values for the hard–wall potential are displayed as well. A careful inspection of the data reveals that, as N increases, the expectation values of the system in Eq. (3.2) approach those of the system confined by the hard–wall potential. Moreover, as the confinement radius r_0 increases we approach the expectation values of the free hydrogen atom, see [15]. This situation can also be observed in Figures 3.6, 3.7 and 3.8 in which the relative expectation value differences (defined similarly to Eq.(3.9)) with respect to the expectation values of the system confined by the hard–wall potential are displayed as function of $1/N^{0.7}$. Interestingly, the curves for the expectation value $\langle r^{-1} \rangle$ in Figure 3.6 approach the limit of the hard–wall results from below, while those for the expectation values $\langle r \rangle$ and $\langle r^2 \rangle$ in Figures 3.7 and 3.8 approach it from above. This behaviour is due to opposite trends in the wave functions of the confined hydrogen atom for increasing N. On one hand, the increase in N restricts the extend of the wave functions beyond r_0, and thus the expectation values $\langle r \rangle$ and $\langle r^2 \rangle$ become smaller. At the same time, the change in the slope of the potential for $r < r_0$ shifts the wave functions away from the origin and towards r_0 resulting an increase in the expectation value $\langle r^{-1} \rangle$.

3.5 Physical Properties

Since the work of Michels at al. [47], it was recognized that it is essential to calculate physical properties associated with ground state energies and wave functions. For the confined hydrogen atom, nuclear magnetic shielding [4, 41] given by

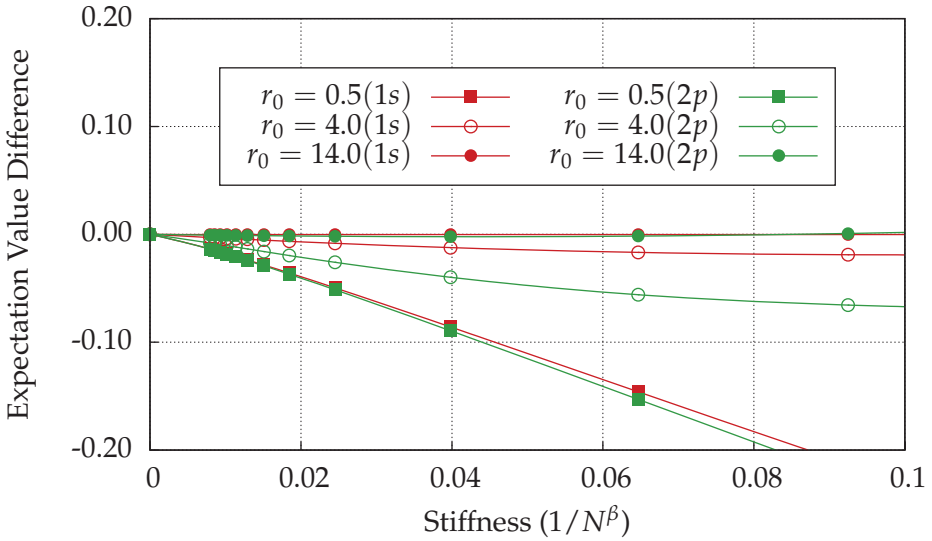

Figure 3.6: Behaviour of relative expectation value $\langle r^{-1} \rangle$ differences, with respect to hard–wall expectation values [47], for radii $r_0 = 0.5, r_0 = 4.0$ and $r_0 = 14.0$ for $1s$ and $2p$ with $\beta = 0.7$.

the diamagnetic screening constant, dipole polarisability[3] in the Kirkwood [34] approximation and pressure [4, 41, 65] are some of the most important ones. Diamagnetic screening constant is given by

$$\sigma_d = \frac{\left\langle r^{-1} \right\rangle}{3\mu_0 c^2}, \tag{3.12}$$

where μ_0 is the magnetic constant (permeability of the vacuum), and c is the speed of light. The observed NMR resonance frequencies for the various nuclei are usually given as chemical shifts, δ, in parts per million with respect to a reference. Chemical shifts arise because the magnetic field, B, experienced by a specific nucleus differs from the applied field, B_0, as shown in $B = B_0 (1 - \sigma_t)$, where σ_t is the total screening constant. The screening constant, σ, is a scalar quantity that is the trace of second–rank tensor as identified by

$$\sigma = \frac{1}{3}\left(\sigma_{xx} + \sigma_{yy} + \sigma_{zz}\right).$$

[3]One should note that dipole polarisabilities calculated in the Kirkwood approximation are not exact dipole polarisability values. We take a detail study of the dipole polarisability in Chapter 4.

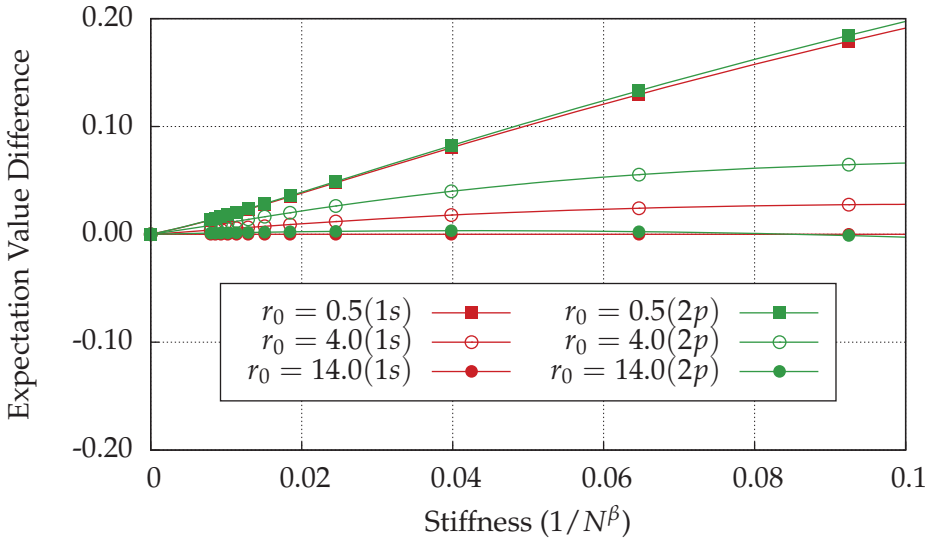

Figure 3.7: Behaviour of relative expectation value $\langle r \rangle$ differences, with respect to hard–wall expectation values [47], for radii $r_0 = 0.5, r_0 = 4.0$ and $r_0 = 14.0$ for $1s$ and $2p$ with $\beta = 0.7$.

In high–resolution NMR solution experiment, one normally measures the average screening, σ, due to rapid molecular tumbling in solution. The total screening constant, σ_t, consists of two components, a diamagnetic screening constant, σ_d, and a parametric screening constant, σ_p such that

$$\sigma_t = \sigma_d + \sigma_p.$$

The diamagnetic contribution to the screening constant, σ_d, involves rotation of electrons around the nucleus and is important for ^1H NMR.

Polarisability in the Kirkwood approximation is given by

$$\alpha_K = \frac{4}{9} \left\langle r^2 \right\rangle^2, \tag{3.13}$$

and pressure is calculated by

$$P = -\frac{1}{4\pi r_0^2} \left. \frac{\mathrm{d}E}{\mathrm{d}r} \right|_{r=r_0}. \tag{3.14}$$

Since we already investigated radial expectation values in Section 3.4, it is trivial

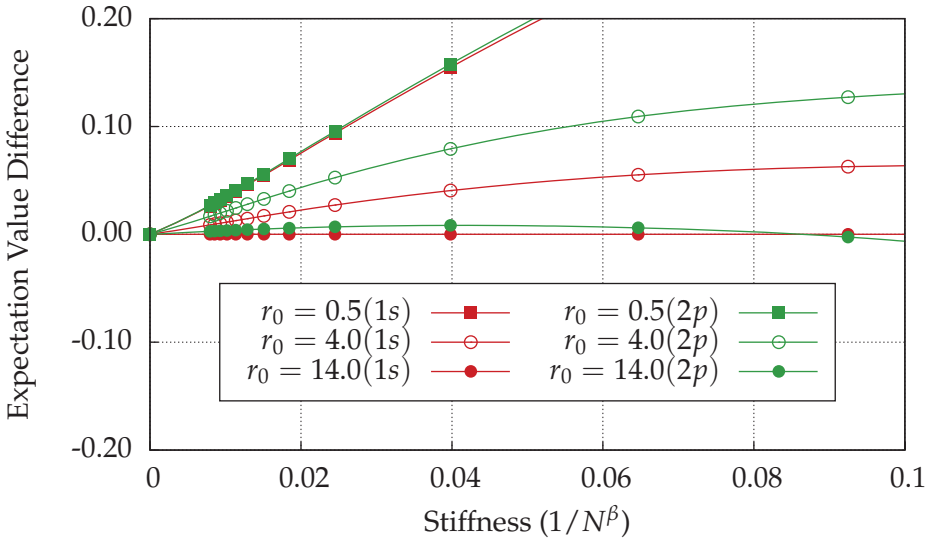

Figure 3.8: Behaviour of relative expectation value $\langle r^2 \rangle$ differences, with respect to hard–wall expectation values [47], for radii $r_0 = 0.5, r_0 = 4.0$ and $r_0 = 14.0$ for $1s$ and $2p$ with $\beta = 0.7$.

to calculate these values for the soft–wall confined hydrogen atom. It is worthy to note that the purpose of this section is to illustrate the fact that these quantities can be calculated with ease. Table 3.7 presents the polarisabilities of a soft-wall confined hydrogen atom in the Kirkwood approximation. Nuclear magnetic shielding values for various radii and stiffness levels are given in Table 3.8. And, finally, Table 3.9 depicts the pressure changes for a soft–wall confined hydrogen atom. It is not surprising to observe that the numerical values tend monotonically towards the values of free hydrogen atom.

Table 3.4: $\langle r^{-1} \rangle$ for $1s, 2s$ and $2p$ states.

r_0/N	5	30	50	300	1000	Hard-wall [5]
			$1s$			
0.5	2.997101666084	4.217423405091	4.462563154917	4.937280565039	5.045811429883	5.114044005817
1.0	1.969874326624	2.345927749952	2.435595581457	2.623535259164	2.669626213516	2.699145601709
2.0	1.381647048912	1.416280069860	1.441631962305	1.505553008033	1.523253024984	1.535161706433
3.0	1.182740123127	1.146253934721	1.154550571194	1.181562454782	1.190019267697	1.196038911029
4.0	1.093844145888	1.048335862740	1.050549420881	1.061313673136	1.065164928339	1.068128869980
5.0	1.050040513762	1.014184933809	1.014502635679	1.018129162730	1.019627307623	1.020951410022
8.0	1.009010631004	1.000014009140	1.000030082520	1.000035190754	1.000067357867	1.000294519368
10.0	1.003287091651	1.000013462428	1.000012809037	1.000011180125	1.000010648481	1.000011692821
$+\infty$						1.000000000000
			$2s$			
0.5	3.006937224210	5.157300351809	5.492626061296	6.109931858202	6.249254944169	6.339617044443
1.0	1.876041931468	2.740794052960	2.869639252667	3.120464614330	3.180855823720	3.220106088679
2.0	1.176181001324	1.461710874003	1.505611778302	1.602842821187	1.628847481405	1.646270138977
3.0	0.891121367424	0.998208312842	1.019067606325	1.074286751050	1.090572192052	1.101807847166
4.0	0.726587650498	0.744261537377	0.754696530818	0.791091444630	0.803001371213	0.811449809228
5.0	0.616660846404	0.581851678467	0.586245172832	0.611020019384	0.620118031511	0.626761896507
8.0	0.434238989247	0.351590493757	0.349458773521	0.356010291597	0.359629228422	0.362517019168
10.0	0.372316448058	0.295532807471	0.293135830712	0.295427460237	0.297274517872	0.298837430642
$+\infty$						0.250000000000
			$2p$			
0.5	2.021143946975	3.057104385556	3.247150068500	3.610590421187	3.693405511259	3.743969324235
1.0	1.255592705961	1.618680345589	1.690071606975	1.836541044986	1.872240403911	1.894589973231
2.0	0.791287319051	0.870073483621	0.892897689385	0.947670712342	0.962581867283	0.972343283603
3.0	0.611022131589	0.614019354041	0.623851260423	0.652787090426	0.661513469760	0.667442484298
4.0	0.512789054433	0.485421007694	0.489818293206	0.507290351596	0.513131993885	0.517234054760
5.0	0.450509213842	0.409129222488	0.410783153622	0.422014309432	0.426199612595	0.429229629938
8.0	0.352307744374	0.302241167301	0.301110316353	0.304306479531	0.306076341165	0.307472580370
10.0	0.319153684449	0.273696168660	0.272403218487	0.273594870010	0.274561930084	0.275370901669
$+\infty$						0.250000000000

Table 3.5: $\langle r \rangle$ for $1s, 2s$ and $2p$ states.

r_0/N	5	30	50	300	1000	Hard-wall [5]
			$1s$			
0.5	0.426727031602	0.295328195770	0.278624800961	0.251249548520	0.245737668220	0.242490864909
1.0	0.663735590809	0.542790845313	0.521555948904	0.482332852819	0.473619738273	0.468317654189
2.0	0.982375081099	0.942115428955	0.922839946454	0.878282996070	0.866765299696	0.859353174267
3.0	1.182808475343	1.217895234029	1.206253718713	1.170873265520	1.160341627190	1.153206302642
4.0	1.308773513053	1.379635342844	1.375018487752	1.354079380901	1.346869193515	1.341709680766
5.0	1.385941965246	1.456784165208	1.455855404303	1.446581184510	1.442865016052	1.440025713179
8.0	1.475146752176	1.499140730169	1.499246771270	1.499043491463	1.498909998576	1.498697359886
10.0	1.490171263895	1.500045150873	1.500058321991	1.500050976497	1.500043342927	1.499936378772
$+\infty$						1.500000000000
			$2s$			
0.5	0.544896607212	0.309624486976	0.290016535978	0.259979915765	0.254058476171	0.250584160442
1.0	0.890145010630	0.595896184054	0.567525707556	0.519818854967	0.509536459409	0.503320800950
2.0	1.454891280644	1.161059098846	1.124383296614	1.051313770433	1.033363169195	1.021978923588
3.0	1.940801343169	1.739942730490	1.702404452911	1.610663339428	1.585362020290	1.568684837349
4.0	2.378631855562	2.334859655329	2.303165282251	2.200041254701	2.168060902743	2.146227032148
5.0	2.777033278332	2.923589773432	2.903402140946	2.799183460244	2.762636201186	2.736823894320
8.0	3.757432696954	4.402094840676	4.421728697111	4.356328813901	4.321543874933	4.294622827259
10.0	4.252743364268	5.075604703566	5.109939497273	5.075102983680	5.047976910225	5.025764746350
$+\infty$						6.000000000000
			$2p$			
0.5	0.552805723607	0.359718451953	0.338448774427	0.304219296025	0.297375415177	0.293372329060
1.0	0.893359566074	0.681866461055	0.652578840374	0.600075368233	0.588554320309	0.581592021699
2.0	1.427316222333	1.278219887686	1.244494197209	1.171229771950	1.152800391877	1.141079082073
3.0	1.860137083071	1.826176301792	1.795867174167	1.713785737299	1.690560736704	1.675175170130
4.0	2.229958645873	2.330569054676	2.307870834054	2.224627056855	2.198230614490	2.180112919952
5.0	2.553234622989	2.791662603136	2.778756035730	2.699778214846	2.671634436332	2.651680860602
8.0	3.320305260430	3.899070710384	3.915142381901	3.867052181355	3.841192731623	3.821144671631
10.0	3.703531776651	4.394302352164	4.419955511347	4.395248429759	4.375707168113	4.359641624918
$+\infty$						5.000000000000

Table 3.6: $\langle r^2 \rangle$ for $1s$, $2s$ and $2p$ states.

r_0/N	5	30	50	300	1000	Hard-wall [5]
			$1s$			
0.5	0.213288238814	0.099857695718	0.088773785793	0.072085535875	0.068940525768	0.067128353709
1.0	0.522940211790	0.341630999882	0.314905227744	0.268692238921	0.258949678150	0.253127838756
2.0	1.173840466856	1.059661581981	1.014555970115	0.915213997301	0.890495190944	0.874825394134
3.0	1.739639302875	1.829728535505	1.791209115401	1.678897977190	1.646447104381	1.624768629063
4.0	2.170627535092	2.422301893794	2.402859581764	2.318589777800	2.290268518627	2.270311332217
5.0	2.471349326550	2.764914350798	2.760044333823	2.715511122924	2.698034322164	2.684971686682
8.0	2.870164759578	2.993316260789	2.994013108247	2.992602857333	2.991693718808	2.990632403134
10.0	2.946516662354	2.999836127552	2.999939610675	2.999878163064	2.999815887372	2.999459508866
$+\infty$						3.000000000000
			$2s$			
0.5	0.373721239472	0.123137515076	0.108034093294	0.086803614184	0.082892891302	0.080654594362
1.0	0.994549822336	0.455716253602	0.413452474439	0.346941726160	0.333368105029	0.325322011605
2.0	2.630768886133	1.713585804471	1.608526548360	1.408671545123	1.361533348530	1.332090458615
3.0	4.619339221279	3.771140498819	3.615206236662	3.247829616088	3.149730637313	3.085882627579
4.0	6.838062605902	6.608497181291	6.437913482526	5.902390830856	5.740753465054	5.631603212642
5.0	9.191186728987	10.084421418603	9.950180385881	9.289692161113	9.063590788983	8.905502665899
8.0	16.334647820623	21.926804004823	22.109608761444	21.472595502116	21.140067955508	20.884945066449
10.0	20.729390634042	29.116085364427	29.510997160460	29.097683846923	28.781351828043	28.524320123988
$+\infty$						42.00000000000
			$2p$			
0.5	0.333101494313	0.138897815255	0.122881475258	0.099239575217	0.094819854150	0.092285829550
1.0	0.872309437217	0.500303785647	0.457931945401	0.386980154538	0.372229519676	0.363464365379
2.0	2.237411263226	1.767164610338	1.673862014029	1.481316715634	1.434824200640	1.405665140785
3.0	3.817155965619	3.627325808475	3.505205440908	3.188698962427	3.102080307763	3.045404821779
4.0	5.509718828732	5.944322441588	5.824878901388	5.405466069531	5.276154508597	5.188390046474
5.0	7.253938156064	8.587028918395	8.502616828543	8.014892063591	7.845237297725	7.726190758434
8.0	12.422744033871	17.153042427050	17.297164494257	16.849332226547	16.612606868807	16.430636936153
10.0	15.582401614048	22.168839033206	22.447758759912	22.171301315012	21.956137890750	21.780647272389
$+\infty$						30.00000000000

Table 3.7: Polarisabilities in the Kirkwood [34] approximation α_K $\left[10^{-24}\mathrm{cm}^3\right]$ for a soft–wall confined hydrogen atom.

r_0	$N = 5$	$N = 30$	$N = 50$	$N = 300$	$N = 1000$
0.5	0.002996	0.000657	0.000519	0.000342	0.000313
1.0	0.018010	0.007687	0.006531	0.004755	0.004416
2.0	0.090748	0.073953	0.067791	0.055165	0.052226
3.0	0.199315	0.220493	0.211307	0.185639	0.178532
4.0	0.310307	0.386436	0.380257	0.354053	0.345457
5.0	0.402244	0.503482	0.501710	0.485651	0.479420
8.0	0.542543	0.590101	0.590375	0.589819	0.589461
10.0	0.571793	0.592674	0.592715	0.592691	0.592666
$+\infty$					0.592739

Table 3.8: Nuclear magnetic shielding σ_d $[e^2/3\mu c^2]$ for a soft–wall confined hydrogen atom.

r_0	$N = 5$	$N = 30$	$N = 50$	$N = 300$	$N = 1000$
0.5	2.997102	4.217423	4.462563	4.937281	5.045811
1.0	1.969874	2.345928	2.435596	2.623535	2.669626
2.0	1.381647	1.416280	1.441632	1.505553	1.523253
3.0	1.182740	1.146254	1.154551	1.181562	1.190019
4.0	1.093844	1.048336	1.050549	1.061314	1.065165
5.0	1.050041	1.014185	1.014503	1.018129	1.019627
8.0	1.009011	1.000014	1.000024	1.000035	1.000067
10.0	1.003287	1.000003	1.000003	1.000005	1.000005
$+\infty$					1.000000

Table 3.9: Pressure P [atm] changes for a soft–wall confined hydrogen atom.

r_0	$N = 5$	$N = 30$	$N = 50$	$N = 300$	$N = 1000$
0.5	4.87471864	13.32735727	15.55897040	20.24330335	21.36385852
1.0	0.19088209	0.38144374	0.43337617	0.54673756	0.57515324
2.0	0.00633954	0.00852321	0.00945549	0.01174679	0.01237727
3.0	0.00074167	0.00067841	0.00074207	0.00092990	0.00098728
4.0	0.00014367	0.00008144	0.00008763	0.00011199	0.00012039
5.0	0.00003663	0.00001129	0.00001182	0.00001543	0.00001685
8.0	0.00000149	0.00000004	0.00000003	0.00000004	0.00000005
10.0	0.00000028	0.00000000	0.00000000	0.00000000	0.00000000
$+\infty$					0.00000000

Chapter 4

The Even–Tempered Basis Sets

Advances in the capacities and capabilities of computers have had an enormous impact on theoretical calculations supporting experimental work in the last two decades. *Ab–initio* electronic–structure methods implemented in many software packages are the default standard to explain, or predict molecular properties. The quality of these properties however depends on the chosen model and quality of data and/or the parameters supplied to the software. The parameters in *ab–initio* calculations are those defining the functions of the basis set required for expanding the atomic or molecular orbitals, or electron density. In order to achieve an acceptable accuracy, a careful choice of these parameters is very important. In practice, popular software packages for *ab–initio* quantum chemical calculations contain internally defined basis sets from which the user must select an appropriate set. However, sometimes, one needs custom fitted basis sets designed particularly for the system at hand.

The first step in any *ab–initio* theoretical calculation of atoms, or molecules is the determination of atomic and molecular wave functions, which are usually built up from a set of one–electron functions centred at the origin of an atom. The major requirement is that the set has a size that the functions are either a good representation, or, able to adjust to be a good representation of the exact solution, at least in the most significant regions for the property considered. A

series of calculations with improving basis sets is usually applied to one atom or molecule until certain convergence criteria are reached. The error in the calculation is estimated from the sensitivity of the results to further refinements in the basis sets. The existence of vast multitude of basis sets is attributable to the fact that finding an ideal set of functions is very difficult.

The truncation of the finite basis set is an important source of error in molecular electronic structure calculations. Therefore, recent research follows a more systematic approach to producing basis sets for electronic structure calculations. As the available basis sets increase in size, choice of the right set that has the desired accuracy and efficiency in terms of computation time needs to be done carefully.

The computer time required for *ab–initio* calculations depends on the number of basis functions in the set. Particularly, the time needed for the integral evaluation scales up the fourth power of number of functions. Therefore, there is great interest in finding small basis sets that provide results close to the exact solution.

In this chapter, first, we give a brief introduction to basis set theory together with orbital approximation. Secondly, we present a basis set study on soft–wall confined hydrogen atom. Numerical method introduced in the Chapter 3 is only capable of calculating total energy shifts of a soft–wall confined hydrogen atom. In order to calculate physical properties of soft–wall hydrogen atom, as well as similar calculations for multi–electron systems, it is necessary to use a quantum chemistry software package, such as Gaussian 09, where basis sets are utilized to approximate the wave function and hence calculate approximate physical properties. Current publicly available basis sets designed for free hydrogen atom are not adequate to study physical properties of a soft–wall confined hydrogen atom, let alone multi–electron systems. It is natural to expect that such basis sets would result in accurate enough wave function approximations of a soft–wall confined hydrogen atom with sufficiently large confinement radii r_0 where stiffness level N is arbitrary.

However, it would be naïve to think that the same basis set would successfully approximate a wave function when the radius r_0 approaches zero and permeability of the walls decreases greatly. Therefore, we see it fit to energy optimise a basis set for a soft–wall confined hydrogen atom which would give the most accurate approximation for all radii and stiffness values. As a result, we will have a basis set that can be used to calculate physical properties of soft–wall confined systems with high accuracy.

4.1 Orbital Approximation

In the Born–Oppenheimer approximation, for a system with n electrons and m nuclei, the non–relativistic time–independent electronic Schrödinger equation is

$$\left\{\sum_{i=1}^{n}\left(-\frac{1}{2}\nabla_i^2-\sum_{\alpha=1}^{m}\frac{Z_{i\alpha}}{r_{i\alpha}}\right)+\sum_{i<j}^{n}\frac{1}{r_{ij}}+\sum_{\alpha<\beta}^{m}\frac{Z_\alpha Z_\beta}{R_{\alpha\beta}}\right\}\Psi=E\Psi, \tag{4.1}$$

where ∇_i^2 is the Laplacian operator of the i-th electron, Z_α the nuclear charge of the α nucleus, $r_{i\alpha}$ the distance between electron i and nucleus α, r_{ij} the distance between electrons i and j, and $R_{\alpha\beta}$ the internuclear distance between nuclei α and β. In *ab initio* methods, the exact electrostatic Hamiltonian of the system is considered, where all the electrostatic interactions between nuclei and electrons are considered at the non–relativistic level.

In Eq. (4.1), the Hamiltonian of a system composed of pointwise positive and negative charges appears such that the finite size of the atomic nuclei is neglected. Even though Eq. (4.1) is a non–relativistic approximation, we have an analytic solution only for simple systems such as hydrogen–like atoms or almost exact solutions for few electron systems.

The first attempt made to resolve this issue is using the independent particle model, or, orbital approximation. It is a simplified model in which the electron–electron repulsion is approximated by one–particle effective potential. Under

this simplification, the electronic wave function can be written as a product of one–electron functions. If this product is anti–symmetrised, as the Pauli principle demands, the resulting simpler wave function for a closed shell system is the Slater determinant,

$$\Psi = \frac{1}{\sqrt{n!}} \left| \phi_1 \alpha(1)\, \phi_1 \beta(2) \cdots \phi_{n/2} \alpha(n-1)\, \phi_{n/2} \beta(n) \right|, \tag{4.2}$$

where $\left\{\phi_i\right\}_{i=1}^{n}$ is the set of one–electron wave functions, or, orbitals. When the variational principle is applied to Eq. (4.1) with the function (4.2) and the orbitals being orthonormalised, the resulting set of differential equations is known as the Hartree–Fock (HF) equations [22, 31, 63]. In the case of a single nucleus, the HF equations can be solved numerically. In 1951, Roothaan [57] and Hall [29, 30] proposed the development of the orbitals as a linear combination of a known basis set. For instance, in a molecule, the molecular orbitals are written as a linear combination of atomic centred orbitals (LCAO). Including such orbitals in the HF equations, a set of algebraic equations is obtained, the so–called Hartree–Fock–Roothaan–Hall equations. They can be solved using standard matrix techniques. If the set in which the orbitals are expanded were a complete basis set, the LCAO approximation would be exact independent of the chosen basis set. Unfortunately, the sets used must be constrained to a limited number of basis functions for practical calculations. This non–completeness of the basis set introduces the so–called basis set truncation error. The expansion of the wave function as a linear combination of basis set functions will effect the accuracy of the Hartree–Fock–Roothaan–Hall equations. Since the basis set is not complete, its choice is a systematic source of error in *ab–initio* molecular calculations.

The electron–correlation energy was first introduced by Löwdin [44] in 1959. This energy was defined as the difference between the exact electronic energy of the physical system and the limit HF energy, and gives a measure for the quality the HF approximation. The first proposed method to evaluate correlation energies was

the configuration interaction (CI) method. The occupied and virtual orbitals are first obtained from HF calculations. With these orbitals, one constructs "excited" Slater determinants, where the Hamiltonian matrix is obtained as expectation values over these determinants. Diagonalising the Hamiltonian matrix recovers part of the correlation energy. This contribution is dependent on the truncations in the poly–electronic basis set (set of orbitals and number of Slater determinants). Of course, a large number of correlation methods have been introduced since. For a review of some of these techniques, see [25], and citations therein.

4.2 Gaussian Basis Sets

In most applications of quantum chemistry, calculations for molecules are performed using linear combinations of atomic orbitals to form molecular orbitals (LCAO–MO). This means that molecular orbitals are expanded in a finite linear combination of atomic orbitals

$$\psi_i = \sum_{j=1}^{n} c_{ji}\phi_j,$$

where ψ_i is the i–th molecular orbital, c_{ji} are the coefficients of the linear combitation, ϕ_j is the j–th atomic orbital, and n is the number of atomic orbitals. Atomic orbitals are solutions of the Hartree–Fock equations for an atom, i.e., a wave function representing a single electron in the multi–electron atom. Slater type orbitals (STOs) were originally used as basis functions due to their similarity to the atomic orbitals of the hydrogen atom. Their general shape has the following form

$$\phi_{nlm}(r,\theta,\phi) = AY_{lm}(\theta,\phi)r^{n-1}\exp\left(-\xi r\right),$$

where A is the normalisation constant, ξ is called the exponent, r,θ,ϕ are spherical coordinates, Y_{lm} are spherical harmonics, and n,l,m are the principal, angular, and

magnetic quantum numbers, respectively.The excellent behaviour shown by the STO functions in the near and far regions of the atomic nucleus is well–known. They satisfy the nuclear cusp condition because of their exponential relationship with the nucleus–electron distance. This fact allows the STO basis sets to reproduce correctly the regions near the nucleus. In addition, they decay properly in the long range.

Unfortunately, the initial and successful work developed for atomic calculations with STO functions was abandoned due to the complexity in the evaluation of two–electron multi–center integrals required in molecular calculations. Hence, exponential functions on r^2 (*Gaussian type orbitals*, or GTOs) became the standard basis employed in molecular electronic structure calculations.

Gaussian basis sets [12, 13] are composed of Gaussian–type orbitals (GTOs) of the form

$$\phi_{nlm}\left(r,\theta,\phi\right) = NY_{lm}\left(\theta,\phi\right)r^{2n-2-l}\exp\left(-\xi r^2\right), \tag{4.3}$$

where N is the normalisation constant, ξ is known as the exponent, and Y_{lm} are spherical harmonic functions. The indices n, m and l determine the type of orbital, i.e., s, p, d, etc. Basis functions of this explicit form are also known as Gaussian primitives, and, for reasons of balance and efficiency, a linear combination of a number of primitives is often put together to form contracted functions,

$$\psi = \sum_i n_i\phi_i,$$

where n_i are known as contraction coefficients kept fixed in the variational procedure.

How the optimisation of exponents of a basis set is done depends on their intended usage. For instance, if one is primarily focused on electronic properties of atoms, or, molecules, then using a basis set that has been optimised specifically for that purpose is likely to produce very good results. In this section, we will be

focusing on energy–optimised basis sets, where the exponents are optimised to minimise the total electronic energy as such basis sets are considered to be of more general purpose. Although all exponents may be optimised using common minimisation algorithms such as Broyden–Fletcher–Goldfarb–Shanno and simplex [54], an alternative option is to optimise a single exponent, then produce additional exponents using mathematical relationships such as well–tempered, even–tempered and Legendre polynomials. Such methods are incredibly useful for large basis sets where optimisation of every individual primitive is difficult, as discussed, for example, by Petersson [52].

Many–electron self–consistent field (SCF) computations scale up by M^4, where M is the number of basis functions. This, in return, forces one to restrict the number of functions used in the calculations. Furthermore, Gaussian basis functions have (quasi–)linear dependencies, which can cause numerical instabilities in calculations. Often, time and resource consuming non–linear optimisation of the Gaussian functions is required. To avoid such full optimisations, a number of different methods were introduced to fit some functional form to Gaussian exponents that would give results close to fully optimised basis set. The even–tempered technique [55] uses only two optimisation parameters. Other functionals with more optimisation parameters were also introduced [32, 36, 52], but the even–tempered basis is considered to span the Hilbert space most evenly.

The even–tempered atomic orbital basis is a set of nuclear–centred functions defined by

$$\psi_{nlm}\left(r,\theta,\phi\right) = N_l(\gamma_i)Y_{lm}(\theta,\phi)r^l\exp\left(-\gamma_i r^p\right), \quad p = 1 \text{ or } 2,$$

where Y_{lm} is the solid spherical harmonic. A uniform power of r in the radial dependence for each distinct symmetry l is characteristic of the basis, as well as

exponents written in terms of α and β,

$$\gamma_i = \alpha\beta^k, \quad \text{for} \quad \alpha > 0, \quad \beta > 1, \tag{4.4}$$

for $k = 1, \ldots, M$, so that the Gaussian exponents γ_i form a geometric progression. Here the two parameters that need to be optimised are α and β. The functional in Eq. (4.4) can be applied to Gaussians of angular momentum $l = 0, 1, 2, \ldots$, corresponding to s–, p–, d–,... orbitals, respectively. Schmidt and Ruedenberg [60] proposed that even–tempered basis sets are asymptotically complete when α and β considered to be functions of M and this claim has been proven by Kryachko et al. [37] where they present empirical formulae for generating systematic sequences of even–tempered basis sets. However, it is possible to show that the even–tempered basis is incomplete when β remains constant [16].

4.3 Computational Details

In order to determine the Gaussian exponents γ_i, we employ a non–linear conjugate gradient method. For an N–dimensional function $f(\mathbf{x})$, $\mathbf{x} \in \mathbb{R}^N$, the method uses the gradient $\nabla_{\mathbf{x}} f$ of the function to obtain a local minimum. It works when the function is approximately quadratic near the minimum.

We implement this method due to it is efficiency and easily applicable nature, and overall shape of the energy surface of the problem. The basis for a non–linear conjugate gradient method is to effectively apply the linear conjugate gradient method, where the residual is replaced by the gradient. A model quadratic function is never explicitly formed, so it is always combined with a line search method. Local minima for each radius and stiffness level, is located at the bottom of an energy "valley" where the behaviour resembles a quadratic behaviour, see Figure 4.1. However, we had to modify the original algorithm as we cannot use an adaptive step size due to lack of a functional form. In addition, although the

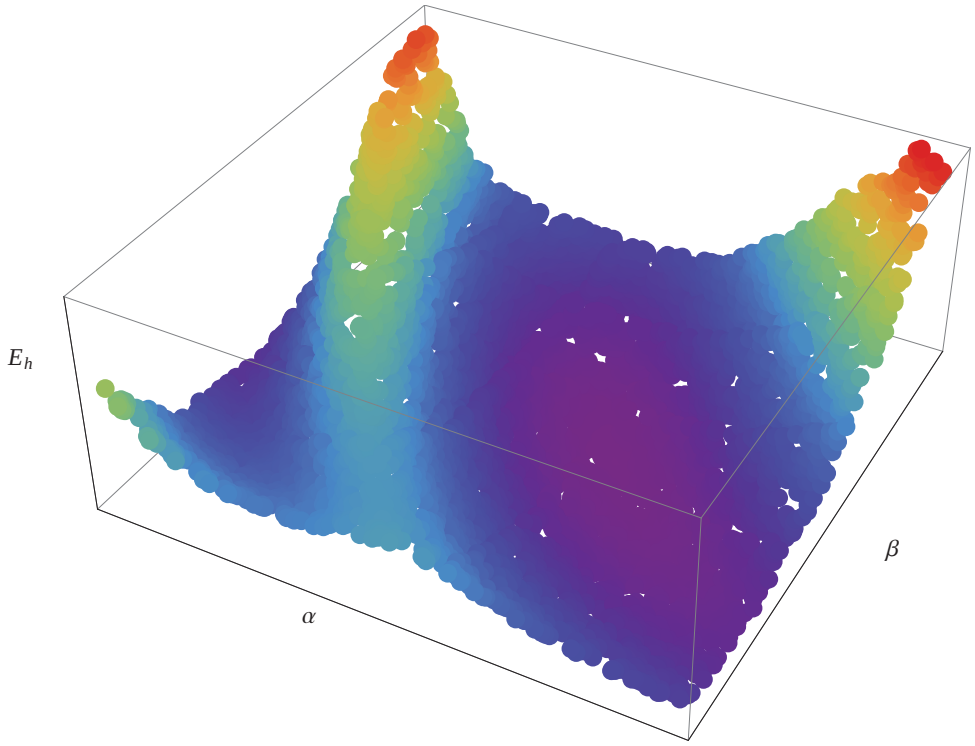

Figure 4.1: An example valley ($r_0 = 9, N = 30$) of changing total energy with respect to changing exponents α and β in Eq. (4.4).

choice of the step size λ_n for the conjugate directions $\mathbf{s_n}$ for a non-linear problem, like the one at hand, is a matter of heuristics or taste, we utilised the one suggested by Polak-Ribiére, i.e.,

$$\lambda_n = \frac{\Delta\mathbf{x}_n \left(\Delta\mathbf{x}_n - \Delta\mathbf{x}_{n-1}\right)}{\Delta\mathbf{x}_{n-1}^T \cdot \Delta\mathbf{x}_{n-1}},$$

with an additional step

$$\lambda_n = \max\left\{0, \lambda_n\right\},$$

which provides a direction reset automatically. Convergence criteria is based on the total energy difference threshold. For sufficiently large radii, we set this value to 10^{-10} Hartree. The algorithm stops when it reaches the energy difference threshold. For relatively soft walls, this threshold is not larger than 10^{-9} Hartree. However, with increasing stiffness and decreasing radius, this value needs to be lowered for numerical instability. For small radii and high stiffness levels, we were forced to decrease the convergence threshold of the total energy down to 10^{-3} Hartree.

All calculations have been carried out using *Wolfram Mathematica [69]* as *Mathematica* is able to handle very small and very large numbers efficiently. Each term of the Hamiltonian that goes into integration has been coded into *Mathematica* as most of these integrals are already known. Hence, we increase the efficiency by bypassing the actual integral evaluations. We ran individual calculations for each radius in the range $r_0 = 0.5, \ldots, 10$ where stiffness $N \in \{2, 5, 10, 20\}$. Each optimisation started with an initial pair $(\alpha, \beta) = (\alpha_0, \beta_0)$ that has been chosen from randomly generated pairs with the lowest energy in pre–defined intervals for both Gaussian exponents α and β. Every optimisation has been run with $5, 10, 15$ and 20 Gaussian functions. We chose to stop at $M = 20$ as adding more function did not result in a significant change in the minimal energy, neither for small nor for large stiffness. Optimised exponents are presented in Tables 4.1 and 4.2.

Table 4.1: Optimised exponent α for the soft–wall confined hydrogen atom.

r_0/N	2	5	10	20
0.5	0.8449901	1.8479106	2.4482584	3.4834735
1.0	0.4288235	0.7244657	0.9165578	1.2619454
1.5	0.2916991	0.4156655	0.4887258	0.6479075
2.0	0.2231050	0.2803730	0.3069455	0.3918201
2.5	0.1818367	0.2071580	0.2127706	0.2618203
3.0	0.1542356	0.1623552	0.1578393	0.1875333
4.0	0.1195753	0.1117317	0.0999142	0.1113650
5.0	0.0986542	0.0847631	0.0719216	0.0759551
6.0	0.0846328	0.0684663	0.0565076	0.0571530
7.0	0.0745706	0.0577658	0.0472407	0.0462296
8.0	0.0669924	0.0503127	0.0413037	0.0394541
9.0	0.0610760	0.0448869	0.0373117	0.0350362
10.0	0.0563267	0.0407988	0.0345232	0.0320394

Using gathered data, we were able to fit surfaces for both optimized exponents α and β both in terms of r_0 and N. The following functional forms give results within %1 lowest sum of absolute error. Deviation of the energy due to this error is negligible. The optimised exponent α can be obtained from

$$f_\alpha(r_0, N) = A_1 r_0^{A_2} \log(N + A_3) + A_4,$$

Table 4.2: Optimised exponent β for the soft–wall confined hydrogen atom.

r_0/N	2	5	10	20
0.5	1.7745493	2.1810663	2.6264559	2.9885192
1.0	1.7982507	2.1333990	2.3534143	2.4568655
1.5	1.8075812	2.1284928	2.3052870	2.3522688
2.0	1.8127127	2.1272885	2.2914538	2.3314742
2.5	1.8160020	2.1268582	2.2863848	2.3273126
3.0	1.8183076	2.1266678	2.2842257	2.3264757
4.0	1.8213507	2.1265166	2.2826838	2.3262725
5.0	1.8232853	2.1264629	2.2822404	2.3262642
6.0	1.8246324	2.1264392	2.2820869	2.3262638
7.0	1.8256284	2.1264272	2.2820265	2.3262638
8.0	1.8263968	2.1264205	2.2820004	2.3262638
9.0	1.8270090	2.1264165	2.2819882	2.3262638
10.0	1.8275090	2.1264139	2.2819822	2.3262638

whereas exponent β can be obtained by

$$f_\beta(r_0, N) = B_1 + \frac{B_2}{r_0} + B_3 \log(N) + \frac{B_4}{r_0^2} + B_5 \log(N)^2 + \frac{B_6 \log(N)}{r_0}$$

with $A_i, B_j \in \mathbb{R}$. Surface plots of f_α and f_β can be seen in Figures 4.2 and 4.3. In addition, Figures 4.4 and 4.5 show changes in exponents α and β with respect to changing r_0 and N.

4.4 Comparison to the Numerov Method

We next demonstrate the accuracy of the Gaussian basis sets mentioned in Section 4.3. We compare the energies calculated using even–tempered basis sets to the numerical energies obtained from the Numerov method.

Table 4.3 lists data for the convergence in ground state energy for a soft–wall confined hydrogen atom by using different number of Gaussian basis functions with optimized exponents. It is evident that with increasing number of Gaussian functions, the energy of the system, for any radius and stiffness level, becomes

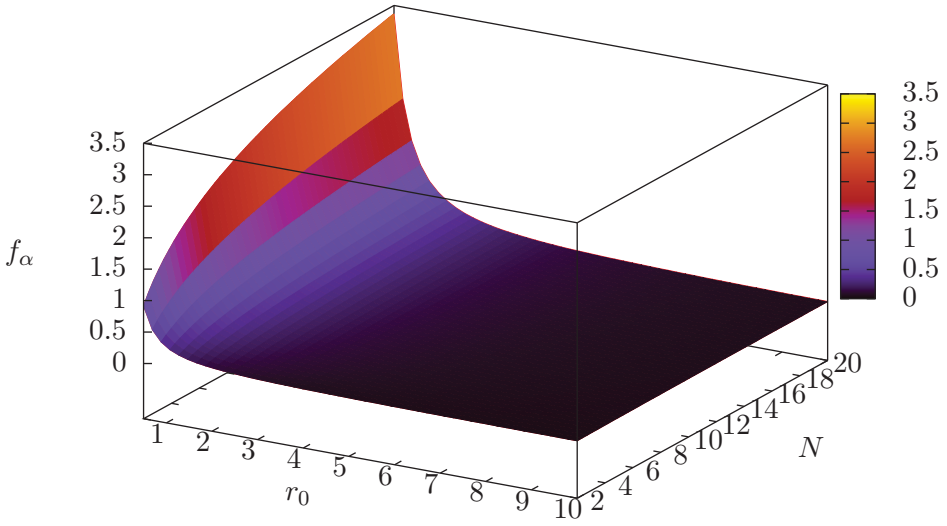

Figure 4.2: Surface plot of function f_α.

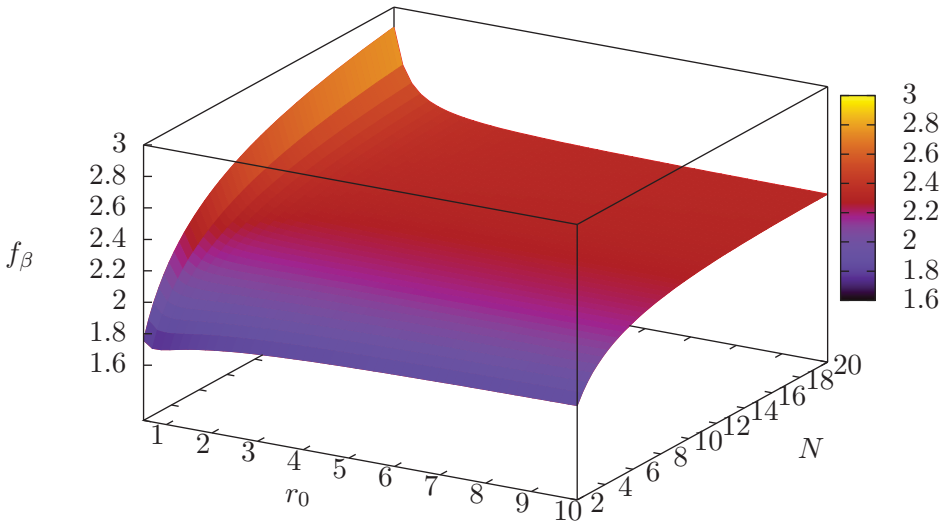

Figure 4.3: Surface plot of function f_β.

closer to the Numerov method's numerical result. This convergence is much faster for small stiffness N and much slower for higher N. One of the reasons for such a behaviour is that the wave function becomes considerably compressed with decreasing r_0 and increasing N. Therefore, it becomes difficult to represent such a

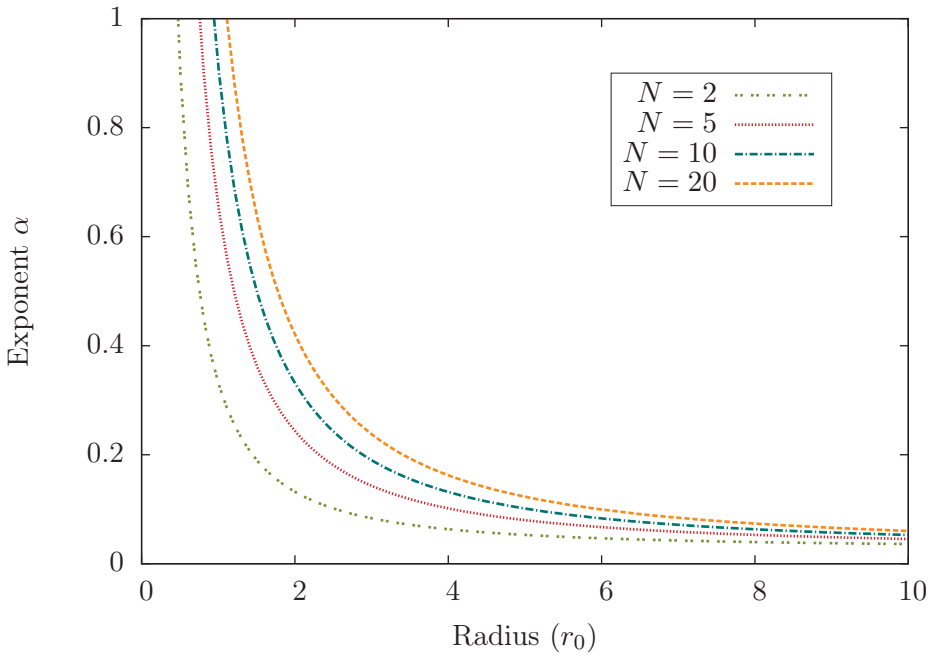

Figure 4.4: Change in exponent α with respect to varying radius with different stiffness levels.

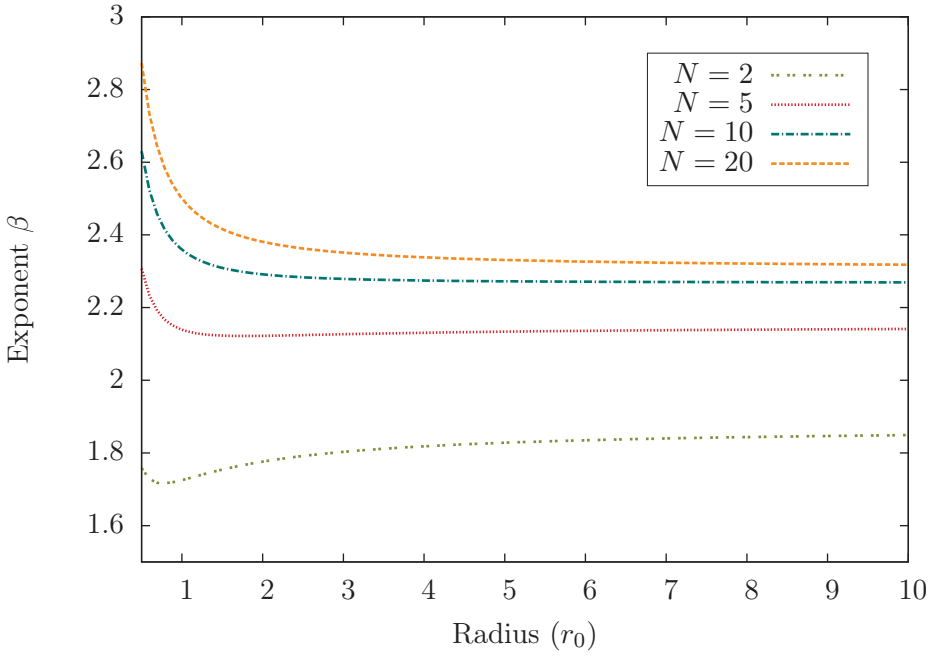

Figure 4.5: Change in exponent β with respect to varying radius with different stiffness levels.

wave function with so many Gaussian functions in this region.

As we mentioned in the previous section, we chose to stop our optimization scheme at $M = 20$ Gaussian functions because, for small and large stiffness N, there

Table 4.3: Convergence of ground state energy eigenvalues for the soft–wall confined hydrogen atom.

r_0/M	5	10	20	Numerov
		$N = 2$		
0.5	2.1691414	2.1686715	2.1686385	2.1686378
2.0	−0.0873566	−0.0877805	−0.0878006	−0.0878014
5.0	−0.4039320	−0.4043344	−0.4043459	−0.4043462
8.0	−0.4579223	−0.4583265	−0.4583342	−0.4583341
10.0	−0.4719760	−0.4723851	−0.4723927	−0.4723929
		$N = 20$		
0.5	10.8129323	10.5020423	10.3480080	7.8198240
2.0	−0.1579184	−0.1777180	−0.1885275	−0.2679730
5.0	−0.4960529	−0.4959198	−0.4960145	−0.4975368
8.0	−0.4995574	−0.4999617	−0.4999606	−0.4999732
10.0	−0.4995626	−0.4999943	−0.4999983	−0.4999986

is no significant improvement to the energy. This can be observed in Figures 4.6–4.9. One should note that with increasing stiffness level and decreasing radii, the average percentage error in energy difference with respect to numerical calculations become rather large. This, unfortunately, can cause numerically unstable results for the system. Improvement in the optimisation method may not be of much help as it is also due to the nature of the wave function in these "tight" regions. Notice that with increasing N the asymptotic behaviour becomes less and less Gaussian–like. Nevertheless, we choose to present the data set as it follows the correct behaviour and, given a better algorithm scheme, we believe the results can be improved. One other thing to note is the "spike" seen in Figures 4.6–4.9 around $r_0 = 1.5$. Interestingly, this is close to the proximity of the radius where the zero–energy wave function occurs. The optimisation algorithm assumes a steady change in the energy surface. Therefore, the optimised exponents follow a specific trend, in this case, as noted before, an exponential behaviour. However, this perhaps causes the mentioned spike in the energy difference. In other words, basis set optimised at radius $r_0 = 1.5$ does not fully reflect the true nature of the wave function. One way to fix this is to perform an individual optimisation for radii around $r_0 = 1.5$. However, this would disturb the smooth trend of the

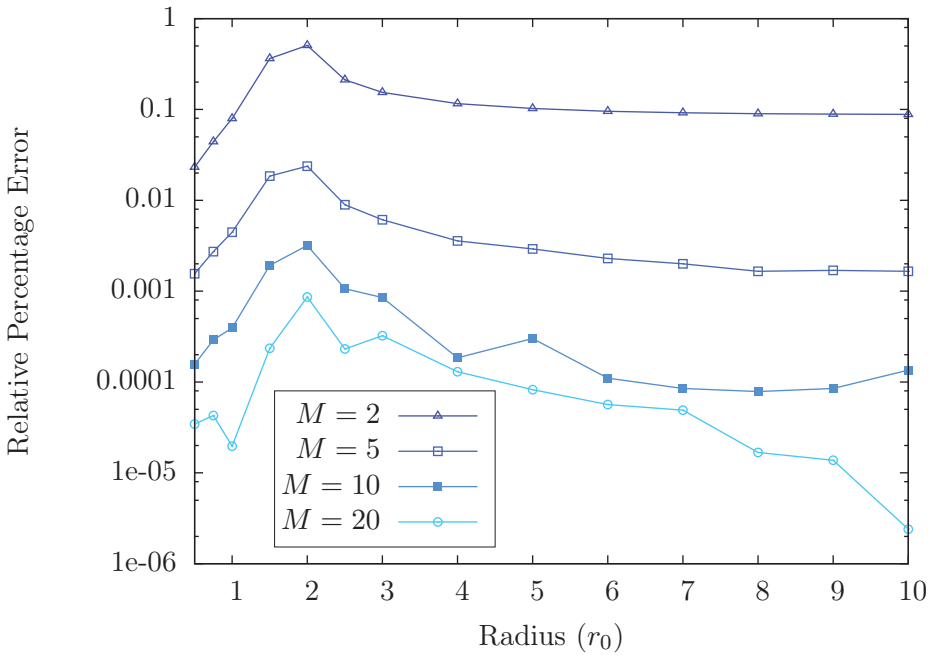

Figure 4.6: Relative percentage error change in the electronic energy with respect to the Numerov numerical method with changing radius for stiffness $N = 2$.

optimised exponents of the basis set. It should be also noted that the error at $r_0 = 1.5$ when $N = 10$ is significantly larger than the error when $N = 20$. We suspect that this might be one of the many shortcomings of our optimisation algorithm for this particular system, and/or numerical instabilities introduced during the optimisation process. One reason why our algorithm fails might be the fact that the non–linear conjugate gradient method cannot detect the true minimum when the radius of the soft–wall gets very small and permeability of the walls decrease. This is due to the significantly large number of local minima existing in this tight regime.

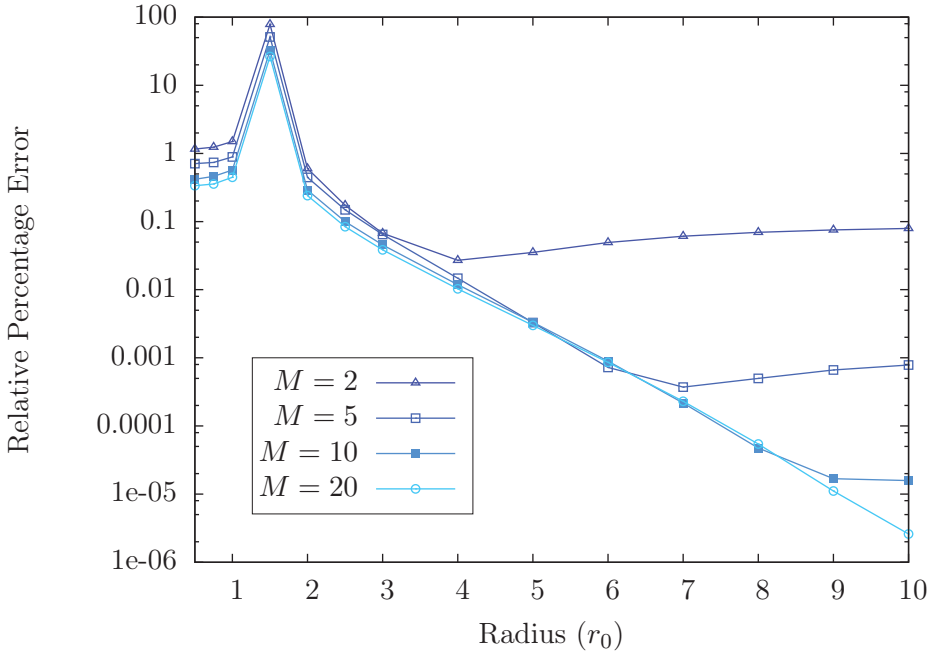

Figure 4.7: Relative percentage error change in the electronic energy with respect to the Numerov numerical method with changing radius for stiffness $N = 5$.

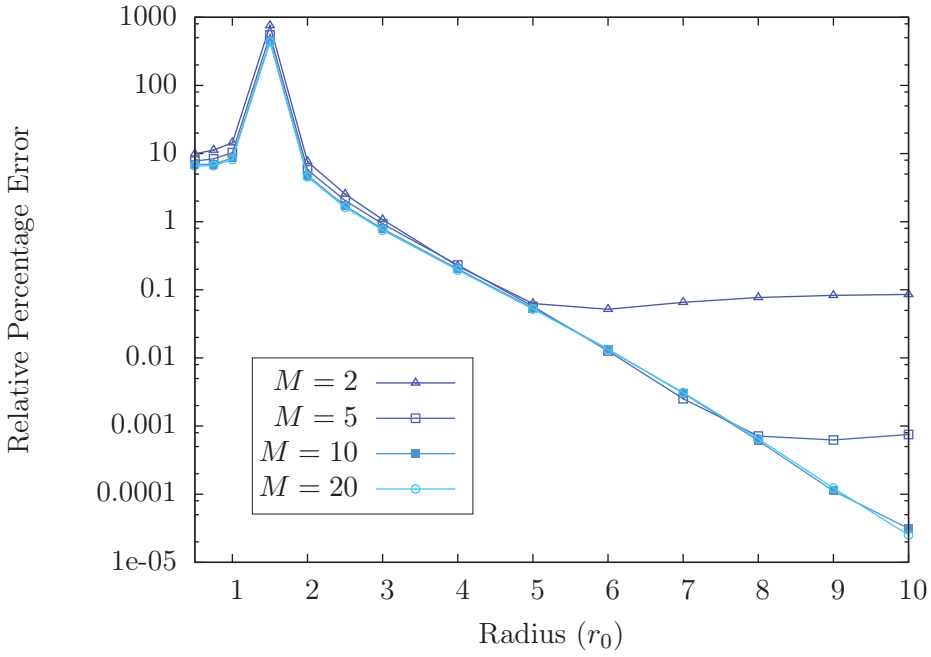

Figure 4.8: Relative percentage error change in the electronic energy with respect to the Numerov numerical method with changing radius for stiffness $N = 10$.

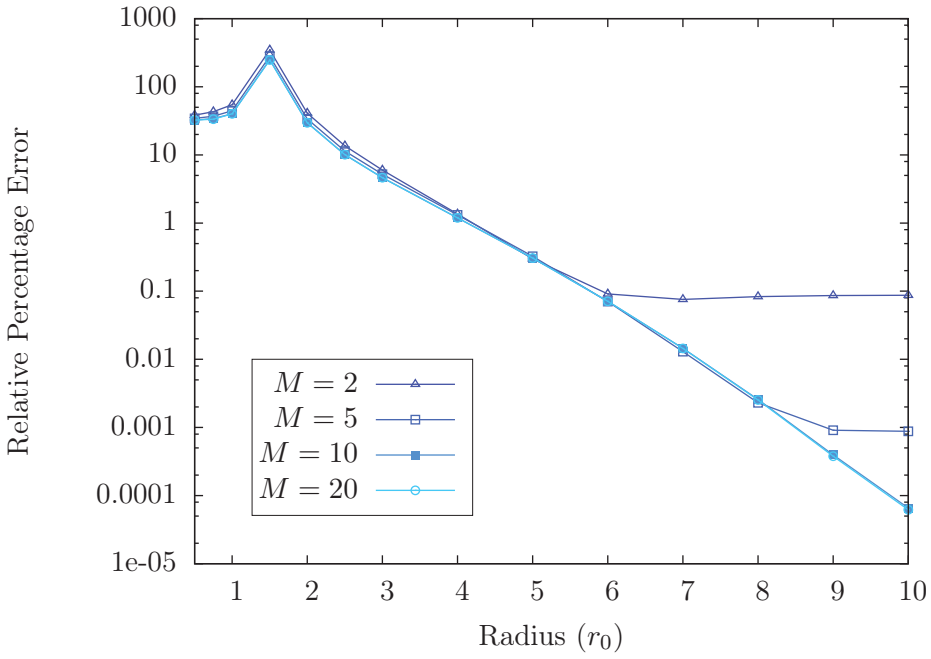

Figure 4.9: Relative percentage error change in the electronic energy with respect to the Numerov numerical method with changing radius for stiffness $N = 20$.

4.5 Dipole Polarisability of Soft–Wall Confined Hydrogen Atom

Dipole polarisabilities[1] are important in many areas of chemistry and physics. In electromagnetic field–matter interactions, for instance, the response of a neutral particle to an applied field such as a laser is determined by polarisabilities.

The interaction of a particle with an external electric field is characterised by induced electric multipole moments. The induced dipole moment is related to the electric field through the atomic dipole polarisability. From this, the static electric dipole polarisability can be defined as a measure of the distortion of the electronic density under the effect of a static external electric field.

Polarisabilities determine the behaviour of neutral particles in the interaction with other particles such as in collision phenomena. Some of the important relationships between polarizabilities and other physical properties are listen in Table 4.4.

[1]Interested reader many want to check Appendix D for a brief description.

Table 4.4: The relationship between the dipole polarisability α and other physical quantities.

Quantity	Relation to α[a]
Dielectric constant[b]	$\varepsilon = 1 + 4\pi\alpha$
Refractive index[b]	$\eta = 1 + 2\pi\alpha$
Ion mobility in gas[c]	$K = 13.876\sqrt{\alpha\mu}$ cm^2/volt·sec
van der Waals constant between system A and B	$C_6 = \frac{3}{2}\left(\frac{\alpha_A\alpha_B}{\sqrt{\alpha_A/n_A} + \sqrt{\alpha_B/n_B}}\right)$
Long range electron– or ion–atom interaction potential[d]	$U = -e^2\alpha/2r^4$

[a] α is in units of Å^3.
[b] For a dilute non–polar gas.
[c] μ is the reduced mass.
[d] For singly charged ions r is the separation between colliding pair of particles, and e is the charge of an electron.

In this section, using even–tempered basis sets, we present the dipole polarisability of soft–wall confined hydrogen atom. We have run individual *Gaussian* 09 [23] calculations where the basis set is energy optimised even–tempered basis set discussed in Section 4.3.

Gaussian 09 is not currently capable of running calculations on systems having polynomial potentials, i.e. of the form

$$V(r) = a_0 r^n + a_1 r^{n-1} + \cdots + a_{n-1} r + a_n$$

for $a_i \in \mathbb{R}$ and $n \in \mathbb{Z}$. In order to simulate a polynomial behaviour similar to that of soft–wall potential, it was necessary to use a pseudo–potential of the form

$$V_{\text{pseudo}}(r) = A r^{\gamma+2} \mathrm{e}^{-\xi r^2}.$$

Here, $A \in \mathbb{R}$ and $\gamma \in \mathbb{N}^*$. This function mimics the behaviour of the soft–wall potential for sufficiently small values of ξ. It is easy to see that

$$V_{\text{pseudo}}(r) \sim V_s(r),$$

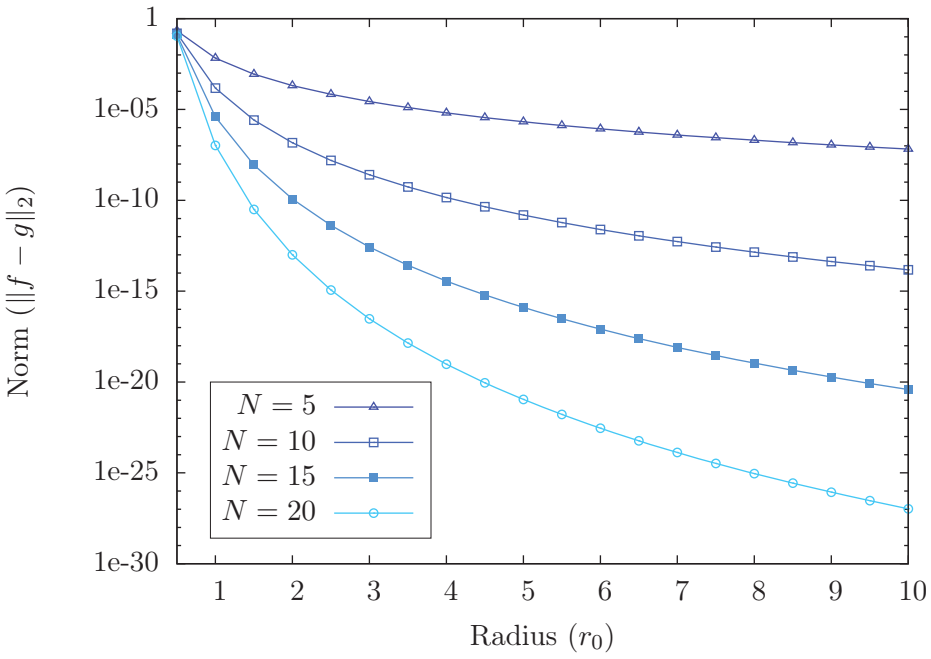

Figure 4.10: Change in L^2 norm over radius with various N. Here, we choose $\xi = 10^{-8}$.

when ξ is small. The trick of using a pseudo–potential in our calculations has a negligible effect. In order to demonstrate the negligible effect of using such a pseudo–potential, we show that the difference between the two functions quickly converges zero for sufficiently small values of ξ. Since both $V_{\text{pseudo}}(r)$ and $V_s(r)$ are square–integrable functions, we can use the norm

$$\|f-g\|_2 = \left(\int_0^{+\infty} (f-g)^2 \, \mathrm{d}\mu\right)^{1/2}$$

to demonstrate this effect. Evaluating the norm in the range $(0, r_0)$ reveals that with increasing radius and stiffness, the similarity of these functions gets better. As per usual, the most problematic region is the most inner one. Norm at $r_0 = 0.5$ for any stiffness is of order 10^{-1}. However, this value drops off quickly. A plot of the norm vs. radius with different N is shown in Figure 4.10. Although $\xi = 10^{-4}$ would be sufficient enough for most of the calculations, for the sake of safety, we set $\xi = 10^{-8}$.

Dipole polarisability calculations in *Gaussian* 09 can be requested with the method

Table 4.5: Dipole polarisability (α) shifts for the soft-wall confined hydrogen atom.

r_0/N	2	5	10	20	Hard–wall [14]
0.5	0.3081363	0.0401424	0.0141991	0.0052122	0.0020300
2.0	2.0092895	1.0392709	0.7724152	0.5097479	0.3401565
5.0	3.8376210	3.6423213	3.7235522	3.5456747	3.4029447
8.0	4.3183668	4.3640944	4.4391208	4.4504448	4.4527846
10.0	4.4119524	4.4591518	4.4888680	4.4957282	4.4967546

keyword "Polar" which requests that the dipole electric field polarisabilities (and hyperpolarisabilities, if possible) be calculated. No geometry change or derivatives are implied. This method uses static frequencies to calculate polarisabilities and hyperpolarisabilities. We calculated the dipole polarisabilities of a soft–wall confined hydrogen atom as easy as using the method keyword in our calculations. Results of these calculations are populated in Table 4.5. One can observe that with increasing stiffness the dipole polarisability of a soft–wall confined hydrogen atom approaches that of hard–wall confined hydrogen atom as one expects. It is also important to note a particular behaviour in regards to polarisability changes of soft–wall confined hydrogen atom. A careful examination of Fig. 4.5 reveals that for small radii ($r_0 < 4$), the polarisability of the system gets smaller for increasing stiffness. This is due to, first, shrinking spatial confinement, and, second, the increasing stiffness of the walls. Decreasing radius and increasing stiffness restricts the electron movements. Hence, polarisability gets smaller in this region. And for large radii, we see that polarisability is very close to the polarisability of hard–wall confined hydrogen. This is an expected behaviour as the radius gets larger, we approach free hydrogen polarisability

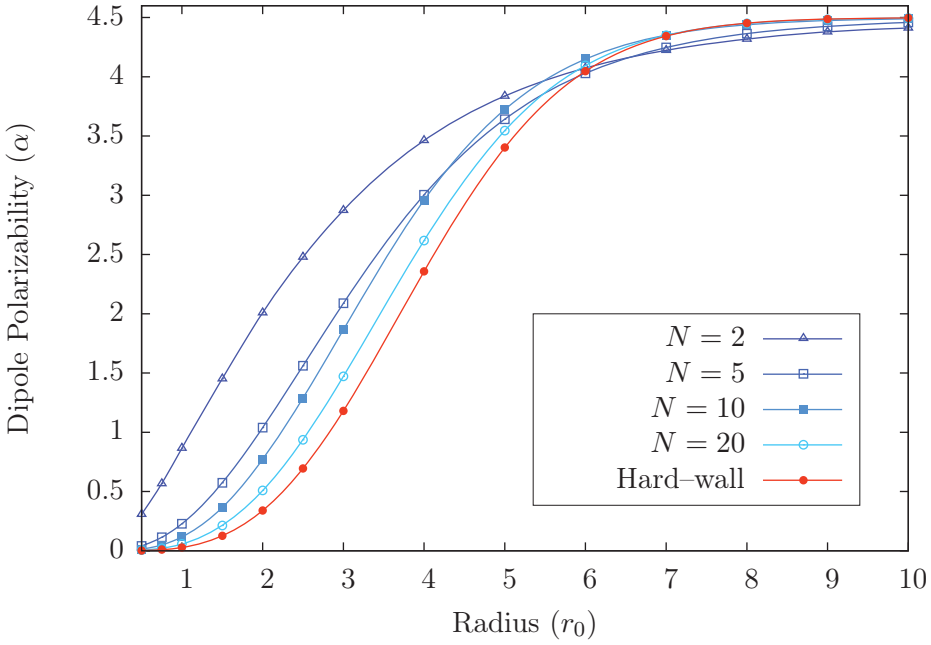

Figure 4.11: Dipole polarisability change for the soft–wall confined hydrogen with respect to radius and stiffness of the confinement.

Chapter 5

The Soft–Wall Confined Helium and Argon

Interest to the hard–wall confined hydrogen atom also kindled an interest in the hard–wall confined multi–electron systems. In is only natural to follow this trend and try to investigate multi–electron systems confined in a soft–wall confinement. Therefore, we devote this chapter to study the physical properties of the soft–wall confined helium and argon atoms. We will be taking a similar approach to the one we used in studying the soft–wall confined hydrogen atom in Chapter 4.

5.1 Recent Studies

Helium is the simplest multi–electron system. Unlike the hydrogen atom, in helium it is possible to study physical properties such as the electronic correlation, which is an essential property of the electronic structure for atoms and molecules.

Similarly to the hard–wall confined hydrogen atom, a systematic study of how energy and the electron correlation changes as a function of pressure, or, the confining cavity dimension is an important aspect to the hard–wall confined

helium atom. Although this problem carries similar properties compared to the hard–wall confined hydrogen atom, the solution is much harder due to the electron–electron interaction term in the Schödinger equation. Very first results on a hard–wall confined helium atom originated in 1952 by ten Seldam and de Groot [61]. They performed a variational calculation on the hard–wall confined helium system. The trial wave function was based on an ansatz proposed by Hylleraas in 1929. They multiplied this ansatz by cut–off functions to ensure that Dirichlet boundary condition is satisfied where the trial wave function takes the form

$$\psi(s,t,u) = \left(r_0 - \frac{s-t}{2}\right)\left(r_0 - \frac{s+t}{2}\right)\left(c_0 + c_1 t + c_2 t^2\right)\mathrm{e}^{-ks},$$

where r_0 is the spherical box radius; c_0, c_1, c_2 and k are the variational parameters; s, t and u denote the Hyleleraas coordinates defined as

$$s = r_1 + r_2,$$

$$t = -r_1 + r_2,$$

$$u = r_{12}.$$

Here, r_1, r_2 and r_{12} are the distances between nucleus to electron 1, nucleus to electron 2 and distance between electron 1 and 2, respectively. The cut–off functions correspond to

$$r_0 - r_1 = r_0 - \frac{s-t}{2} \quad \text{and} \quad r_0 - r_2 = r_0 - \frac{s+t}{2}.$$

In comparison to the free helium atom, inclusion of such cut–off functions increases both the number of terms on the trial wave function and, consequently, the number of integrals to be evaluated. Their calculations showed that ground state energies of the confined helium atom are higher than of those of the free atom. This is expected as confinement within an impenetrable box raises the energy eigenvalues. Some of their results are presented in Table 5.1.

Table 5.1: Ground state energy of confined helium atom by ten Seldam and Groot[61]. Distances and energies are given in bohrs and hartrees, respectively.

r_0	2.572	2.916	6.176	$+\infty$
E	−2.76204	−2.84812	−2.90162	−2.90243

They also were able to compute the pressure by differentiating the energy with respect to the volume

$$P = -\frac{\partial E}{\partial V} = -\left[\frac{1}{4\pi r^2}\frac{\partial E}{\partial r}\right]_{r=r_0},$$

where $\partial E/\partial V$ is determined by means of a numerical derivative. In a later work [62], they also presented polarisabilities for the confined helium atom in the Kirkwood approximation, where for spherical atoms the polarisability takes the form

$$\alpha = \frac{4}{9n}\left(\left\langle r_1^2\right\rangle + \left\langle r_2^2\right\rangle\right),$$

where

$$\left\langle r_i^2\right\rangle = \frac{\int \psi^* r_i^2 \psi \mathrm{d}V}{\int \psi^* \psi \mathrm{d}V}, \quad i = 1, 2.$$

Table 5.2: Ground state energy of hard–wall confined helium atom computed by several authors. Distances and energies are given in bohrs and hartrees, respectively.

r_0	Ref. [26]	Ref. [45]	Ref. [56]	Ref. [33]	Ref. [7]	Ref. [10]
2.0	−2.5977	−2.6026	−2.5028	−2.6051	−2.6040	−2.5998
2.2	−2.7074		−2.6947		−2.7145	−2.7088
2.4	−2.7760		−2.7302		−2.7836	−2.7765
2.6	−2.8194		−2.8358		−2.8271	−2.8191
2.8	−2.8472		−2.8570		−2.8472	−2.8462
3.0	−2.8652	−2.8708	−2.8684	−2.8727	−2.8548	−2.8636
3.5				−2.8935	−2.8935	−2.8851
4.0	−2.8956	−2.8988	−2.8764	−2.9003	−2.9004	−2.8931
4.5					−2.9026	−2.9863
5.0	−2.9004	−2.9020	−2.8764	−2.9032	−2.9034	−2.8979
6.0		−2.9024		−2.9035	−2.9037	−2.8990
7.0		−2.9025			−2.9037	
$+\infty$	−2.9024		−2.8764	−2.9037	−2.9037	−2.8999

The most accurate work on the hard–wall confined helium atom ground state

Table 5.3: Ground state energies for hard-wall confined helium as a function of the spatial variable r_0 compared to literature values. PT and VPT denote first–order perturbation theory and the fifth–order variational perturbation theory calculations from Montgomery et. al [49]. Variational energies calculated using a 10–term generalised Hylleraas basis set [21] are labelled GHB. FPPT refers to those obtained by using perturbation theory with a free particle zeroth–order wave function [39].The energies obtained using a generalised Laguerre polynomial expansion [39] are denoted by GLP.

r_0	PT	VPT	GHB	FPPT	GLP
0.1	906.6319	906.562423	906.6575	907.3076	907.562500
0.2	206.2212	206.151713	206.1696	206.9099	
0.3	82.4041	82.334517	82.3403	83.1064	
0.4	41.0502	40.980281	40.9826	41.7663	
0.5	22.8117	22.741303	22.7423	23.5419	22.741303
0.6	13.3893	13.318127	13.3186		
0.7	7.9973	7.925216	7.9254		
0.8	4.6837	4.610408	4.6105		
0.9	2.5379	2.463236	2.4633		
1.0	1.0921	1.015755	1.0158		1.015755
1.1	0.0872	0.009026	0.0091		
1.2	−0.6284	−0.708802	−0.7087		
1.3	−1.1482	−1.231051	−1.2309		
1.4	−1.5318	−1.617330	−1.6172		
1.5	−1.8185	−1.906961	−1.9067		
2.0	−2.4980	−2.604046	−2.6036		−2.604038
3.0	−2.7335	−2.872443	−2.8718		−2.872495
4.0	−2.7492	−2.900534	−2.8997		−2.900485
5.0	−2.7500	−2.903408	−2.9028		−2.903410
6.0	−2.7500	−2.903650	−2.9033		−2.903696
$+\infty$	−2.7500	−2.903669	−2.9035		
Exact		−2.903724			

energy shifts have been presented by Montgomery et. al [49]. They solved the time–independent Schrödinger equation using the first–order Rayleigh–Schrödinger perturbation theory, and then extended the calculations using fifth–order variational perturbation theory. Ground state hard–wall confined helium atom results of Montgomery et. al [49] are presented in Table 5.3 together with various other results from literature.

The electron correlation energy is defined as the difference between the Hartree–

Fock energy and the exact total energy

$$E_{corr} = E_{HF} - E_{exact}.$$

Gimarc [26] was the first author to analyse the confined helium atom problem by systematically studying the correlation energy. Although the correlation energies for free atoms are known at the time, Gimarc was interested in the effect of spatial confinement on the correlation energy. They found that the correlation energy is relatively insensitive to significant changes to the size r_0 of the spherical confinement.

Ludeña and Gregory [45] were the first to report CI calculations by using a basis set that consisted of $6s$, $4p$ and $4d$ orbitals, spanned by 41 functions. Not only their results were improvements to previous work but they concluded that the correlation energy grows slightly when the box radius is reduced as one expects.

Throughout literature, there has been many reported results improving on previous work in one way, or the other. Aquino et. al [6] approached this problem by using a wave function expansion in term of generalised Hylleraas basis sets, where the Hamiltonian is expressed in Hylleraas coordinates

$$\begin{aligned} H = & -\frac{1}{2}\left(\frac{\partial^2}{\partial r_1^2} + \frac{2}{r_1}\frac{\partial}{\partial r_1} + \frac{\partial^2}{\partial r_{12}^2} + \frac{2}{r_{12}}\frac{\partial}{\partial r_{12}} + 2\mathbf{r}_1 \cdot \mathbf{r}_{12}\frac{\partial^2}{\partial r_1 \partial r_{12}}\right) \\ & -\frac{1}{2}\left(\frac{\partial^2}{\partial r_2^2} + \frac{2}{r_2}\frac{\partial}{\partial r_2} + \frac{\partial^2}{\partial r_{12}^2} + \frac{2}{r_{12}}\frac{\partial}{\partial r_{12}} + 2\mathbf{r}_2 \cdot \mathbf{r}_{12}\frac{\partial^2}{\partial r_2 \partial r_{12}}\right) \\ & -\frac{Z}{r_1} - \frac{Z}{r_2} + \frac{1}{r_{12}}, \end{aligned}$$

where $\mathbf{r}_1$ and $\mathbf{r}_2$ refers to the unit vectors for electron–nucleus distances and $\mathbf{r}_{12}$ is the inter–electronic distance. The trial wave function in terms of the chosen basis

including the cut–off factors has the form

$$\psi = \left(1 - \frac{r_1}{r_0}\right)\left(1 - \frac{r_2}{r_0}\right)\sum_k^M c_k \left(1 + P_{12}\right) r_1^{n_k} r_2^{m_k} r_{12}^{l_k} \mathrm{e}^{-\alpha_k r_1 - \beta_k r_2 - \gamma_k r_{12}},$$

where coefficients c_k and exponents $\{\alpha, \beta, \gamma\}$ are variational parameters, while P_{12} is the two particle exchange operator. In their calculations they used expansions with $M = 1, 5$ and $M = 10$ terms where exponents are controlled by the relation $n + m + l \leq 2$. As expected the lowest energies were given by 10–term expansion. They also obtained the ionization radius, the atomic pressure and the expectation value $\langle r_{12} \rangle$ for the confined helium atom.

Aquino et al. [7] extended their calculations by using $M = 20, 30$ and $M = 40$ generalised Haylleraas wave functions spanned according to $n + m + l \leq 5$. Their calculations with $M = 40$ showed significant improvements for tight confinement regimes. Some of their results are presented in Table 5.2.

5.2 The Soft-Wall Confined Helium

In this section, we present results for the soft–wall confined helium. In our calculations we use an even–tempered basis set spanned by $20s15p10d5f4g3h$ functions. All calculations are carried out using *Gaussian '09* [23] at full CI level.

Table 5.4 contains the ground state energy shifts for the soft–wall confined helium atom. These results are compared to Montgomery at. al [49] who used variational perturbation theory (VPT) to calculate the ground state of a hard–wall confined helium atom. To the best of our knowledge, the results presented in [49] are the most up to date ones. As expected, the trend in energy with respect to the confinement radius and stiffness is very similar to hydrogen case, i.e. with increasing stiffness the ground state energy approaches the hard–wall confined

Table 5.4: Ground state energy shifts of a soft–wall confined helium atom with respect to changing radius (r_0) and stiffness (N).

r_0/N	2	5	10	20	VPT [49]
0.5	1.0430997	3.6063966	7.2548701	14.7214540	22.741303
1.0	−1.4682529	−1.4828801	−1.1430589	−0.1113855	1.015755
1.5	−2.1485202	−2.4166504	−2.4154448	−2.1714886	−1.906961
2.0	−2.4363568	−2.7007607	−2.7423842	−2.6754580	−2.604046
3.0	−2.6737619	−2.8553786	−2.8813648	−2.8770162	−2.872443
4.0	−2.7675201	−2.8886043	−2.8998425	−2.9001250	−2.900053
5.0	−2.8138361	−2.8978804	−2.9027063	−2.9029756	−2.903408
6.0	−2.8400001	−2.9009692	−2.9031748	−2.9032807	−2.903650

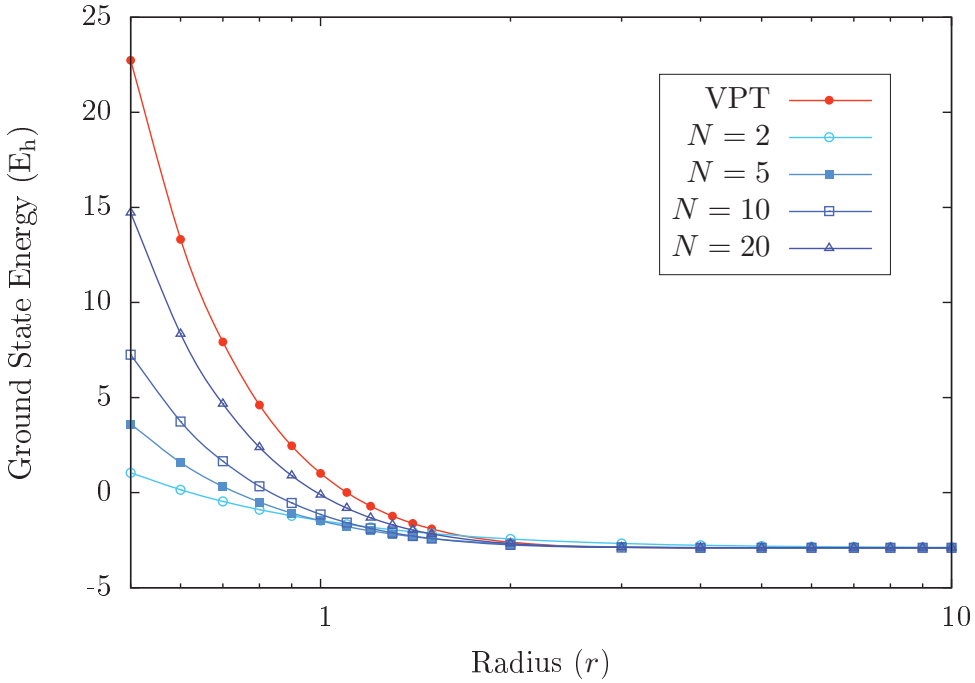

Figure 5.1: Ground state energy shifts of a soft–wall confined helium atom.

helium atom, see also Figure 5.1.

Similarly, one can observe dipole polarisability shifts for the soft–wall confined helium atom in Table 5.5 where the data is plotted in Figure 5.2.

One of the other electronic structure properties that can be investigated is electron correlation. The basis set correlation energy is computed by

$$\mathrm{E}_{corr}^{basis} = \mathrm{E}_{exact}^{basis} - \mathrm{E}_{HF}^{basis}.$$

Table 5.5: Dipole polarisability shifts of soft–wall confined helium atom with respect to changing radius (r_0) and stiffness (N).

r_0/N	2	5	10	20
0.5	0.09679	0.03037	0.01357	0.00524
1.0	0.25303	0.15092	0.10136	0.05664
1.5	0.40735	0.33751	0.28097	0.19170
2.0	0.54475	0.54575	0.51689	0.40133
3.0	0.76186	0.90773	0.96584	0.87539
4.0	0.91506	1.13710	1.22932	1.19813
5.0	1.02319	1.25965	1.33582	1.33504
6.0	1.10068	1.32075	1.37040	1.37490

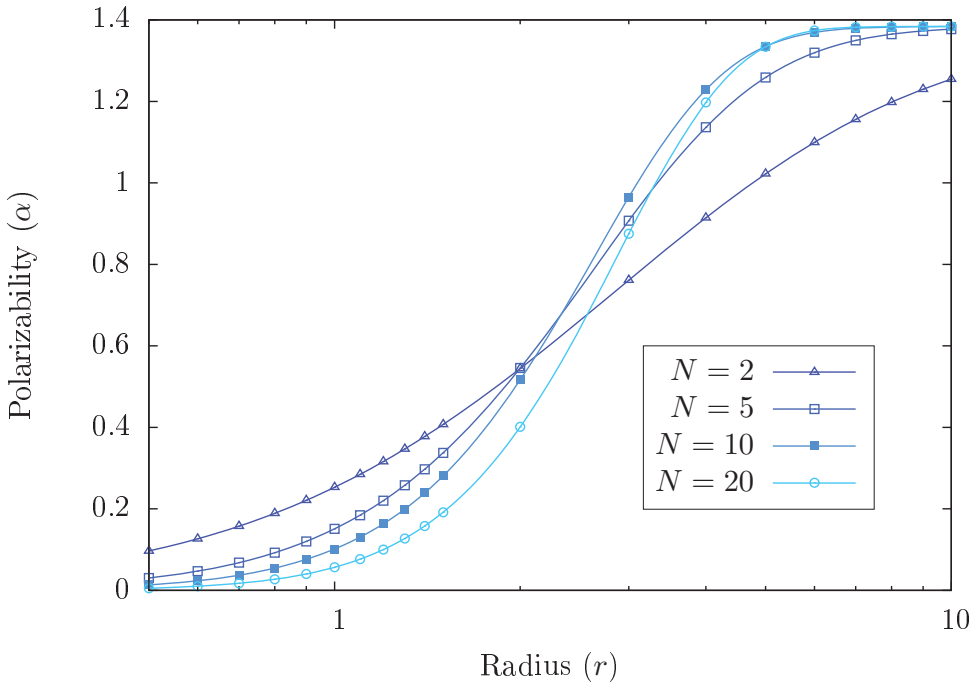

Figure 5.2: Dipole polarisability changes for a soft–wall confined helium atom for various radii and stiffness values.

Table 5.6: Change in the electron correlation energy of a soft–wall confined helium atom for various r_0 and N.

r_0/N	2	5	10	20
0.5	0.0421707	0.0444112	0.0471078	0.0498617
1.0	0.0411690	0.0420228	0.0433361	0.0453181
1.5	0.0408703	0.0410855	0.0415128	0.0424621
2.0	0.0408061	0.0408887	0.0409930	0.0412498
3.0	0.0408761	0.0411649	0.0413031	0.0412083
4.0	0.0409806	0.0414226	0.0416028	0.0416140
5.0	0.0410609	0.0415249	0.0416525	0.0416782
6.0	0.0411153	0.0415440	0.0416253	0.0416449

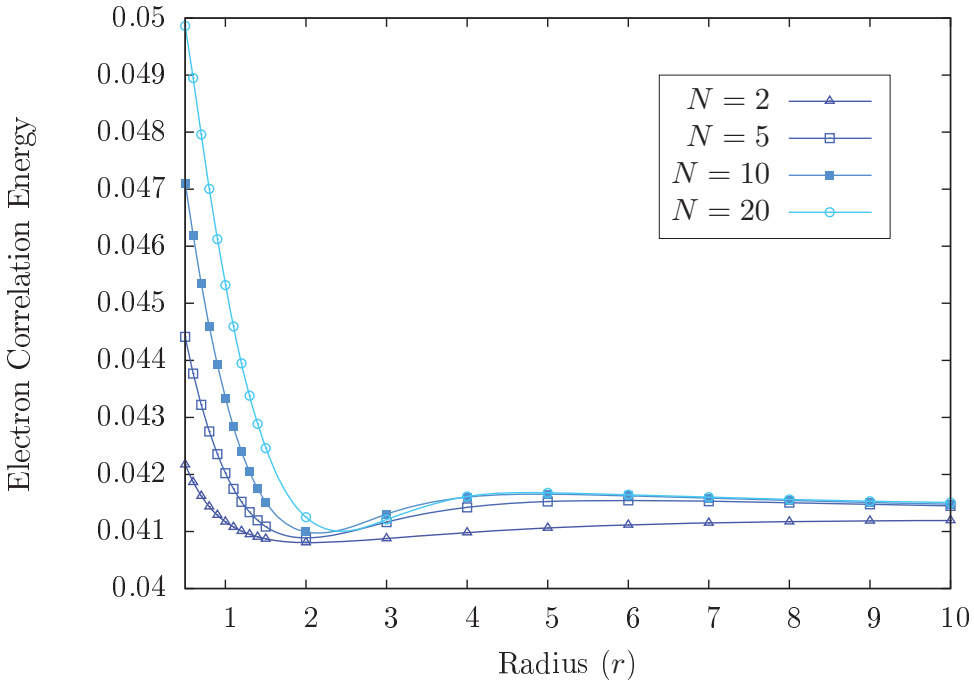

Figure 5.3: Soft–wall confined helium atom correlation energy change.

Using the data from *Gaussian* 09 calculations, it is easy to extract the electron correlation energy for each individual case of a soft–wall confined helium atom.

As expected, with increasing radius and stiffness of the confinement, correlation energies get close to the free helium correlation energy, which is $E_{corr}^{exact} = 0.042044384$. For small radii, $r_0 = (0.5, 4)$, E_{corr}^{basis} first decreases and then increases. We believe the decrease happens around the radius that corresponds to the zero–energy wave function where electrons become unbound. And, the increase is due to spatial confinement which reaches a very tight regime. See Figure 5.3.

Table 5.7: Ground state energy shifts of a soft–wall confined argon atom for various r_0 and N.

r_0/N	2	5	10	20
0.5	−479.09391	−420.23970	−329.45587	−80.70723
0.6	−490.78639	−450.22437	−396.78407	−248.74221
0.7	−498.55832	−469.50401	−434.42614	−344.12469
0.8	−504.01995	−484.51852	−457.58429	−396.80654
0.9	−508.02226	−495.32308	−474.86927	−432.77699
1.0	−511.05261	−502.86400	−489.08159	−455.63490
1.1	−513.40798	−508.27595	−498.92301	−475.24336
1.2	−515.27853	−512.25824	−505.86887	−488.77853
1.3	−516.79100	−515.25143	−510.88274	−498.34231
1.4	−518.03273	−517.54220	−514.57377	−505.23967
1.5	−519.06565	−519.32272	−517.33710	−510.30220
2.0	−522.33002	−524.07361	−524.06842	−522.09346
3.0	−524.94834	−526.62626	−526.94180	−526.70593
4.0	−525.95768	−527.18746	−527.36478	−527.33701
5.0	−526.44757	−527.34981	−527.43918	−527.44142
6.0	−526.71910	−527.40492	−527.45094	−527.45486
7.0	−526.88298	−527.42534	−527.45051	−527.45304
8.0	−526.98771	−527.43300	−527.44797	−527.44984
9.0	−527.05729	−527.43553	−527.44534	−527.44725
10.0	−527.10469	−527.43585	−527.44301	−527.44531

5.3 The Soft–Wall Confined Argon

To the best of our knowledge, there are no studies on any form of confined argon atom. Therefore, we see it fit to present an analysis of a soft–wall confined argon atom.

We follow a similar approach to the soft–wall confined hydrogen and helium atoms where we use an even–tempered basis set spanned by $20s15p10d5f4g3h$. All calculations have been performed with strict convergence criteria of $\epsilon = 10^{-9}$ at CCSD(T) level. Table 5.7 presents the results of our calculations where Figure 5.4 depicts the data. It is not surprising to see exactly the same behaviour of change in energy due to varying radii and stiffness levels similar to the soft–wall confined hydrogen and helium atoms.

We should note that as the radius of the confinement gets smaller, calculations take

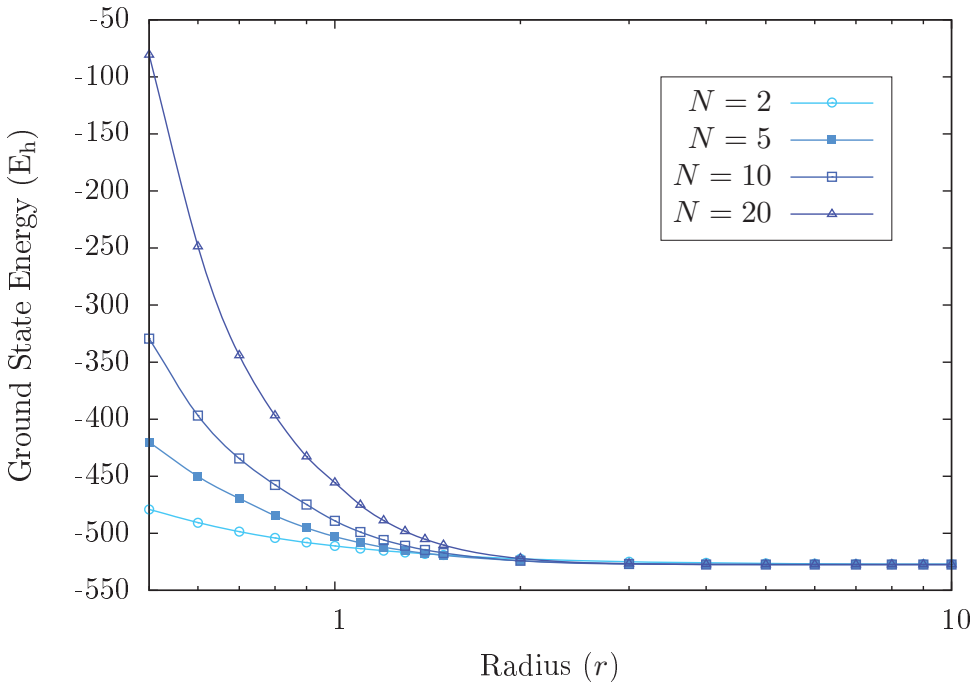

Figure 5.4: Ground state energy shifts of a soft–wall confined argon atom.

longer to finish. In addition, we had several difficulties with configuration of the atomic orbitals. In order to solve numerical errors due to wrong configuration, we used the configuration of the previous successful calculation. This significantly lowered the calculation intensity and duration as the system starts with already configured orbitals. Another factor that effects the duration of the calculations is the polarisation calculations we asked *Gaussian '09* [23] to perform. We present the dipole polarisability shifts of the soft–wall confined argon atom in Table 5.8. Once again, it is worthy to note that change in the dipole polarisability follows a similar trend to that of the soft–wall confined hydrogen and helium atoms. Figure 5.5 depicts this behaviour.

Another physical property that is very interesting to observe is the electron correlation. It is very easy to extract this information as *Gaussian '09* [23] already calculates everything we need. Table 5.9 and Figure 5.6 presents the results of the electron correlation calculations for a soft–wall confined argon atom. It is very interesting to note that we do *not* see any similarities to the electron correlation shifts of a soft–wall confined helium atom as depicted in Figure 5.3. This is due the

Table 5.8: Dipole polarisability shifts of a soft–wall confined argon atom with respect to changing radius (r_0) and stiffness (N).

r_0/N	2	5	10	20
0.5	1.11680	0.90668	0.75361	0.00001
0.6	1.26297	0.90136	0.75365	0.00017
0.7	1.42418	0.90756	0.75464	0.00115
0.8	1.59338	0.93594	0.75521	0.00474
0.9	1.76603	0.99879	0.76711	0.01414
1.0	1.94045	1.08978	0.80487	0.03358
1.1	2.11371	1.20369	0.86684	0.06764
1.2	2.28656	1.33630	0.95138	0.12047
1.3	2.46467	1.48413	1.05691	0.19531
1.4	2.62671	1.64438	1.18187	0.29420
1.5	2.79370	1.81478	1.32473	0.41796
2.0	3.58657	2.76467	2.25663	1.37554
3.0	4.94496	4.82280	4.70058	4.11137
4.0	6.03206	6.70406	7.11704	6.63102
5.0	6.89327	8.17170	8.96221	8.47606
6.0	7.57965	9.21568	10.10197	9.71301
7.0	8.12996	9.90814	10.67469	10.49826
8.0	8.57376	10.34374	10.92463	10.96675
9.0	8.93826	10.62446	11.04758	11.21710
10.0	9.23497	10.79623	11.09017	11.31799

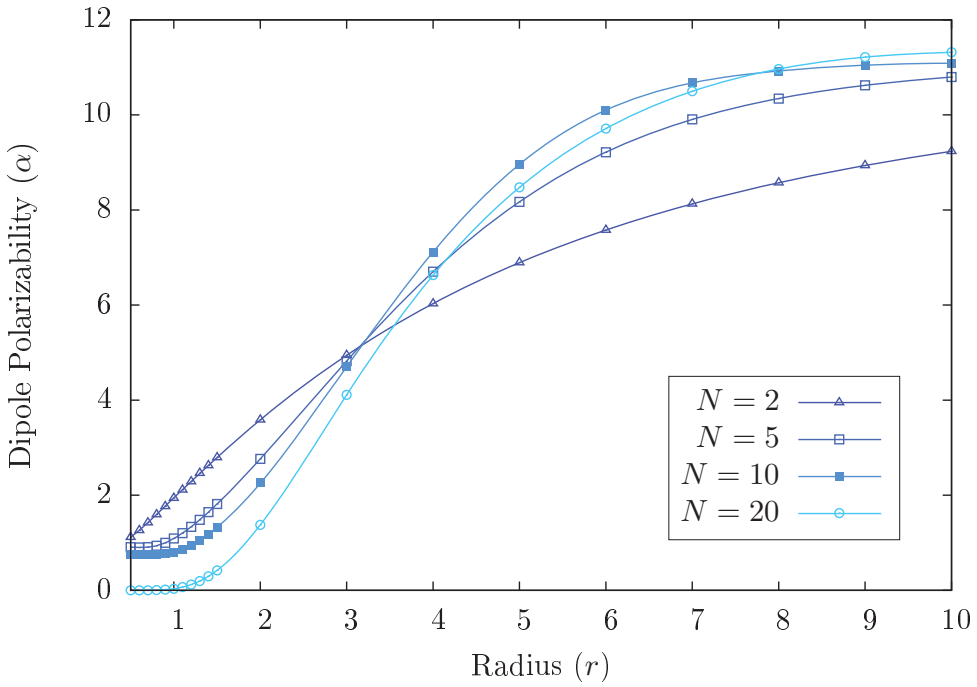

Figure 5.5: Dipole polarisability changes for a soft–wall confined argon atom for various radii and stiffness values.

range we carry our calculations. Although we use exactly the same range for the confinement radius r_0, in order to see a similar decrease around the zero–energy wave function, we need to carry out calculations for radii much smaller than $r_0 = 0.5$. This is another validation that a spatial confinement forces the wave functions towards the nucleus, and hence causing the confined systems to attain higher energies compared to the unconfined systems.

Table 5.9: Change in the electron correlation energy of a soft–wall confined argon atom for various r_0 and N.

r_0/N	2	5	10	20
0.5	0.77596	0.88757	0.90332	0.92948
0.6	0.75752	0.85459	0.86895	0.89185
0.7	0.74320	0.82906	0.84234	0.86272
0.8	0.73165	0.80858	0.82097	0.83934
0.9	0.72209	0.79169	0.80335	0.82007
1.0	0.71400	0.77748	0.78851	0.80384
1.1	0.70703	0.76531	0.77580	0.78994
1.2	0.70096	0.75475	0.76477	0.77788
1.3	0.69561	0.74549	0.75509	0.76730
1.4	0.69084	0.73729	0.74651	0.75793
1.5	0.68655	0.72996	0.73884	0.74955
2.0	0.67019	0.70247	0.71003	0.71812
3.0	0.65080	0.67144	0.67733	0.68256
4.0	0.63924	0.65438	0.65920	0.66294
5.0	0.63136	0.64378	0.64782	0.65070
6.0	0.62555	0.63676	0.64018	0.64255
7.0	0.62103	0.63196	0.63487	0.63693
8.0	0.61740	0.62864	0.63110	0.63301
9.0	0.61439	0.62635	0.62841	0.63026
10.0	0.61184	0.62481	0.62652	0.62838

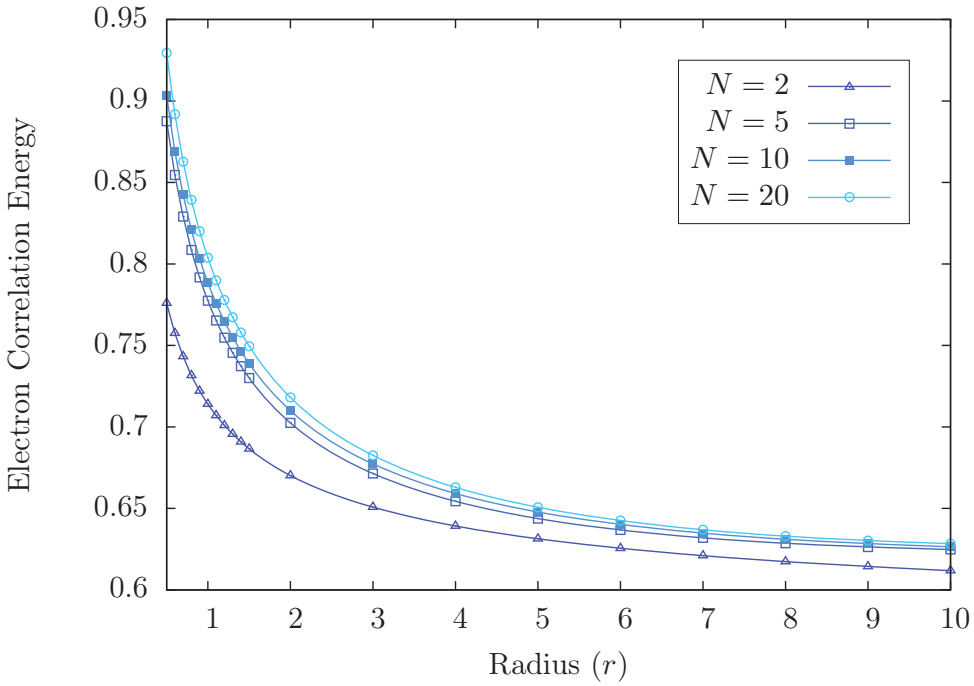

Figure 5.6: The electron correlation energy change for a soft–wall confined argon atom.

Chapter 6

Conclusions and Future Perspective

In this thesis, we investigated confined atomic systems. Our departure point was the celebrated hard–wall confined hydrogen atom studied by Michel et al. [47] in 1937. Based on the idea developed by Michel et al., we were able to study the confined hydrogen atom model on a different perspective with a more flexible confining potential. In their model the confining potential has the following form

$$-\frac{1}{r} + V_h(r) = -\frac{1}{r} + \begin{cases} 0 & \text{if} \quad r \leq r_0, \\ +\infty & \text{if} \quad r > r_0. \end{cases}$$

Whereas, in our approach, we use the following confining potential

$$V_s(r) = \left(\frac{r}{r_0}\right)^N.$$

It is readily seen that $V_s(r) \to V_h(s)$ as $N \to +\infty$. Therefore, with our approach one is not restricted only to the hard–wall confinement. With an additional parameter N to the confining potential, we are able to manipulate the stiffness of the confining cavity. Thus, by increasing the stiffness parameter, one can observe the transition of a system placed in a "soft" spherical box to a one that is confined in an hard–wall spherical box. This flexibility brings several advantages over the hard–wall alternative. First of all, we do not require a boundary condition for the

wave function. Secondly and even more importantly, a soft–wall potential does not possess a discontinuity like the hard–wall potential (or some other penetrable boxes in use). This greatly simplifies its use in conjunction with existing numerical algorithms/software packages to study (unconfined) many–electron systems, and opens the way for quantum theoretical studies of atoms, or molecules in relatively stiff potentials to simulate high pressures.

Having noticed these advantages, we started our study with a numerical approach to the problem as the problem does not have an analytical solution. After careful calculations and simulations, it is evident that the soft–wall confined system with high stiffness levels mimics the hard–wall confined system. In addition, there is a smooth and predictable transition from soft-wall confinement to hard–wall confinement with increasing stiffness level N confirming the mathematical convergence of $V_s(r)$ to $V_h(r)$.

The natural next step was to investigate if we can implement this idea to multi–electron systems. As helium is the simplest multi–electron atom, it was the apparent choice for the next step. To do that, we designed energy optimised even–tempered basis sets for the soft–wall confined hydrogen atom for various stiffness values. Using these basis sets, once again, we were able to confirm that with increasing stiffness level, we are able to approach hard–wall confined helium atom results.

In order to confirm our assumptions, we also carried a detailed study on the soft–wall confined argon atom. We followed a similar technique used for studying the soft–wall confined hydrogen and helium atoms. It was not surprising to conclude that both energy eigenvalues and the dipole polarisabilities of the two systems undergo the same transition in the same interval for the confinement radius. However, it was interesting to note a rather different behaviour when it comes to the electron correlation of the soft–wall confined argon atom. Although our calculations have been carried out within the same range of radius, we were

not able to see a decrease in the electron correlation energy around the radius corresponding to the zero–energy wave function of the helium atom. This was merely due to the radius that corresponds to the zero–energy wave function for the soft–wall confined argon atom being way out in the range of our study. Therefore, this is yet another confirmation to our conclusions that systems trapped in cavities attain much higher energies compared to those of free systems.

Our framework for this thesis was set in non–relativistic mechanics. An interesting extension to this topic would be studying the relativistic soft–wall confined systems.

Aside from the mathematically trivial case, particle in a box is usually the first problem that an undergraduate student of non–relativistic quantum mechanics is asked to solve. Normally, the student goes further into obtaining the bound states solution of a particle in a finite square well. It is much later that one gets involved with more involved problems like the three dimensional Coulomb problem. Unfortunately, in relativistic quantum mechanics the story is reversed. One can hardly find a textbook on relativistic quantum mechanics where one dimensional problem of particle in a potential box is solved before the relativistic hydrogen atom is. The difficulty is that if this is to be done from the start, then ones is forced to get into subtle issues like Klein paradox, electron–positron pair production, stability of the vacuum and appropriate boundary conditions. In fact, the subtleties are so exasperating to the extend that Adler [1] ruled out this problem all together and noted that "*. . . rules out any consideration of an infinite square well in the relativistic theory.*" In non–relativistic case, one finds a subspace of the solution space that satisfies the physical boundary conditions. This makes the non–relativistic Hamiltonian self–adjoint. However, in relativistic case, the solution space of some problems is far too small to support a self–adjoint structure for the Dirac Hamiltonian. Some attempts to overcome this problem were made by performing what is called self–adjoint extension of Hamiltonian resulting in a larger solution space. For example, boundary conditions could be relaxed without

violating the physics of the problem and/or the potential is slightly modified or regularised. For the one dimensional Dirac equation with the box potential, this approach made it possible to find a subspace that satisfies the appropriate boundary conditions in which a real energy spectrum could be obtained [2, 3, 58].

In 1932, Plesset [53] studied the Dirac electron in simple fields by transforming the relativistic wave equations for the Dirac electron into a symmetric canonical form. In his elegant work, he was able to investigate the characteristics of solutions of these relativistic equations for simple fields. Following his work, Titchmarsh [66] extended the results presented by Plesset [53] using eigenfunction expansions. This method allowed Titchmarsh to investigate various types of the potential functions from simple polynomial ones to reciprocal higher order ones. Although it is natural to expect that one would study hard–wall confined Dirac particle, it was not until 2013 that this new avenue is taken under study. Very first study on treatment of a hard–wall confined Dirac particle presented by Bakke [9] in 2013. In their work, they discussed the confinement of a Dirac particle to a hard–wall confining potential induced by non–inertial effects. They showed that the geometry of the manifold can play the role of a hard–wall confining potential due to non–inertial effects yielding bound state solutions of the Dirac equation analogous to having a Dirac particle confined to a quantum dot with a hard–wall confining potential. Although their approach is one of the first attempts, it does bring a very elegant solution to the relativistic particle confined in a hard–wall potential.

Relativistic effects on molecular properties and energies are ubiquitous in chemistry. Their consideration in quantum chemical calculations requires Dirac's theory of the electron, whose application is not without obstacles. Douglas-Kroll-Hess theory accomplishes a decoupling of positive– and negative–energy eigenstates of the Dirac one–electron Hamiltonian by an expansion in the external potential. At low orders, this expansion already converges and provides efficient relativistic Hamiltonians to be used in routine quantum chemical calculations.

As a first step towards calculating ground state energy shift of a soft–wall confined relativistic hydrogen atom, one can employ Gaussian09's Douglas-Kroll-Hess approximation method with basis sets introduced in Chapter 4. This will also provide an insight into relativistic effects. It is our belief that introducing a soft–wall potential, similar to the one introduced in this thesis, into the one–particle Dirac equation will bring its complications. The Klein paradox [35]–[59] and self–adjointness of the relativistic Hamiltonian operator are some of those complications that needs to be addressed. In addition, since there will be no analytic solution, it will be necessary to approach the problem numerically in a similar fashion in Chapter 3. Although the work on studying a relativistic particle in a soft–wall potential requires extensive work on both theoretical and numerical aspects, it is certainly an interesting and natural extension of this thesis.

Appendix A

Atomic Units

Electronic structure theorists generally employ "atomic units" (a.u.) on which three defining base units are the fundamental natural constants e (electronic charge), m_e (electronic mass), $\hbar$ (reduced Plank's constant) rather than arbitrary chosen macroscopic objects. These units have many advantages. First of all, they bring the electronic Schrödinger equation to its simplest form, expressed in pure numbers only. This way the equation can be solved once for all without worrying about remeasuring physical quantities. The atomic units are also sensibly proportioned and sized such that the key atomic properties tend to have values of order of unity. For instance, the hydrogenic 1s orbital radius turns out to be exactly 1 a.u. of length. By working out the combination of e, m_e and $\hbar$ which practical units match those of a desired physical property, such as energy ($m_e e^4/\hbar^2$), length ($\hbar^2/m_e e^2$), and so forth, one obtains the corresponding atomic unit of that property which is usually designated simply as "a.u." rather than assigned a special symbol and name of each property. Tables A.1–A.3 provide conversion factors from a.u. to SI units and a variety of practical units in common usage. An abbreviated exponential notation is used in which 7.6554(4) means 7.6554×10^4.

Table A.1: Conversion factors from atomic units to SI units.

Atomic unit (base units)	SI Value	Name (symbol)
Mass (m_e)	9.10939(−31) kg	Mass of the electron
Charge (e)	1.602188(−19) C	Electronic charge
Angular momentum ($\hbar$)	1.05457(−34) J/(s·rad)	Plank's constant/2π
Energy ($m_e e^4/\hbar^2$)	4.35975(−18) J	Hartree (H)
Length ($\hbar^2/m_e e^2$)	5.29177(−11) m	Bohr; Bohr radius (a_0)
Time ($\hbar^3/m_e e^4$)	2.41888(−17) s	Jiffy
Elect. dipole moment ($\hbar^2/m_e e$)	8.47836(−30) C·m	2.54177 Debye (D) units
Mag. dipole moment ($e\hbar/2m_e$)	9.27402(−24) J/T	Bohr magneton (μ_B)

Table A.2: Fundamental constants in atomic and SI units.

Physical constant	Symbol	Value (a.u.)	Value (SI)
Rydberg constant	R_∞	2.29253(2)	1.03737(−23) m^{-1}
Planck constant	h	6.28319(= 2π)	6.62608(−34) J·s
Speed of light	c	1.37036(2)	2.99792(8) m/s
Proton mass	m_p	1.83615(3)	1.67262(−27) kg
Atomic mass unit	amu	1.82289(3)	1.66054(−27) kg
Fine structure constant	α	7.29735(−3)	7.29735(−3)

Table A.3: Energy conversion table for non–SI units

	Value in non–SI units					
Unit	a.u.	kcal/mol	eV	cm^{-1}	Hz	K
a.u.	1	6.27510(2)	2.72114(1)	2.19475(5)	6.57968(15)	3.15773(5)
kcal/mol	1.59360(−3)	1	4.33641(−2)	3.49755(2)	1.04854(13)	5.03217(2)
eV	3.67493(−2)	2.30605(1)	1	8.06554(3)	2.41799(14)	1.16044(4)
cm^{-1}	4.55634(−6)	2.85914(−3)	1.23984(−4)	1	2.99792(10)	1.43877
Hz	1.51983(−16)	9.5371(−14)	4.13567(−15)	3.33564(−11)	1	4.79922(−11)
K	3.16683(−6)	1.98722(−3)	8.61739(−5)	6.95039(−1)	2.08367(10)	1

Appendix B

Kummer's Differential Equation

A confluent hypergeometric function is a solution of a confluent hypergeometric differential equation, which is a degenerate form of a hypergeometric differential equation where two of the three regular singularities merge into an irregular singularity. The term "confluent" refers to the merging of singular points of families of differential equations. Kummer's function $M(a, b, c)$, introduced by Kummer in 1837, is a solution to Kummer's differential equation of the form

$$x\frac{\mathrm{d}^2y}{\mathrm{d}x^2} + (b - x)\frac{\mathrm{d}y}{\mathrm{d}x} - ay = 0,$$

with a regular point at 0 and an irregular singularity at $+\infty$. It has two linearly independent solutions; $M(a, b, x)$ and $U(a, b, x)$. Kummer's function of the first kind, M, is a generalized hypergeometric series given by

$$M(a, b, x) = \sum_{n=0}^{+\infty} \frac{(a)_n x^n}{(b)_n n!} = {}_1F_1(a, b, x),$$

where

$$(a)_n = a(a + 1)(a + 2) \cdots (a + n - 1)$$

is the rising factorial. If a and b are integers, $a < 0$ and either $b > 0$ or $b < a$, then the series yields a polynomial with a finite number of terms. If b is a non-positive

integer, then ${}_1F_1(a,b,x)$ is undefined.

Another solution of Kummer's equation is the Tricomi confluent hypergeometric function $U(a,b,x)$ introduced by Francesco Tricomi in 1947. The function U is defined in terms of Kummer's function M by

$$U(a,b,x) = \frac{\Gamma(1-b)}{\Gamma(a-b+1)}M(a,b,x) + \frac{\Gamma(b-1)}{\Gamma(a)}x^{1-b}M(a-b+1,2-b,x).$$

$M(a,b,x)$ can be represented as an integral

$$M(a,b,x) = \frac{\Gamma(b)}{\Gamma(a)\Gamma(b-a)}\int_0^1 e^{xu}u^{a-1}(1-u)^{b-a-1}\mathrm{d}u,$$

for $Re(b) > Re(a) > 0$. In addition, U can be obtained by the Laplace integral

$$U(a,b,x) = \frac{1}{\Gamma(a)}\int_0^{+\infty} e^{-xt}t^{a-1}(1+t)^{b-a-1}\mathrm{d}t,$$

where $Re(a) > 0$. This integral defines a solution in the right half-plane $Re(x) > 0$.

Finally, we mention the connection with Laguerre polynomials. In terms of these polynomials, Kummer's functions have several expansions. Most widely used one is the following expansion

$$L_n^m(x) = \frac{(n+m)!}{n!m!}{}_1F_1(-n,m+1,x).$$

We refer to these polynomials as *generalized Laguerre polynomials*, because the independent definition that may be introduced does not presume that m is a non-negative integer. The independent definition is

$$L_n^m(x) = \frac{1}{n!}e^x x^{-m}\frac{\mathrm{d}^n}{\mathrm{d}x^n}\left(x^{n+m}e^{-x}\right).$$

Appendix C

Numerov Method

Numerov's numerical method [50, 51] is used in standard applications to solve ordinary second–order differential equations in which the first–order derivative does not appear, i.e., differential equations of the form

$$\left(\frac{\mathrm{d}^2}{\mathrm{d}r^2} + f(r)\right)\psi(r) = g(r), \tag{C.1}$$

where $f(r)$ and $g(r)$ are continuous functions on a predefined domain, say $[a, b]$. We want to solve this equation as a boundary value problem, i.e., $\psi(a)$ and $\psi(b)$ are given. The first thing is to choose a step size h for the interval. This implies the solution $\psi(r)$ is obtained as a discrete set of points on the defined mesh. Thus, Eq. (C.1), on the mesh, is

$$\left(\frac{\mathrm{d}^2}{\mathrm{d}r^2} + f_i\right)\psi_i = g_i,$$

for all i, where $f_i = f(i)$. It is well known that the three–point central difference formula for the second derivative is given by

$$\psi_i'' = \frac{\psi_{i+1} - 2\psi_i + \psi_{i-1}}{h^2} - \frac{h^2}{12}\psi'''' + O\left(h^4\right), \tag{C.2}$$

where $\psi_{i\pm k} = \psi(r_i \pm kh)$, for $k \in \{-1, 0, 1\}$. Eq. (C.1) can be used to calculate the fourth–order derivative ψ''''. Substitution of (C.2) into (C.1) yields

$$\psi'''' = -\frac{1}{h^2}\left[f_{i+1}\psi_{i+1} - 2f_i\psi_i + f_{i-1}\psi_{i-1} - g_{i+1} + 2g_i - g_{i-1}\right] + O\left(h^2\right).$$

Thus, Eq. (C.2) becomes

$$\left(1 + \frac{h^2}{12}f_{i+1}\right)\psi_{i+1} = 2\left(1 - \frac{5h^2}{12}f_i\right)\psi_i - \left(1 + \frac{h^2}{12}f_{i+1}\right)\psi_{i-1} + \frac{h^2}{12}\left(g_{i+1} + 10g_i + g_{i-1}\right) + O\left(h^6\right).$$

Above relation is the desired one that connects ψ_{i+1}, ψ_i and ψ_{i-1}. The error is one order smaller than fourth–order Runge–Kutta.

In our case, $g(r) = 0$. Hence, forward and backward relations are given by rather simpler formulae

$$\left(1 + \frac{h^2}{12}f_{i+1}\right)\psi_{i+1} = 2\left(1 - \frac{5h^2}{12}f_i\right)\psi_i - \left(1 + \frac{h^2}{12}f_{i-1}\right)\psi_{i-1},$$
$$\left(1 + \frac{h^2}{12}f_{i-1}\right)\psi_{i-1} = 2\left(1 - \frac{5h^2}{12}f_i\right)\psi_i - \left(1 + \frac{h^2}{12}f_{i+1}\right)\psi_{i+1}.$$

Once we have two values of the solution ψ_i at successive mesh points, we can generate the entire solution. The boundary conditions, along with asymptotic nature of the function, are used to specify these two required initial values.

Appendix D

The Static Dipole Polarisability

The expression for the static dipole polarisability follows from perturbation theory. The perturbation expression for the ground state energy E_0 is given by

$$E_0 = E_0^{(0)} + E_0^{(1)} + E_0^{(2)} + \cdots \tag{D.1}$$

$$= E_0^{(0)} + \left\langle 0 \middle| H^{(1)} \middle| 0 \right\rangle + \sum_{n \neq 0} \frac{\left| \left\langle 0 \middle| H^{(1)} \middle| n \right\rangle \right|^2}{E_0 - E_n} + \cdots \tag{D.2}$$

A homogeneous electric field perturbation along the z–axis, $H^{(1)} = -\mu_z F$, gives

$$E_0 = E_0^{(0)} - \langle 0 \left| \mu_z \right| 0 \rangle F + \left\{ \sum_{n \neq 0} \frac{\left| \langle 0 \left| \mu_z \right| n \rangle \right|^2}{E_0 - E_n} \right\} F^2 + \cdots \tag{D.3}$$

The dipole polarisability is defined as the second derivative of the expression in Eq.(D.3) with respect to the field strength F which results in the following expression

$$\alpha_{zz} = -\left(\frac{\mathrm{d}^2 E}{\mathrm{d}F^2} \right)\Bigg|_{F=0} = 2 \sum_{n \neq 0} \frac{\left| \langle 0 \left| \mu_z \right| n \rangle \right|^2}{E_0 - E_n}. \tag{D.4}$$

Note that the first derivative results in the expectation value of the dipole moment operator $\langle 0 \left| \mu_z \right| 0 \rangle$ which gives the permanent electric dipole moment.

Eq. (D.4) shows the dipole polarisability α_{zz} with two subscripts. This is due to the

fact that the dipole polarisability is regarded as a second rank tensor. When an external field is applied along the z–axis, a dipole maybe induced with components μ_z, μ_y and μ_z, where

$$\mu_i = \alpha_{iz} F_z, \quad i = x, y, x.$$

In general, the diagonal element α_{zz} dominates the other two when the electric field is along the z–axis as the induced dipole moment is usually almost parallel to the applied electric field. For example, in a closed shell atom the dipole polarisability can be reduced to a scalar quantity in which the only surviving polarisability tensor component is the one parallel to the applied electric field.

Appendix E

Hilbert Spaces

Hilbert spaces arise naturally in many applications. Therefore, we see it fit to make a brief introduction here. Throughout the description, we consider linear complex spaces for completeness. We begin with definition of an inner product.

Definition 1 *An* inner product *defined on a complex linear space X is a map*

$$\langle \cdot, \cdot \rangle : X \times X \to \mathbf{C},$$

such that for all $\mathbf{x}, \mathbf{y}, \mathbf{z} \in X$ and $\alpha, \beta \in \mathbf{C}$,

1. $\langle \mathbf{x}, \mathbf{x} \rangle \geq 0$,
2. $\langle \mathbf{x}, \mathbf{x} \rangle = 0$ *if and only if* $\mathbf{x} = \mathbf{0}$,
3. $\langle \mathbf{x}, \mathbf{y} \rangle = \langle \mathbf{y}, \mathbf{x} \rangle^*$,
4. $\langle \mathbf{x}, \alpha\mathbf{y} + \beta\mathbf{z} \rangle = \alpha^* \langle \mathbf{x}, \mathbf{y} \rangle + \beta^* \langle \mathbf{x}, \mathbf{z} \rangle$.

We call a linear space with an inner product an inner product space.

Note that if X is a real linear space, $\langle \cdot, \cdot \rangle$ becomes bilinear as the operation is linear in both first and second arguments.

For a linear space X, we can define a 2–norm on X by

$$\|\mathbf{x}\| = \sqrt{\langle \mathbf{x}, \mathbf{x} \rangle}. \tag{E.1}$$

Thus, any inner product space is a linear normed space.

Definition 2 *A* Hilbert space *is a complete inner product space.*

In particular, every Hilbert space is a Banach space with respect to the norm defined in (E.1). In what follows, we will present examples that occur frequently in many application in physics, chemistry and other natural sciences.

Example 1 *The standard inner product on* $\mathbb{C}^n$ *is given by*

$$\langle \mathbf{x}, \mathbf{y} \rangle = \sum_{i=1}^{n} x_i y_i^*,$$

where $\mathbf{x} = (x_1, x_2, \ldots, x_n)$, $\mathbf{y} = (y_1, y_2, \ldots, y_n)$, *and* $x_i, y_i \in \mathbb{C}$. *This space is complete and, therefore, it is a finite–dimensional Hilbert space.*

Example 2 *Let* $C([a,b])$ *denote the space of all complex–valued continuous functions defined on* $[a,b]$. *We define an inner product on* $C([a,b])$ *by*

$$\langle f, g \rangle = \int_a^b f(\xi)\, g(\xi)^*\, \mathrm{d}\xi,$$

where $f, g : [a,b] \to \mathbb{C}$. *This space is not complete, hence, not a Hilbert space. However, the completion of* $C([a,b])$ *with respect to the associated norm*

$$\|f\| = \left(\int_a^b \left| f(\xi) \right|^2 \right)^{1/2} \mathrm{d}\xi,$$

denoted by $L^2([a,b])$*–space of square Lebesgue integrable functions, forms a Hilbert space. Note that, although* $L^p([a,b])$ *spaces are Banach spaces, these are not Hilbert spaces except for* $p = 2$.

Similarly to Example 2, if $\mathbb{T} = \{z \in \mathbb{C} : |z| = 1\}$, then $L^2(\mathbb{T})$ is a Hilbert space of square–integrable functions $f : \mathbb{T} \to \mathbb{C}$ with the inner product

$$\langle f, g \rangle = \int_{\mathbb{T}} f(\xi)\, g(\xi)^* \, \mathrm{d}\xi.$$

Example 3 *We can also define the Hilbert space $\ell^2(\mathbb{Z})$ of doubly infinity complex sequences by*

$$\ell^2(\mathbb{Z}) = \left\{ (z_n)_{n=-\infty}^{+\infty} \,\middle|\, \sum_{n=-\infty}^{+\infty} |z_n|^2 < +\infty \right\}.$$

The space $\ell^2(\mathbb{Z})$ is a linear complex space with operations addition and multiplication by a scalar. An inner product can be given by

$$\langle x, y \rangle = \sum_{n=-\infty}^{+\infty} x_n y_n^*.$$

Example 4 *Let $\mathbb{C}^{n\times m}$ denote the space of all $n \times m$ matrices with complex entries. We define an inner product on $\mathbb{C}^{n\times m}$ by*

$$\langle A, B \rangle = \mathrm{tr}\left(AB^{\dagger}\right),$$

where $\dagger$ denotes the complex-conjugate transpose of a matrix. More specifically, if $A = \left(a_{ij}\right)$ and $B = \left(b_{ij}\right)$, then

$$\langle A, B \rangle = \sum_{i=1}^{n} \sum_{j=1}^{m} a_{ij} b_{ij}^*.$$

This inner product is equal to the one obtained by identification of a matrix in $\mathbb{C}^{n\times m}$ with a vector in $\mathbb{C}^{nm}$. The corresponding norm,

$$\|A\| = \left(\sum_{i=1}^{n} \sum_{j=1}^{m} \left|a_{ij}\right|^2 \right)^{1/2},$$

is called the Hilbert-Schmidt *norm.*

Example 5 *Let $C^k([a, b])$ be the space of functions with k continuous derivatives on $[a, b]$.*

We define an inner product on $C^k([a,b])$ *by*

$$\langle f, g\rangle = \sum_{j=0}^{k} \int_a^b f^{(j)}(\xi)\, g^{(j)}(\xi)^*\, \mathrm{d}\xi.$$

The corresponding norm is given by

$$\|f\| = \left(\sum_{j=0}^{k} \int_a^b \left| f^{(j)}(\xi) \right|^2 \mathrm{d}\xi \right)^{1/2}.$$

The space $C^k([a,b])$ *is an inner product space, however, it is not a complete one. Completion of* $C^k([a,b])$ *with respect to the given norm is a* Sobolev *space denoted by* $H^k((a,b))$.

The inner product structure of Hilbert spaces allows us to introduce the concept of orthogonality, which makes it possible to visualise vectors and linear subspaces of Hilbert spaces in a geometric way.

Definition 3 *Let H be a Hilbert space, and* $\mathbf{x}, \mathbf{y} \in H$. *We say that* $\mathbf{x}$ *and* $\mathbf{y}$ *are orthogonal, written* $\mathbf{x} \perp \mathbf{y}$, *if their inner product,* $\langle \mathbf{x}, \mathbf{y} \rangle$, *is zero, i.e.,* $\langle \mathbf{x}, \mathbf{y} \rangle = 0$. *We say that the subsets A and B are orthogonal, if* $\mathbf{x} \perp \mathbf{y}$ *for every* $\mathbf{x} \in A$ *and* $\mathbf{y} \in B$. *The orthogonal complement of* $A^\perp$ *of a subset A is the set of vectors orthogonal to A,*

$$A^\perp = \left\{ \mathbf{x} \in H \,\middle|\, \mathbf{x} \perp \mathbf{y} \text{ for all } \mathbf{y} \in A \right\}.$$

Therefore, a subset U of non–zero vectors in a Hilbert space H is orthogonal if any two distinct elements in U are orthogonal. A set of vectors U is orthonormal if is orthogonal and $\|\mathbf{u}\| = 1$ for all $\mathbf{u} \in U$, in which case vectors are said to be normalised. An orthonormal basis for a Hilbert space is an orthonormal set such that every vector in the space can be writing as a linear combination of those in the basis. Every Hilbert space has an orthonormal basis which may be finite, countably infinite, or uncountable. The reason behind mentioning orthonormal basis sets is the fact that *separable* Hilbert spaces – Hilbert spaces with finite or countable infinite orthonormal basis set – play an important role in quantum theory.

Example 6 *A set of vectors* $\{\mathbf{e}_1, \mathbf{e}_2, \ldots, \mathbf{e}_n\}$ *is an orthonormal basis of the finite dimensional Hilbert space* $\mathbb{C}^n$ *if*

1. $\left\langle \mathbf{e}_i, \mathbf{e}_j \right\rangle = \delta_{ij}$ *for* $1 \leq i, j \leq n$,

2. *for all* $\mathbf{x} \in \mathbb{C}^n$, *there are unique coordinates* $x_k \in \mathbb{C}$ *such that*

$$\mathbf{x} = \sum_{i=1}^{n} x_i \mathbf{e}_i,$$

where δ_{ij} *is the Kronecker delta*

$$\mathbf{e}_i \cdot \mathbf{e}_j = \delta_{ij} = \delta_{ji} = \begin{cases} 1 & \text{if } i = j, \\ 0 & \text{otherwise.} \end{cases} \tag{E.2}$$

The orthogonality of the basis implies that we can recover each coordinate of a given vector $\mathbf{x}$ *simply by* $x_k = \langle \mathbf{e}_k, \mathbf{x} \rangle$. *For example, the standard orthonormal basis of* $\mathbb{C}^n$ *consists of the vectors*

$$\mathbf{e}_1 = (1, 0, 0, \ldots, 0), \quad \mathbf{e}_2 = (0, 1, 0, \ldots, 0), \quad \ldots, \quad \mathbf{e}_n = (0, 0, 0, \ldots, 1).$$

Example 7 *The set of functions* $\{e_n(x) \,|n \in \mathbb{Z}\}$, *where*

$$e_n(x) = \frac{1}{\sqrt{2\pi}} \mathrm{e}^{\mathrm{i}nx},$$

is an orthonormal basis of the space $L^2(\mathbb{T})$ *of* 2π*–periodic functions, called the Fourier basis. The inverse Fourier transform* $\mathcal{F}^{-1} : \ell^2(\mathbb{Z}) \to L^2(\mathbb{T})$ *defined by*

$$\mathcal{F}^{-1}(c_k) = \frac{1}{\sqrt{2\pi}} \sum_{k=-\infty}^{+\infty} c_k \mathrm{e}^{\mathrm{i}kx},$$

is a Hilbert space isomorphism between $\ell^2(\mathbb{Z})$ *and* $L^2(\mathbb{T})$. *Both Hilbert spaces are separable with a countably infinite basis.*

The introduction of quantum mechanics in the 1920s is one of the most profound events in the history of our understanding of the atomic world. The theory itself developed with an impressive pace and researchers did not have time to think much about the mathematical structures they employed. It was von Neumann who realized that Hilbert spaces are the natural settings for quantum mechanics.

One of the simplest quantum mechanical systems is the particle in a box model which describes the movement of a single particle, like an electron, between two impenetrable walls, a system similar to the models used in this thesis. The state of such a particle is described, at time t, by the term $\psi(\cdot, t) \in L^2([0, L])$ which is a vector in the Hilbert space of complex valued square–integrable functions on $[0, L]$. This function is called the wave function of the particle. Of course, this description in not valid in Newtonian mechanics where the state of a particle is described by the position and the velocity of the particle at any time t. The physical interpretation of the wave function is that $\left|\psi\right|^2$ is a probability density. If the position ξ of the particle is measured at some time t, then the probability of observing the particle in the interval $0 \leq a < b \leq L$ is given by

$$P(a \leq \xi \leq b, t) = \frac{\int_a^b \left|\psi(\xi, t)\right|^2 \mathrm{d}\xi}{\int_0^L \left|\psi(\xi, t)\right|^2 \mathrm{d}\xi}.$$

Another way in which L^2–spaces arise naturally is as energy spaces. The quantity

$$\int \left|f(\xi)\right|^2 \mathrm{d}\xi$$

often represents the total energy of a physical system, or, some other fundamental quantity where one considers systems that this quantity is finite. For instance, in fluid mechanics, if $\mathbf{u}(\mathbf{x})$ is the velocity of a fluid at the point $\mathbf{x}$, then

$$\int_V |\mathbf{u}(\mathbf{x})|^2 \mathrm{d}\mathbf{x}$$

is proportional to the kinetic energy of the fluid in volume V. This energy should be finite in any finite volume V. Another example is the electromagnetic field described by two vector fields, the electric field $\mathbf{E}$ and the magnetic field $\mathbf{B}$. In suitable units, the energy of the electromagnetic field in a region Ω is given by

$$\int_\Omega \left\{ |\mathbf{E}(\mathbf{x})|^2 + |\mathbf{B}(\mathbf{x})|^2 \right\} d\mathbf{x}.$$

The requirement of the finite energy leads naturally to the requirement that $\mathbf{E}$ and $\mathbf{B}$ belong to appropriate L^2–spaces.

Appendix F

Variational Methods

F.1 The Ritz–Rayleigh Variational Method

The Ritz–Rayleigh variational method is a useful and accurate tool for solving problems in different fields such as quantum chemistry, molecular physics and solid state physics, among others. This method allows us to approximate the ground state energy of a system without directly solving the Schrödinger equation. The variational method is based on the following theorem.

Theorem 1 *Given a system whose Hamiltonian operator $\mathcal{H}$ is time independent and whose lowest-energy eigenvalue is E_0, if ϕ is any normalized, well–behaved function of the coordinates of the system's particles that satisfies the boundary conditions of the problem, then*

$$\int \phi^* \mathcal{H} \phi \, d\tau \geq E_0. \tag{F.1}$$

Proof F.1.1 *Let $\{\psi\}_{k\in\Delta}$ be a complete, orthonormal set of eigenfunctions of $\mathcal{H}$, where Δ is an indexing set. Assume that*

$$\phi = \sum_k a_k \psi_k, \tag{F.2}$$

where

$$\mathcal{H}\psi_k = E_k \psi_k.$$

Substitution of (F.2) into (F.1) yields

$$\int \phi^* \mathcal{H} \phi \mathrm{d}\tau = \int \sum_k a_k^* \psi_k^* \mathcal{H} \sum_j a_j \psi_j \mathrm{d}\tau = \int \sum_k a_k^* \psi_k^* \sum_j a_j \mathcal{H} \psi_j \mathrm{d}\tau.$$

Assuming the validity of interchanging the integration and infinite summations, we get

$$\begin{aligned} \int \phi^* \mathcal{H} \phi \mathrm{d}\tau &= \int \sum_k a_k^* \psi_k^* \sum_j a_j E_j \psi_j \mathrm{d}\tau \\ &= \sum_k \sum_j a_k^* a_j E_j \int \psi_k^* \psi_j \mathrm{d}\tau = \sum_k \sum_j a_k^* a_j E_j \delta_{kj}. \end{aligned}$$

Hence, we have

$$\int \phi^* \mathcal{H} \phi \mathrm{d}\tau = \sum_k a_k^* a_k E_k = \sum_k |a_k|^2 E_k.$$

Since E_0 is the lowest energy eigenvalue of $\mathcal{H}$, we have $E_k \geq E_0$, or, equivalently,

$$\sum_k |a_k|^2 E_k \geq \sum_k |a_k|^2 E_0,$$

which implies

$$\int \phi^* \mathcal{H} \phi \mathrm{d}\tau = \sum_k |a_k|^2 E_k \geq \sum_k |a_k|^2 E_0.$$

Because ϕ is normalized, we have

$$\int \phi^* \phi \mathrm{d}\tau = 1.$$

Then, we have

$$1 = \int \phi^* \phi \mathrm{d}\tau = \int \sum_k a_k^* \psi_k^* \sum_j a_j \psi_j \mathrm{d}\tau = \sum_k |a_k|^2 .$$

Hence, we finally see that

$$\int \phi^* \mathcal{H} \phi \mathrm{d}\tau = \sum_k |a_k|^2 E_k \geq \sum_k |a_k|^2 E_0 = E_0.$$

Remark 5 *If ϕ is not a normalized function, then to apply the variational theorem we multiply ϕ by a normalization constant N so that $N\phi$ is normalized. Replacing ϕ by $N\phi$, we have*

$$|N|^2 \int \phi^* \mathcal{H} \phi \mathrm{d}\tau \geq E_0,$$

or, equivalently,

$$\frac{\int \phi^* \mathcal{H} \phi \mathrm{d}\tau}{\int \phi^* \phi \mathrm{d}\tau} \geq E_0, \tag{F.3}$$

where

$$|N|^2 = \frac{1}{\int \phi^* \phi \mathrm{d}\tau}.$$

Remark 6 *The function ϕ is called a trial variation function, and the integral in (F.1) is called the variational integral.*

F.2 The Method of Linear Variation Functions

A special kind of variation function widely used in the study of molecules is the linear variation function. A linear variation function is a linear combination of n linearly independent functions $f_1, f_2, \ldots, f_n$:

$$\phi = c_1 f_1 + c_2 f_2 + \cdots + c_n f_n = \sum_{i=1}^{n} c_i f_i,$$

where ϕ is the trial function and the coefficients c_i are parameters to be determined by minimizing the variational integral. The basis functions f_i must satisfy the boundary conditions of the problem.

Employing Theorem 1, we have

$$\int \phi^* \phi \mathrm{d}\tau = \int \sum_{i=1}^{n} c_i f_i \sum_{k=1}^{n} c_k f_k \mathrm{d}\tau = \sum_{i=1}^{n} \sum_{k=1}^{n} c_i c_k \int f_i f_k \mathrm{d}\tau.$$

We define the overlap integral S_{ik} as

$$S_{ik} \stackrel{\text{def}}{=} \int f_i f_k \mathrm{d}\tau. \tag{F.4}$$

Thus, we have

$$\int \phi^* \phi \mathrm{d}\tau = \sum_{i=1}^{n} \sum_{k=1}^{n} c_i c_k S_{ik}.$$

Note that S_{ik} is not necessarily equal to δ_{ik}, since there is no reason to suppose that the functions f_i are mutually orthogonal. They are not necessarily the eigenfunctions of any operator. For the sake of simplicity, we assume that the functions f_i are real-valued functions. The numerator of inequality (F.3) is

$$\int \phi^* \mathcal{H} \phi \mathrm{d}\tau = \int \sum_{i=1}^{n} c_i f_i \mathcal{H} \sum_{k=1}^{n} c_k f_k \mathrm{d}\tau = \sum_{i=1}^{n} \sum_{k=1}^{n} c_i c_k \int f_i \mathcal{H} f_k \mathrm{d}\tau.$$

Let

$$H_{ik} \stackrel{\text{def}}{=} \int f_i \mathcal{H} f_k \mathrm{d}\tau.$$

Thus, we write

$$\int \phi^* \mathcal{H} \phi \mathrm{d}\tau = \sum_{i=1}^{n} \sum_{k=1}^{n} c_i c_k H_{ik}.$$

The variational integral W is then given by

$$W = \frac{\int \phi^* \mathcal{H} \phi \mathrm{d}\tau}{\int \phi^* \phi \mathrm{d}\tau} = \frac{\sum_{i=1}^{n} \sum_{k=1}^{n} c_i c_k H_{ik}}{\sum_{i=1}^{n} \sum_{k=1}^{n} c_i c_k S_{ik}},$$

or, equivalently,

$$W \sum_{i=1}^{n} \sum_{k=1}^{n} c_i c_k S_{ik} = \sum_{i=1}^{n} \sum_{k=1}^{n} c_i c_k H_{ik}. \tag{F.5}$$

We now minimize W so as to approach as closely as we can to E_0. The variational integral W is a function of the n independent variables $c_1, c_2, \ldots, c_n$, i.e., $W = W(c_1, c_2, \ldots, c_n)$. A necessary condition for a minimum in a function W of several variables is that its partial derivative with respect to each of the variables must be

zero at the minimum:

$$\frac{\partial W}{\partial c_j} = 0,$$

for $j \in \{1, 2, \ldots, n\}$. Differentiating (F.5) partially with respect to each c_i, we obtain n equations, for $j \in \{1, 2, \ldots, n\}$:

$$\frac{\partial W}{\partial c_j} \sum_{i=1}^{n} \sum_{k=1}^{n} c_i c_k S_{ik} + W \frac{\partial}{\partial c_j} \sum_{i=1}^{n} \sum_{k=1}^{n} c_i c_k S_{ik} = \frac{\partial}{\partial c_j} \sum_{i=1}^{n} \sum_{k=1}^{n} c_i c_k H_{ik}.$$

It is easily seen that

$$\frac{\partial}{\partial c_j} \sum_{i=1}^{n} \sum_{k=1}^{n} c_i c_k S_{ik} = \sum_{i=1}^{n} \sum_{k=1}^{n} \left[\frac{\partial}{\partial c_j} (c_i c_k) \right] S_{ik} = \sum_{i=1}^{n} \sum_{k=1}^{n} \left(c_k \frac{\partial c_i}{\partial c_j} + c_i \frac{\partial c_k}{\partial c_j} \right) S_{ik}.$$

The coefficients c_i are independent variables and therefore

$$\frac{\partial c_i}{\partial c_j} = \delta_{ji} = \begin{cases} 0 & \text{if } i \neq j, \\ 1 & \text{if } i = j. \end{cases},$$

which implies

$$\begin{aligned} \frac{\partial}{\partial c_j} \sum_{i=1}^{n} \sum_{k=1}^{n} c_i c_k S_{ik} &= \sum_{k=1}^{n} \sum_{i=1}^{n} c_k \delta_{ji} S_{ik} + \sum_{i=1}^{n} \sum_{k=1}^{n} c_i \delta_{jk} S_{ik} \\ &= \sum_{k=1}^{n} c_k S_{jk} + \sum_{i=1}^{n} c_i S_{ij} \\ &= \sum_{k=1}^{n} c_k S_{jk} + \sum_{k=1}^{n} c_k S_{kj} = \sum_{k=1}^{n} c_k S_{jk} + \sum_{k=1}^{n} c_k S_{jk} \\ &= 2 \sum_{k=1}^{n} c_k S_{jk}, \end{aligned}$$

since

$$S_{ij} = S_{ji}^{*} = S_{ji}.$$

Similarly, we have

$$\frac{\partial}{\partial c_j} \sum_{i=1}^{n} \sum_{k=1}^{n} c_i c_k H_{ik} = 2 \sum_{k=1}^{n} c_k H_{jk}.$$

Hence, we get

$$2W \sum_{k=1}^{n} c_k S_{jk} = 2 \sum_{k=1}^{n} c_k H_{jk},$$

or, equivalently,

$$\sum_{k=1}^{n} \left[\left(H_{jk} - S_{jk} W \right) c_k \right] = 0, \tag{F.6}$$

for $j \in \{1, 2, \ldots, n\}$. Eq. (F.6) is a set of n simultaneous, linear, homogeneous equations in n unknowns $c_1, c_2, \ldots, c_n$. For the general case of n functions $f_1, f_2, \ldots, f_n$, we have

$$\begin{aligned}
(H_{11} - S_{11} W)\, c_1 + (H_{12} - S_{12} W)\, c_2 + \cdots + (H_{1n} - S_{1n} W)\, c_n &= 0, \\
(H_{21} - S_{21} W)\, c_1 + (H_{22} - S_{22} W)\, c_2 + \cdots + (H_{2n} - S_{2n} W)\, c_n &= 0, \\
&\vdots \\
(H_{n1} - S_{n1} W)\, c_1 + (H_{n2} - S_{n2} W)\, c_2 + \cdots + (H_{nn} - S_{nn} W)\, c_n &= 0.
\end{aligned}$$

We know that for a homogeneous system to have a non-trivial solution, the determinant of the coefficients must vanish, i.e.,

$$\det \left(H_{ji} - S_{ji} W \right) = 0,$$

or, equivalently,

$$\begin{vmatrix}
H_{11} - S_{11} W & H_{12} - S_{12} W & \cdots & H_{1n} - S_{1n} W \\
H_{21} - S_{21} W & H_{22} - S_{22} W & \cdots & H_{2n} - S_{2n} W \\
\vdots & \vdots & \ddots & \vdots \\
H_{n1} - S_{n1} W & H_{n2} - S_{n2} W & \cdots & H_{nn} - S_{nn} W
\end{vmatrix} = 0. \tag{F.7}$$

Expansion of the determinant gives an algebraic equation of degree n in the unknown W. This algebraic equation has n roots which can be shown to be real. Arranging these roots in order of increasing value, we denote them as

$$W_1 \leq W_2 \leq \cdots \leq W_n.$$

If we number the bound states of the system in order of increasing energy, we have

$$E_0 \leq E_1 \leq \cdots \leq E_n \leq E_{n+1} \leq \cdots ,$$

where E_i denote the true energies of various states. From Theorem 1, it can be easily shown that

$$E_0 \leq W_1, \qquad E_0 \leq W_2, \qquad \ldots, \qquad E_0 \leq W_n.$$

Thus, the linear variation method provides upper bounds to the energies of the lowest n bound states of the system.

Bibliography

[1] C. Adler, *The relativistic one-dimensional square potential*, American Journal of Physics, 39 (1971), pp. 305–309.

[2] V. Alonso and S. Vincenzo, *General boundary conditions for a Dirac particle in a box and their non-relativistic limits*, Journal of Physics A: Mathematical and General, 30 (1997), p. 8573.

[3] ——, *Some remarks about the 'free' Dirac particle in a one-dimensional box*, Journal of Physics A: Mathematical and General, 32 (1999), p. 5277.

[4] N. Aquino, *Accurate energy eigenvalues for enclosed hydrogen atom within spherical impenetrable boxes*, International Journal of Quantum Chemistry, 54 (1995), pp. 107–115.

[5] N. Aquino, G. Campoy, and H. Montgomery, *Highly accurate solutions for the confined hydrogen atom*, International Journal of Quantum Chemistry, 107 (2007), pp. 1548–1558.

[6] N. Aquino, A. Flores-Riveros, and J. Rivas-Silva, *The compressed helium atom variationally treated via a correlated hylleraas wave function*, Physics Letters A, 307 (2003), pp. 326 – 336.

[7] N. Aquino, J. Garza, A. Flores-Riveros, J. F. Rivas-Silva, and K. D. Sen, *Confined helium atom low-lying s states analyzed through correlated Hylleraas wave*

functions and the Kohn-Sham model, The Journal of Chemical Physics, 124 (2006), p. 054311.

[8] N. W. Ashcroft, *Metallic hydrogen: A high-temperature superconductor?*, Physical Review Letters, 21 (1968), pp. 1748–1749.

[9] K. BAKKE, *Confinement of a Dirac particle to a hard-wall confining potential induced by noninertial effects*, Modern Physics Letters B, 27 (2013), p. 1350018.

[10] A. Banerjee, C. Kamal, and A. Chowdhury, *Calculation of ground- and excited-state energies of confined helium atom*, Physics Letters A, 350 (2006), pp. 121 – 125.

[11] M. Born, *Zur Quantenmechanik der stövorgänge*, Zeitschrift für Physik, 37 (1926), pp. 863–867.

[12] S. Boys, *Electronic wave functions. 1. a general method of calculation for the stationary states of any molecular system*, Proceedings of the Royal Society of London Series A-Mathematical and Physical Sciences, 200 (1950), pp. 542–554.

[13] S. Boys, G. Cook, C. Reeves, and I. Shavitt, *Automatic fundamental calculations of molecular structure*, Nature, 178 (1956), pp. 1207–1209.

[14] B. Burrows and M. Cohen, *Exact solutions for perturbed confined hydrogen atoms: Polarizabilities and nuclear shielding factors*, Physical Review A, 72 (2005), p. 032508.

[15] J. Dahl, *Introduction to the Quantum World of Atoms and Molecules*, World Scientific, Singapore, 1st ed., 2001.

[16] E. Davidson and D. Feller, *Basis set selection for molecular calculations*, Chemical Reviews, 86 (1986), pp. 681–696.

[17] S. de Groot and C. ten Seldam, *On the energy levels of a model of the compressed hydrogen atom*, Physica, 12 (1946), pp. 669–682.

[18] P. Decleva, G. De Alti, G. Fronzoni, and M. Stener, *Theoretical study of*

resonances in the metal core photoionization of M@C_{60} (M = Li, Na, K), Journal of Physics B: Atomic, Molecular and Optical Physics, 32 (1999), p. 4523.

[19] R. Dutt, A. Mukherjee, and Y. Varshni, *Dipole polarizability of hydrogen atom at high pressures*, Physics Letters A, 280 (2001), pp. 318 – 324.

[20] J. Ferreyra and C. Proetto, *Exact solution of the compressed hydrogen atom*, American Journal of Physics, 81 (2013), pp. 860–865.

[21] A. Flores-Riveros, N. Aquino, and H. M. Jr., *Spherically compressed helium atom described by perturbative and variational methods*, Physics Letters A, 374 (2010), pp. 1246 – 1252.

[22] V. Fock, *Näherungsmethode zur Lösung des quantenmechanischen Mehrkörperproblems*, Zeitschrift für Physik, 61 (1930), pp. 126–148.

[23] M. Frisch, G. Trucks, H. Schlegel, G. Scuseria, M. Robb, J. Cheeseman, G. Scalmani, V. Barone, B. Mennucci, G. Petersson, H. Nakatsuji, M. Caricato, X. Li, H. Hratchian, A. Izmaylov, J. Bloino, G. Zheng, J. Sonnenberg, M. Hada, M. Ehara, K. Toyota, R. Fukuda, J. Hasegawa, M. Ishida, T. Nakajima, Y. Honda, O. Kitao, H. Nakai, T. Vreven, J. A. Montgomery, J. Peralta, F. Ogliaro, M. Bearpark, J. Heyd, E. Brothers, K. Kudin, V. Staroverov, R. Kobayashi, J. Normand, K. Raghavachari, A. Rendell, J. Burant, S. Iyengar, J. Tomasi, M. Cossi, N. Rega, J. Millam, M. Klene, J. Knox, J. Cross, V. Bakken, C. Adamo, J. Jaramillo, R. Gomperts, R. Stratmann, O. Yazyev, A. Austin, R. Cammi, C. Pomelli, J. Ochterski, R. Martin, K. Morokuma, V. Zakrzewski, G. Voth, P. Salvador, J. Dannenberg, S. Dapprich, A. Daniels, O. Farkas, J. Foresman, J. Ortiz, J. Cioslowski, and D. Fox, *Gaussian 09 Revision A.1*, Gaussian Inc. Wallingford CT, (2009).

[24] P. Froman, S. Yngve, and N. Froman, *The energy levels and the corresponding normalized wave functions for a model of a compressed atom*, Journal of Mathematical Physics, 28 (1987), pp. 1813–1826.

[25] P. Fulde, *Electron Correlations in Molecules and Solids*, Springer–Verlag, Germany, 3rd ed., 2003.

[26] B. M. Gimarc, *Correlation energy of the twoelectron atom in a spherical potential box*, The Journal of Chemical Physics, 47 (1967), pp. 5110–5115.

[27] P. Goodfriend, *On the use of linear variation basis functions that do not satisfy the boundary conditions*, Journal of Physics B: Atomic Molecular and Optical Physics, 23 (1990), p. 1373.

[28] T. Guillot, *A comparison of the interiors of jupiter and saturn*, Planetary and Space Science, 47 (1999), pp. 1183–1200.

[29] G. Hall, *The molecular orbital theory of chemical valency. viii. a method of calculating ionization potentials*, Proceedings of the Royal Society of London. Series A. Mathematical and Physical Sciences, 205 (1951), pp. 541–552.

[30] G. Hall and J. Lennard-Jones, *The molecular orbital theory of chemical valency. vii. molecular structure in terms of equivalent orbitals*, Proceedings of the Royal Society of London. Series A. Mathematical and Physical Sciences, 205 (1951), pp. 357–374.

[31] D. Hartree, *The wave mechanics of an atom with a non-Coulomb central field. part i. theory and methods*, Mathematical Proceedings of the Cambridge Philosophical Society, 24 (1928), pp. 89–110.

[32] S. Huzinaga and M. Klobukowski, *Well-tempered {GTF} basis sets for the atoms k through e*, Chemical Physics Letters, 120 (1985), pp. 509 – 512.

[33] C. Joslin and S. Goldman, *Quantum monte carlo studies of two-electron atoms constrained in spherical boxes*, Journal of Physics B: Atomic, Molecular and Optical Physics, 25 (1992), p. 1965.

[34] J. G. Kirkwood, -, Physikalische Zeitschrift, 33 (1932), p. 57.

[35] O. Klein, *Die reflexion von elektronen an einem potentialsprung nach der relativ-*

istischen dynamik von dirac, Zeitschrift für Physik, 53 (1929), pp. 157–165. 10.1007/BF01339716.

[36] M. Klobukowski, *Comparison of generator formulas for exponential parameters of gaussian basis sets*, Chemical Physics Letters, 214 (1993), pp. 166 – 174.

[37] E. Kryachko and S. Wilson, *Generation of systematic sequences of even-tempered basis sets: Empirical generating formulae*, International Journal of Quantum Chemistry, 93 (2003), pp. 112–120.

[38] C. Laughlin, *On the dipole polarizability of a hydrogen-like atom confined in an impenetrable spherical box*, Journal of Physics B: Atomic, Molecular and Optical Physics, 37 (2004), p. 4085.

[39] C. Laughlin and S.-I. Chu, *A highly accurate study of a helium atom under pressure*, Journal of Physics A: Mathematical and Theoretical, 42 (2009), p. 265004.

[40] E. Ley-Koo and S. Cruz, *The hydrogen atom and the H_2^+ and HeH^{++} molecular ions inside prolate spheroidal boxes*, Journal of Chemical Physics, 74 (1981), pp. 4603–4610.

[41] E. Ley-Koo and S. Rubinstein, *The hydrogen atom within spherical boxes with penetrable walls*, Journal of Chemical Physics, 71 (1979), pp. 351–357.

[42] ——, *The hydrogen atom inside boxes with paraboloidal surfaces*, Journal of Chemical Physics, 73 (1980), pp. 887–893.

[43] E. LeyKoo and S. MateosCortés, *The hydrogen atom in a semiinfinite space limited by a conical boundary*, American Journal of Physics, 61 (1993), pp. 246–249.

[44] P.-O. Löwdin, *Correlation Problem in Many-Electron Quantum Mechanics I. Review of Different Approaches and Discussion of Some Current Ideas*, John Wiley & Sons, Inc., 2007, pp. 207–322.

[45] E. Ludea and M. Gregori, *Configuration interaction calculations for two-electron*

atoms in a spherical box, The Journal of Chemical Physics, 71 (1979), pp. 2235–2240.

[46] J. Marin and S. Cruz, *Use of the direct variational method for the study of one- and two-electron atomic systems confined by spherical penetrable boxes*, Journal of Physics B: Atomic, Molecular and Optical Physics, 25 (1992), p. 4365.

[47] A. Michels, J. de Boer, and A. Bijl, *Remarks concerning molecular interaction and their influence on the polarisability*, Physica, 4 (1937), pp. 981–994.

[48] H. Montgomery, *Dynamic dipole polarizabilities of the confined hydrogen atom*, Chemical Physics Letters, 352 (2002), pp. 529 – 532.

[49] H. Montgomery Jr., N. Aquino, and A. Flores-Riveros, *The ground state energy of a helium atom under strong confinement*, Physics Letters A, 374 (2010), pp. 2044 – 2047.

[50] B. Noumerov, *A method of extrapolation of perturbations*, Monthly Notices of the Royal Astronomical Society, 84 (1924), pp. 592–592.

[51] ——, *Note on the numerical integration of* $d^2x/dt^2 = f(x,t)$, Astronomische Nachrichten, 230 (1927), pp. 359–364.

[52] G. Petersson, S. Zhong, J. Montgomery, and M. Frisch, *On the optimization of gaussian basis sets*, The Journal of Chemical Physics, 118 (2003), pp. 1101–1109.

[53] M. Plesset, *The dirac electron in simple fields*, Physical Review, 41 (1932), pp. 278–290.

[54] W. Press, S. Teukolsky, W. Wetterling, and B. P. Flannery, *Numerical Recipes: The Art of Scientific Computing*, Cambridge University Press, Cambridge, 3^{rd} ed., 2007.

[55] C. Reeves, *Use of gaussian functions in the calculation of wavefunctions for small molecules. i. preliminary investigations*, The Journal of Chemical Physics, 39 (1963), pp. 1–10.

[56] R. Rivelino and J. Vianna, *A configuration interaction model to investigate many-electron systems in cavities*, Journal of Physics B: Atomic, Molecular and Optical Physics, 34 (2001), p. L645.

[57] C. Roothaan, *New developments in molecular orbital theory*, Reviews of Modern Physics, 23 (1951), pp. 69–89.

[58] S. Roy and V. Singh, *Fractional total-charge eigenvalues for a fermion in a finite one-dimensional box*, Physics Letters B, 143 (1984), pp. 179 – 182.

[59] F. Sauter, *Zum kleinschen paradoxon"*, Zeitschrift für Physik, 73 (1932), pp. 547–552. 10.1007/BF01349862.

[60] M. Schmidt and K. Ruedenberg, *Effective convergence to complete orbital bases and to the atomic Hartree–Fock limit through systematic sequences of gaussian primitives*, The Journal of Chemical Physics, 71 (1979), pp. 3951–3962.

[61] C. T. Seldam and S. D. Groot, *On the ground state of a model for compressed helium*, Physica, 18 (1952), pp. 891 – 904.

[62] ——, *On the polarizability of a model of the compressed helium atom*, Physica, 18 (1952), pp. 905 – 909.

[63] J. Slater, *Note on Hartree's method*, Physical Review, 35 (1930), pp. 210–211.

[64] A. Sommerfeld and H. Welker, *Künstliche Grenzbedingungen beim Keplerproblem*, Annals of Physics, 424 (1938), pp. 56–65.

[65] D. Suryanarayana and J. Weil, *On the hyperfine splitting of the hydrogen atom in a spherical box*, Journal of Chemical Physics, 64 (1976), pp. 510–513.

[66] E. C. TITCHMARSH, *On the nature of the spectrum in problems of relativistic quantum mechanics*, The Quarterly Journal of Mathematics, 12 (1961), pp. 227–240.

[67] Y. Varshni, *Accurate wavefunctions for the confined hydrogen atom at high pressures*, Journal of Physics B: Atomic, Molecular and Optical Physics, 30 (1997), p. L589.

[68] F. D. Weiss, J. L. Elkind, S. C. O'Brien, R. F. Curl, and R. E. Smalley, *Photophysics of metal complexes of spheroidal carbon shells*, Journal of the American Chemical Society, 110 (1988), pp. 4464–4465.

[69] Wolfram Research Inc., *Mathematica Version 8.0*, (2010). Champaign, Illinois.

Index